WIND SHEAR AND DIFFERENTIAL UPWELLING ALONG THE S W TIP OF AFRICA

MARK R JURY

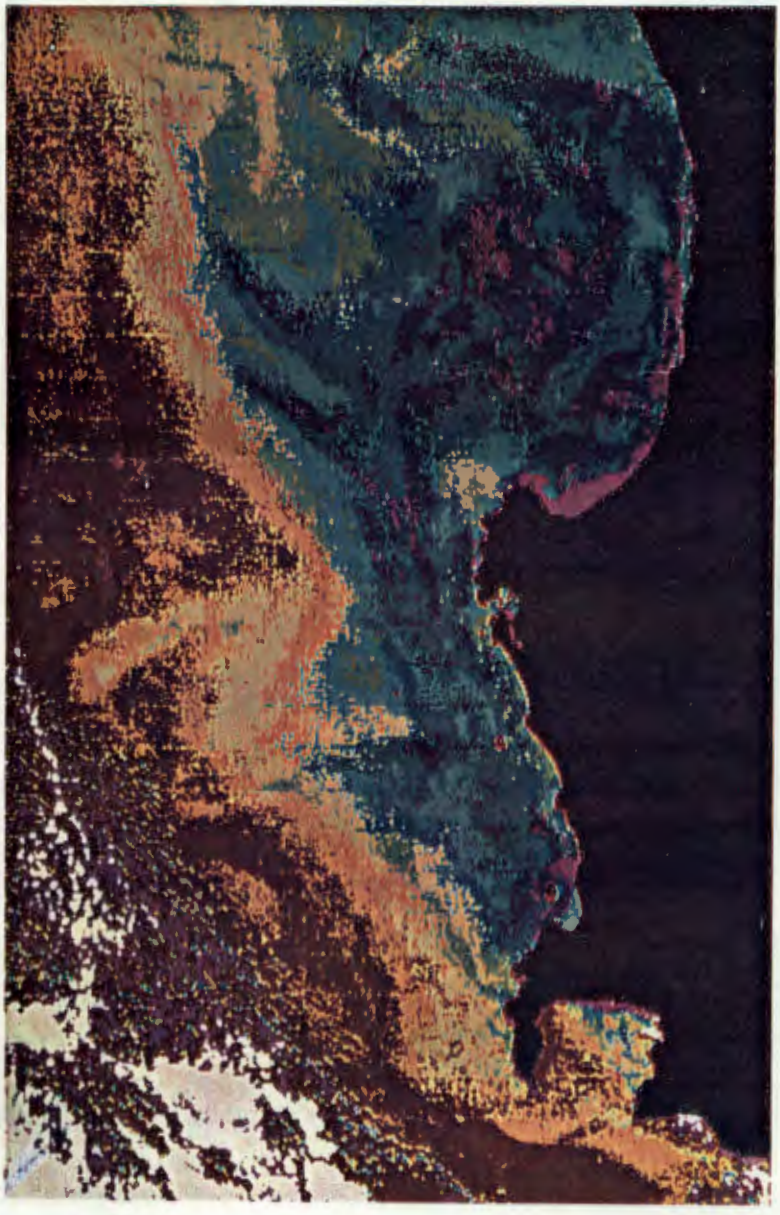

PhD THESIS

PHYSICAL OCEANOGRAPHY

University of Cape Town

1983

ABSTRACT

Along the SW tip of Africa (30-35°S, 17-20°E) topographic irregularities shear the wind stress field giving rise to coastal upwelling with an alongshore variability. The relationship between wind shear and differential upwelling is established using a blend of oceanographic and meteorological investigations. Mesoscale aerial survey case studies form the observational basis from which the spatial variations in winds and upwelling are compared.

Coastal winds, controlled by the pressure gradient between the South Atlantic Anticyclone and a summertime interior low, become modulated through interactions with the circumpolar jet stream. Low level winds accelerate over portions of the southern Benguela current region through deflections forced by three pronounced capes, two with mountain ridges exceeding 1000 m. Selected case studies are utilized to contrast the characteristics of deep and shallow wind flow, and the exposed and sheltered offshore regions. The spatial variability of the low level wind and sea surface temperature fields is correlated by means of aerial survey techniques applied at alongshore spacings of 10 to 50 km. Vertical transect and profile data collected at altitudes up to 1 km illustrate the variable depth of wind flow.

Vertical wind shear controls the interaction of topography and winds. Field results show that vertical shears of $-2\ (10^{-2})s^{-1}$ produce horizontal wind vorticities of $-6\ (10^{-4})s^{-1}$ and alongshore sea surface temperature gradients of $1^{\circ}C\ (10km)^{-1}$, a characteristic of summertime upwelling in the southern Benguela region.

ACKNOWLEDGEMENTS

The Sea Fisheries Research Institute (SFRI) of the Department of Environmental Affairs is gratefully acknowledged for permission to use the data in this thesis. These data remain the copyright of the SFRI. Special thanks goes to the personnel of the Physical Environmental Section of the SFRI, especially to Dr. L.V. Shannon and G. Nelson who directed the CUEX research programme and to J. Froggatt and F. Kamstra who provided technical and logistical support. A routine programme of coastal weather data collection is operated by the SFRI from which a number of figures in this thesis are derived. Moored anemometer data are taken from work prepared for publication by Kamstra.

Sincere appreciation is extended to Prof. G.B. Brundrit of the Department of Physical Oceanography and to Dr. C.S. Keen of the Department of Geography at the University of Cape Town for their supervision and guidance throughout the development of the thesis.

The Electricity Supply Commission is acknowledged for providing assistance in the PhD programme and for the use of facilities in the production of the thesis. A. Albertyn is thanked for word processing of the thesis text.

TABLE OF CONTENTS

LIST OF FIGURES

UNITS TABLE

wind speed	$m\ s^{-1}$
wind vorticity	$10^{-4}\ s^{-1}$
wind stress	dynes (cm^{-2})
wind stress curl	10^{-7} dynes (cm^{-3})
sea surface temperature	^{o}C
air temperature	^{o}C

CHAPTER 1 : INTRODUCTION

A. RATIONALE

This thesis seeks to establish a relationship between wind shear* and differential upwelling along the southwest tip of Africa. It is particularly concerned with mesoscale** phenomena in the atmosphere and ocean. Such phenomena are typically short-lived and therefore require a synchronous acquisition of field data for spatial definition. Aerial survey methods are well suited to this time-space simultaneity and will form the observational basis here. Through the aerial survey results, mesoscale case studies are used to compare spatial variations in horizontal wind and upwelling patterns.

Coastal upwelling along the SW tip of Africa is the result of longshore, equatorward winds driving surface water away from the coast. These southeasterly winds occur most prominently during the summer when the South Atlantic Anticyclone ridges to the south of the African continent. A local pressure gradient, set up by the offshore high and interior low, is modulated by eastward moving mid-latitude troughs producing a

---

* Wind shear will refer to the horizontal variation perpendicular to the surface wind.

** Mesoscale phenomena appear on spatial scales of tens of kilometers over periods of hours. Spatial scales may be quantified as: microscale 1km, mesoscale 1-100km, synoptic scale 100-1000km and macroscale 1000km. Synoptic will also refer to a simultaneous time frame.

recurrent wind/upwelling sequence. These events develop over time scales of a few days with a frequency exceeding 50% during summer. As a result, this season was selected for the observational research programme known as the Cape Upwelling Experiment (CUEX).

The effect of sequentially developing transient weather systems (shown in the following diagram) is not necessarily manifested in the surface wind trajectories but may appear as a change in depth of longshore equatorward winds. Early in the observational programme it was noted that shallow flow depths, associated with coastal lows, were more susceptible to local topographic features than the deeper flows. The contrasting of the surface horizontal wind pattern under differing flow depths was then utilized as the basis for case study analysis in this thesis.

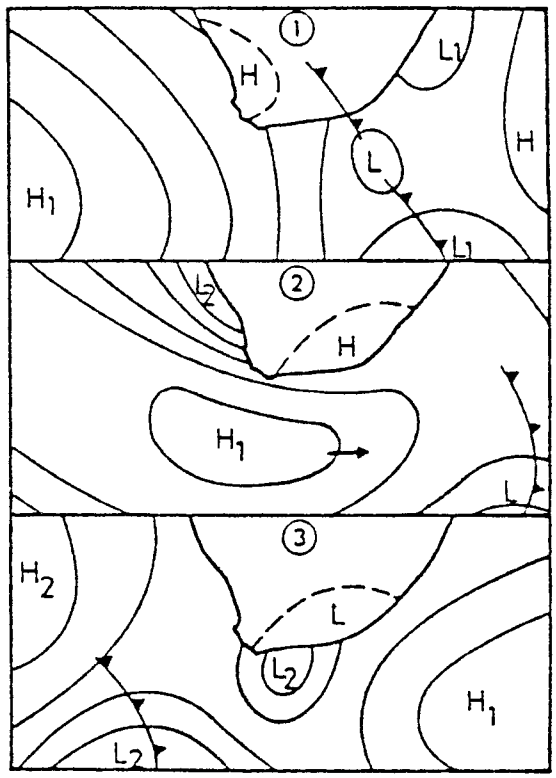

The mesoscale motions governing air-sea dynamics, although readily observable, have received little attention in the southern Benguela region. This thesis documents the perturbations in the coastal wind field which result from topographic deflections and thermal constraints. Each of the major headlands along the SW tip of Africa create a cyclonic horizontal shearing of shallow equatorward winds. The persistence of this sheared wind flow is a triggering mechanism for localised oceanic divergence and differential coastal upwelling. By calling on mesoscale evidence the thesis advances the theoretical considerations of previous studies.

The southern Benguela upwelling region is perhaps uniquely complex in terms of topographic coastal irregularities as seen in Fig.1. Mountainous capes or headlands alternate with low-lying coastal plains, ensuring an alongshore variability in surface friction. Summer-time equatorward flowing winds are perturbed by the topography to a greater or lesser extent depending on the vertical depth of wind flow. The fundamental mechanism which endows the SW tip of Africa with wind shear and differential upwelling is the combination of large and small scale dynamics. While the continental shelf's bathymetry and seasonal winds provide a steady macroscale upwelling mechanism, the topography and mesoscale meteorology create an alternating pattern of active and passive upwelling circulations along the coast.

A vital role in this research is played by the application of mesoscale remote sensing techniques, namely instrumented aerial survey. The data gathering method has advanced air-sea interdisciplinary descriptions elsewhere and provides the means to parameterise wind and thermal variabilities along vast and somewhat remote stretches of coastline. From the mesoscale (space) and synoptic (time) field observations, the immediate and local response of the ocean to atmospheric forcing is evident along the SW tip of Africa.

It is the unique dynamics of the southern Benguela system which produces cold plumes and warm countercurrents via topographic wind shear. These different water masses mix under certain meteorological circumstances to provide a suitable environment for marine bioproductivity. By establishing the alongshore variabilities which link wind shear and differential upwelling, a more complete understanding of the fisheries distribution in the southern Benguela is projected.

The cause-effect relationship between the earth's atmosphere and ocean is becoming understood through advances in data collection and processing techniques. Recent observational studies have made use of these advanced methods in coastal upwelling regions to ensure the renewability of the fisheries resource through scientifically based management. The economic significance and wind-driven nature of currents such

as the Benguela provide a motivation for air-sea interaction research of this type.

B. LITERATURE REVIEW

Early mariners and fishermen realised that a substantial portion of the world's marine life could be found along the cooler, eastern boundary of the major oceans. To more fully document this uneven distribution simple biological and physical observations have been taken from ships exploring the seas since the 1500's. With only limited positioning accuracies these marine observations could approximate global and seasonal oceanic patterns. However the physical studies lacked synoptic, descriptive capabilities until the development of mobile instrumentation and accurate navigation systems for seagoing ships and, more recently, aircraft. Since then the transportation requirements of world trade coupled with the new technology have amassed nearly a century of historical wind and sea surface temperature (SST) data. Such a record of long time averaged data over large oceanic and coastal areas presents an ideal opportunity for the researcher in determining the macroscale forcing functions which drive certain physical oceanographic processes.

CONTRASTING SCALES OF INVESTIGATION

Using the historical data together with digital processing techniques, wind and current distributions have been resolved on time scales of months and spatial scales of thousands of

kilometers. The primary goal of the macroscale studies is the description of seasonally averaged wind and upwelling distributions, an approach particularly suited to areas where monthly trends outweigh weekly weather cycles or mesoscale variations. Data processing in the macroscale studies commences with ship-based marine wind data collected along the coast over decades. The data are inspected for inaccuracies and reduced to sea level using empirical equations. The data are then categorised by month or season and arrayed in a matrix with a one degree latitude/longitude resolution. Wind stress vector components are computed and time averaged over each matrix point. The data, thus averaged, present a reliable macroscale data base from which wind stress curl or vorticity distributions can be calculated and plotted.

Using centered differencing techniques Nelson, Bakun and Parrish (10,11,12,13,45,61,66) have studied the macroscale relationship between cyclonic wind stress curl and enhanced seasonal upwelling along certain portions of the California coast. In a comparison with mean monthly SST's areas of cyclonic wind stress curl were found in spatial agreement with persistent upwelling plumes, particularly next to large capes or headlands. Numerous other authors have incorporated these ideas in explaining persistent upwelling gyres and alongshore current anomalies. The data presentation method favoured by many of the macroscale studies is the marine

atlas accompanied by an interpretive report. It is apparent from these macro-time-scale studies that perturbations in equatorward winds and coastal upwelling occur in sympathy with nearby topographic irregularities.

Macroscale marine-based studies lend a useful data processing technique to this thesis and provide an interpretive framework for relating wind shear and upwelling phenomena. However, to document variabilities with dimensions of less than 40 km, such as found in the southern Benguela, a reduced time and space scale is advantageous. To fulfill these requirements mesoscale aerial survey is the preferred mode of data gathering.

The aerial survey data collection technique compresses time scales while allowing wide areas to be covered. Utilizing sophisticated airborne navigation systems and infrared SST sensors, a series of international studies were initiated in the 1970's by the Coastal Upwelling Ecosystems Analysis (CUEA) Group. The coasts of Oregon (USA), NW Africa and Peru were selected for the purpose of mapping wind and upwelling variabilities in eastern boundary currents using regular interval aerial surveys, at a height of (500 ft.) 152m. In the surveilance of mesoscale phenomena CUEA established a positive correlation between alongshore wind stress and the rate of upwelling. Along the coasts of Peru and NW Africa Stuart, Goodwin, Moody, Duval, Uhart and Watson found that

coastal headlands accelerate equatorward winds and localise upwelling activity (36,59,83,85,89). In the temperate latitudes along the more uniform Oregon coastline, diurnal wind cycles and upwelling events were investigated. Hawkins and other CUEA meteorologists (28,33,39,40,41,49) determined that horizontal and vertical thermal constraints acted to produce seabreezes. By collecting aerial survey wind data over numerous weather cycles the interaction of seabreezes with the prevailing seasonal flow was described. A low seabreeze inversion was found to initiate a bending of surface winds into an alongshore axis off the Oregon coastline. Using similar techniques Findlater and others (4,17,21,31,54) described the SW monsoon wind jet along the coast of Somalia. In response to the stress vectors and curl observed within the jet an upwelling plume was found to persist through the monsoon season off the horn of Africa.

These mesoscale meteorological discoveries have proven the usefulness of aerial survey in clearing the wind/ upwelling picture. Recently a similar data collection strategy was applied to the SW tip of Africa. However the processing of wind data was taken a step further by synthesising the macroscale averaging and mesoscale synoptic approaches. The result is a more refined time and space scale from which wind shear and differential upwelling may be described. In order to put this synthesis into perspective a review of local research may be useful.

BENGUELA STUDIES

The history of wind/upwelling research in the southern Benguela region has derived from the needs of fisheries biologists. Previous research programmes have focused on macroscale upwelling features and associated marine productivity (5,55,62,87). The first application of the aerial survey technique by Andrews and Cram (2) showed that cold water plumes extended northwards from Cape Hangklip, the Cape Peninsula, and Cape Columbine. Using aerial and marine data sources, Bang and others described the variable nature of upwelling phenomena (14,15,16,19). However these studies could not resolve the cause-effect relationship of winds and upwelling due to a lack of mesoscale meteorological observations.

Air-sea interaction processes were first monitored in the southern Benguela using the CUEA aerial survey approach in 1978. As part of the Sea Fisheries Research Institute's (SFRI) Cape Upwelling Experiment (CUEX), a light aircraft was equipped with DECCA navigation, a drift sight, and an infrared SST sensor. Wind and upwelling intensities were mapped and interpreted in terms of temporal cycles, related to the eastwards passage of macroscale weather systems by Shannon, Nelson and Jury (50,77). Concurrently the SFRI monitored the ocean colour, primary productivity and physical oceanographic variables as part of the NIMBUS 7 Ocean Colour Experiment. The mesoscale meteorology was detailed more

precisely in subsequent years by adjusting the area of coverage and resolution of the aerial survey grid pattern. The mesoscale susceptibility of local surface winds to topographic irregularities began to emerge from the background of available data. In the light of previous international studies, this variability of wind stress was thought to have an impact on fisheries through current gyres, nutrient enhancement, primary productivity and recruitment processes and it is such biological processes which motivate this thesis.

MESOSCALE COASTAL METEOROLOGY

The interaction of geographic features, surface winds and ocean currents has been given emphasis in numerous studies through developments in theories and in simulated and observed results. The influence of atmospheric thermal stability on the generation of topographic wind shear has been investigated recently in wind tunnel experiments. Flow behaviour in a scale model with orographic features was observed under different flow speeds and density stratifications. Laboratory results confirmed that when inertia overcame stratification, flow would accelerate over an obstacle. Under density stratified conditions however, the vertical displacement of horizontal wind was inhibited. Flow was forced to deflect around the obstacle leaving a light wind wake or eddy in the lee. In developing the theories to explain such phenomena Atkinson and others (6) have likened

the stratified downslope winds to shallow water flow in a channel. The velocity of flow was found to be inversely correlated with the depth of flow (capped by an inversion layer). A useful parameter was developed to determine whether the flow would accelerate or deflect. This parameter, the Froude number, is given by the ratio of inertia over thermal stratification and could be computed from vertical profile information.

In seeking to substantiate these theories in the field Overland and others (88) used aerial survey techniques to compare horizontal flow fields near mountains with the Froude number calculated from nearby radiosonde data. Case studies of high wind speeds and rapidly decreasing temperatures aloft revealed the formation of a pressure wave and gravity assisted downslope wind accelerations in the lee of the Olympic Mountains (Washington, USA). During stratified flow pronounced deflections resulted in a calm, mesoscale eddy in the lee of the mountain.

These theories and observations which compare vertical and horizontal wind shear in the presence of topography extend the interpretive framework of this thesis. Downslope winds are a common phenomena along the SW tip of Africa and require a better understanding of their mechanisms.

In recent numerical modelling studies of eastern boundary

currents, coastal geometry and bathymetry were shown to induce fluctuations in the geostrophic currents (67). With increasing sophistication in the coastal oceanic circulation models, a greater demand for realistic wind field inputs has developed. The numerical simulation of upwelling along the SW tip of Africa has shown an increasingly differential structure with the input of wind stress fields contained in this thesis (86). To put the synthesis of data processing techniques into a coherent scientific perspective, a review of wind driven upwelling theory is appropriate at this stage.

C. THEORETICAL BACKGROUND

In 1905 Ekman developed theories to explain why the ocean's surface layer, in temperate latitudes, drifts at an angle to the wind stress just above it. The apparent deflection was attributed to the combined effects of the earth's rotation (Coriolis force) and frictional forces (29). This general premise can be applied more specifically to the eastern boundary of an ocean where a coast-parallel equatorward wind deflects the surface water away from the coast thereby creating a mass deficit. In compensation, an ascending motion in the subsurface layers results. This process has come to be known as coastal upwelling (77).

More recent arguments have suggested that the longshore wind stress curl or vorticity influence coastal water circulations (12). In investigating these mechanisms, dynamic conditions

were evaluated to determine how balances between accelerations and other forces were maintained. The presence of a coastline was shown to create an offshore balance between the Coriolis and pressure forces thus overshadowing wind stress. In the alongshore axis, however, wind stress was found to play an equally important role in the balance of forces (34).

Enhanced equatorward drift has been linked by Nelson to the vertical component of wind stress curl (61). Wind-induced Ekman divergence in the surface layer was shown to be balanced by convergence in the subsurface oceanic layer. An area of cyclonic wind stress curl caused a localised oceanic divergence. Such a divergence, superimposed on the existing mass at the coast, would induce a differential upwelling as represented by the following schematic examples for the southern hemisphere.

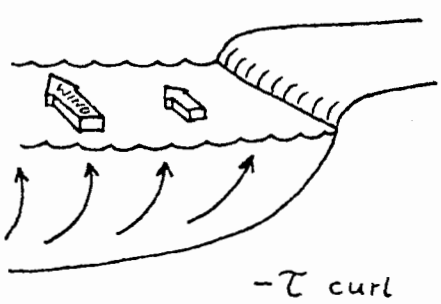

Increasing Upwelling Offshore

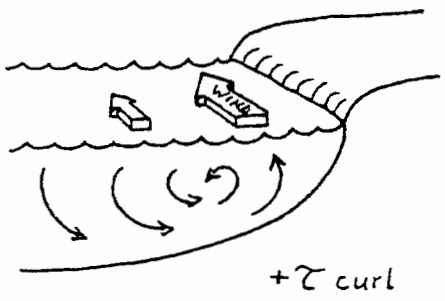

Decreasing Upwelling and Frontal Formations

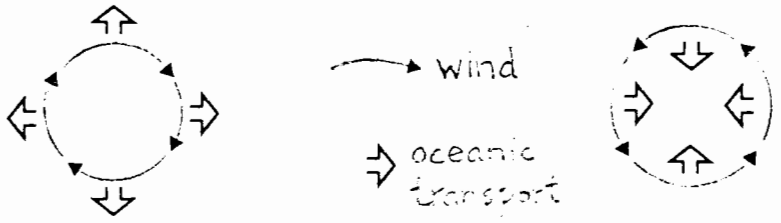

Ekman Divergence Ekman Convergence

The effect of stress curl variations on coastal upwelling appears whenever divergence in the surface wind drift is not balanced by other modes of horizontal oceanic flow. This variability, resulting from wind stress curl and localised oceanic circulation, has been treated in a theoretical light by numerous authors (1,32,34,68).

The link between alongshore wind stress and coastal upwelling, and macroscale wind stress curl and differential upwelling has been explored. However, little observational evidence has been accumulated in a combined approach. By synthesising mesoscale survey techniques and macroscale data analysis methods, attention is drawn to the differential response of coastal upwelling in the presence of cyclonic wind stress curl. A review of the scales of motion which combine or contrast to produce these unique phenomena is given below.

A THEORETICAL FRAMEWORK

Dynamical processes over the continental shelf operate on relatively small horizontal scales of motion where the presence of a coastline is a constraining influence. When focusing on oceanic transport and coastal upwelling processes it is useful to review the fundamental Eulerian equations of motion. Idealizations may then be introduced which simplify these equations to a form appropriate to the study of the coastal upwelling response to wind forcing. A theoretical framework will be developed which will point out the importance of longshore (as against offshore) wind stress. The framework will indicate how the coastal upwelling circulation is maintained and how it is affected by wind stress curl.

A simple theoretical framework for wind-driven upwelling over a continental shelf should distinguish between steady driving forces and secondary interactions or perturbations. The framework must be consistent with field observations, particularly in the surface mixed layer of the ocean. It is useful at this stage to distinguish the various processes according to their characteristic time scales. Firstly, the density field evolves slowly on a seasonal time scale. Thus for upwelling phenomena with a time scale of days, it is reasonable to assume that density changes are controlled by advection and play a passive role. Within this mesoscale time frame, limited to hours and days, interior turbulence and

bottom frictional stresses may be neglected and the major role of the wind emerges. The momentum produced by the wind stress is transferred downward through the surface mixed layer within hours. Wind stress represents the dominant force in a sequence of upwelling events and much of the physics governing phenomena with shorter or longer time scales need not be included in this framework.

In the Eulerian approach to fluid mechanics the motion of a particle is governed by its momentum balance. The rate of change of momentum is the sum of surface stresses (hydrostratic pressure gradients and stress divergence) and interior stresses (density, gravity and Coriolis forces). Of the forces, the vertical shear is important because it transmits the driving force of the wind to the surface layer of a water column. The vertical momentum balance is dominated by the force of gravity. This leads, through a scaling of the terms to the hydrostatic approximation. Horizontal pressure gradients within the water column arise from atmospheric pressure effects, sea surface gradients and inerior density gradients. However, it is the wind stress setting up a sea surface slope which is the dominant contribution to the momentum balance.

A conceptual model of coastal upwelling begins with a steady longshore current in geostrophic balance with the sea surface gradient. In this idealized, steady state condition external

influences such as wind stress are negligible and the water is assumed to be homogeneous. All time derivatives in the transport equations vanish and the offshore velocity is zero due to the presence of a coast. The longshore velocity is in geostrophic balance with the offshore pressure gradient and may be represented, using the x,y,z coordinate system with velocity components u,v,w, as:

$$-fv = -g\frac{\partial \eta}{\partial x} \qquad \text{[Eq.1]}$$

where longshore velocity v depends only on x, g is gravity, f is the Coriolis force and η is the sea surface displacement from a level surface of geopotential.

This conceptual model shows the dominant balance between the longshore current and sea surface gradient or slope but gives no indication of the role played by wind stress and upwelling. Clearly a more realistic framework is necessary to include these secondary processes.

In the dynamics of coastal currents, oceanic transport is determined by a balance between Coriolis force, local acceleration, and wind stress. The ratio of nonlinear momentum advection terms to the Coriolis force is small. Thus a simplified set of governing equations may be introduced which neglect the nonlinear terms and make use of the equation of continuity and the hydrostatic approximation.

The linearized shallow water equations governing particle displacements in the surface mixed layer are:

$$\frac{\partial u}{\partial t} - fv = -g\frac{\partial \eta}{\partial x} + \frac{\tau_x}{\rho H} \qquad \text{[Eq.2]}$$

$$\frac{\partial v}{\partial t} + fu = -g\frac{\partial \eta}{\partial y} + \frac{\tau_y}{\rho H} \qquad \text{[Eq.3]}$$

where ρ is the sea water density, H is the thickness of the surface mixed layer and τ_x and τ_y are wind stress components.

These horizontal momentum balances are supplemented by the continuity equation to incorporate the vertical balance of forces:

$$\frac{\partial u}{\partial x} + \frac{\partial v}{\partial y} = -\frac{\partial w}{\partial z} \qquad \text{[Eq.4]}$$

Assuming that the velocity components are independent of depth and the stress is evenly distributed over H, the depth of the layer H varies with time and horizontal location so that equation 4 may be rewritten as:

$$\frac{\partial H}{\partial t} + H\left(\frac{\partial u}{\partial x} + \frac{\partial v}{\partial y}\right) = 0 \qquad \text{[Eq.5]}$$

It can now be seen in equation 3, that the time variation in the longshore current is forced by the longshore wind stress. However, the offshore component of wind stress in equation 2 only determines smaller scale variations in current, while the geostropic balance is the dominant force.

The stress of the wind, particularly in the longshore direction, is the driving force of coastal upwelling. However there is considerable interaction between the processes represented by equations 2 and 3. In order to highlight the relationship between wind forcing and local Ekman divergence in the surface mixed layer, it is useful to derive the relative vorticity equation from the equations of motion. The pressure terms may be eliminated by differentiating equation 2 with respect to y and equation 3 with respect to x and subtracting. Making use of equation 5 the result may be represented as:

$$\frac{\partial}{\partial t}\left(\frac{\partial v}{\partial x}-\frac{\partial u}{\partial y}\right)=\frac{1}{\rho H}\left(\frac{\partial \tau_y}{\partial x}-\frac{\partial \tau_x}{\partial y}\right)-f\left(\frac{\partial u}{\partial x}+\frac{\partial v}{\partial y}\right) \quad \text{[Eq.6]}$$

Vorticity is seen to be generated by the curl of the frictional forces affecting the surface mixed layer. The vorticity equation 6, derived from the equations of continuity and motion, can be used to supplement the shallow water equations.

Equation 5 shows how the surface oceanic divergence ($\frac{\partial u}{\partial x}+\frac{\partial v}{\partial y}$) is compensated by a reduction in the thickness of the surface mixed layer H and thus by upward vertical motion. The vorticity equation indicates that the wind stress curl ($\frac{\partial \tau_y}{\partial x}-\frac{\partial \tau_x}{\partial y}$) and the surface divergence contribute to an increase in the vorticity of the current ($\frac{\partial v}{\partial x}-\frac{\partial u}{\partial y}$). When considering the scales of motion near a coastal constraint,

it is clear that the current vorticity is dominated by offshore shear in the longshore current.

The mechanism of sea level change due to wind-induced Ekman divergence has been outlined in a simplified theoretical framework. The framework has distinguished the driving force of longshore wind stress from the secondary force of wind stress curl. It is the interaction of the wind stress curl with the coastal geometry which produces local variations in coastal upwelling along the SW tip of Africa.

The above set of equations adequately represent the dynamics of coastal upwelling and are consistent with observational evidence which shows a quick oceanic response to wind forcing. Local winds along the SW tip of Africa impart external impulses to the surface mixed layer on a time scale of days. As a result, the transport field is dominated by barotropic interactions. Changes in the baroclinic field, such as pressure and solenoidal fluctuations, occur on time scales of weeks or more and will not be further investigated.

OVERVIEW OF THESIS

Chapter 1 has provided a backdrop for the exploration of certain mesoscale interactions which occur at the air-sea interface. A rationale for this research was established in the economic importance of fisheries renewability. Wind-driven currents cycle the nutrients along eastern ocean

boundaries and create a favourable environment for biological productivity. The literature review contrasted the various time and space scales of international studies which contributed to the formulation of this thesis. Two data gathering and processing techniques were synthesised from recent wind-upwelling investigations for application along the SW tip of Africa. The history of local research in the southern Benguela was outlined, bringing the literature review up to the 1980's. Recent advances in mesoscale aerial survey data gathering and processing methods were given credit for enabling the description of the wind/upwelling relationship along remote coastlines.

A theoretical framework was formulated in Chapter 1 which extends this relationship beyond the well-known "longshore wind-offshore transport" equations. The possibility of alongshore variations in upwelling due to wind vorticity was brought out in the theoretical framework.

Chapter 2 will develop the ideas and theories into a field application, by first building up a data base through mesoscale aerial survey. Data processing methods will be systematically reviewed and the theoretical approximations handled in a matrix analysis. Digital and manual processing biases will be resolved and the case study patterns subjectively assessed.

In Chapter 3 case study results, selected and categorised by time and space scale will provide an orderly perspective from which to interpret the mesoscale interactions. Topographic surface friction and wind flow depth will be shown to embed a variable level of vorticity or stress curl in the surface summer wind field. The resultant alongshore variation in coastal upwelling is followed through each of the case studies. Chapter 4 will summarize the findings of the case studies and put the contributions of the thesis into perspective. Finally, the clear evidence of the various types of mesoscale motions which link wind shear and alongshore variations in coastal upwelling will be seen as a step towards the renewability of the fisheries resource.

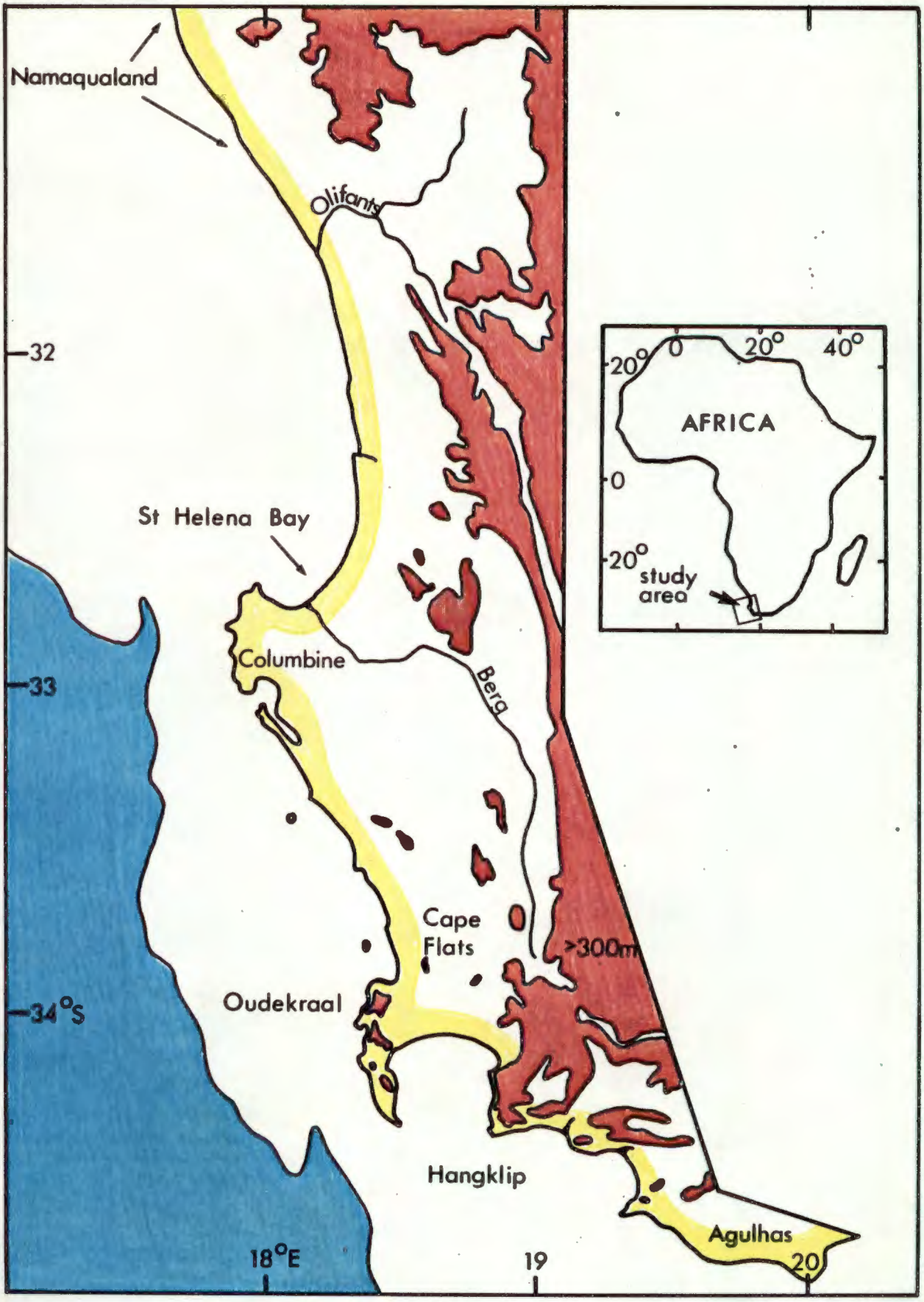

Fig.1 : A detailed topographic and bathymetric reference map of the study area. The 300m contour is colour shaded with brown greater than 300m, yellow along the coast, and blue less than -300m.

CHAPTER 2 : RESEARCH TECHNIQUES AND METHODOLOGY

A. BACKGROUND

A series of physical oceanographic and meteorological (aerial survey) field studies were conducted by the Sea Fisheries Research Institute (SFRI) during the summers of 1979-1980 and 1980-1981. These provided a data base for relating wind forcing and coastal upwelling along the SW tip of Africa. Research was directed towards a better understanding of the physical processes governing the dynamic southern Benguela ecosystem. The enhanced marine bioproductivity, resulting from the rich nutrient supply in the upwelled water, forms the basis for a proliferous fisheries. Past research has shown that the variable nature of southern Benguela upwelling, both in time and space, is the main ingredient in the enhancement process (3).

Coastal winds, which drive the southern Benguela upwelling cell, are governed on scales from 100 to 1000km by the interaction of the South Atlantic Anticyclone with continental lows and easterly moving trough/ridge waves of the circumpolar jet stream. These climatological mechanisms have been extensively covered in the literature (9,35,50,63). On smaller scales of 10 to 100km gradient coastal winds are perturbed by topographic irregularities and attendent thermal contrasts along the SW tip of Africa. These mesoscale circulations feature prominently in the case study data

presented here.

Spatial contrasts in the coastal wind field were monitored by means of an instrumented aircraft flown along precisely scaled horizontal patterns at a height of 152m and on vertical transects up to 1000m using the CUEA methodology. A temporal background to the aircraft-derived data was provided by automatic recording meteorological stations sited at coastal promentaries and by other regional and marine data sources.

B. DATA GATHERING TECHNIQUES

The mesoscale relationship between wind shear and differential upwelling was described via wind and thermal parameters referenced with time and position using an instrumented light aircraft. The survey aircraft was a Partenavia P 68 B twin-enginned, six seater with excellent aerodynamic characteristics for obtaining wind vector measurements via relative drift. A total of 94 aerial surveys (400 hours of flight time) were made. Of these, 29 were selected for case study analysis as described in the table at the end of Chapter 2.

AIRBORNE INSTRUMENTATION

Equipment on board the aircraft included a DECCA navigator for a positioning accuracy to 500m and a standard altitude indicator. The DECCA navigator provides a moving coordinate

reference for mapping purposes. A drift sight was installed which, together with a comparison of indicated and true air speed, permitted a trigonometric computation of wind vectors at 10km intervals along the flight track. Sea surface temperatures (SST) were derived using a Barnes PRT-5 sensor, converting passive infrared energy to a voltage output. The analogue output was continuously recorded on a strip chart with flight positions manually annotated. The entire PRT-5 radiometer system was calibrated at monthly intervals using standard calibrated thermometers in a hot and cold water bath. The strip chart recorder was verified before each flight using a calibrated digital voltmeter with input values determined by the monthly system calibration. The SST data quality was randomly checked during overflights of research vessels. Satisfactory comparisons were found except during calm conditions (with a glassy sea surface) when poor mixing and solar insolation caused positive anomalies.

Ambient air temperatures were monitored using a Rosemont total air temperature sensor mounted on the front of the aircraft. A simple microprocessor developed by the SFRI was used to convert resistance to voltage as input to a Fluke digital voltmeter (DVM). A manual readout of the DVM every 10km horizontally and 32m (100ft) vertically, enabled mapping and profiling of local thermal variations. Ambient temperature data quality was checked by comparison with DF Malan Weather Office temperatures at take off and landing.

A close correlation was found even though no compensation was made for the effect of flight speeds. To correct for frictional warming, indicated flight speeds were maintained at 120 knots, the sensor's calibration speed, particularly during vertical profiling.

DATA RESOLUTIONS

Wind vectors were collected at fixed positions every 10km along DECCA navigation lanes in order to create a uniform resolution of data. The uniformity assisted matrix and manual contouring interpolations. Certain data points were designated to collect site-specific information regarding terrain-induced wind and temperature anomalies.

As the objectives of relating wind shear and differential upwelling parameters were synthesised during the field studies, the data gathering methodology was suitably altered. The data resolution was adjusted by controlling the spacing of the alongshore flight legs. With the crosshore spacing fixed at 10km, the alongshore resolution was scaled to fit recognisable trends and observational needs. For example, in order to survey larger areas in a fixed, 6-hour-maximum flight time, coarse flight grids were devised at alongshore intervals of 50km. Over smaller areas, particularly where topographically deflected winds and small upwelling plumes were expected, alongshore spacings were reduced to 10km. The subjective adjustment of the data resolution could introduce

a degree of bias into the analysis. On the other hand, this adjustment together with a near real-time mapping of the parameter fields, was found to be a useful technique leading to a more clear understanding of the various scales of atmospheric and oceanic motion operating along the SW tip of Africa.

In order to overcome the degree of human biasing, wind velocity contours were analysed through the application of computerised graphics with smoothing subroutines. A further quality check on drift-sight derived wind vectors indicated that accuracies of ± 2 ms^{-1} and ± 7 degrees were achieved in comparison with Weather Office readings and PIBAL ascents. To check whether the observational inaccuracies were compounded by the data processing scheme, random perturbations were added to the matrix analyses. A comparison of digital and manual results showed only minor variations. The limitations imposed by the combination of manual and digital processing were considered to be numerically acceptable, given the magnitude of the wind shear relative to the observational errors.

SURFACE INSTRUMENTATION

Surface based meteorological data were available from the SFRI using Aanderaa automatic sensors to record hourly values of wind speed and direction at 5m above ground level (AGL) and pressure and temperature at 2m AGL. These data were

processed by reading the magnetic tapes onto a minicomputer. A program then listed the data for subsuquent manual analysis and display. In addition, hourly averaged meteorological information were available from an instrumented tower located 30km N of Cape Town. These data included wind speed and direction and temperature lapse rate from 10 to 76m AGL.

Vertical wind and temperature profile data up to 700mb were locally available from the DF Malan Weather Office of the South African Weather Bureau via twice daily radiosonde ascents. World Meteorological Organisation (WMO) standardised radiosondes, tracking equipment and data processing procedures enabled the computation of significant level temperatures and standard level wind vectors.

A marine based data gathering facility (instrumented buoy) was positioned 2km to the W of Oudekraal by the SFRI for selected study periods. The buoy incorporated the Aanderaa meteorological monitoring system together with a true N reference and SST sensor. Logistical complexities, especially mooring problems, limited the period of deployment of this research buoy. In a similar position off Oudekraal an array of four buoys (designed by the SFRI), covering a $100km^2$ area, were moored by Kamstra for a short study period. Wind speeds were recorded using radio receivers at manned shore based stations. In this manner, mesoscale wind circulations were resolved in time and space at the air-land-sea interface off Oudekraal.

C. DATA ANALYSIS METHODOLOGY

The data base supporting the observational link between coastal upwelling and topographic wind shear was formed through 152m aerial surveys conducted during mid-day between the hours of 1000 and 1500 South African Standard Time (SAST). Wind and air temperature data tables, referenced with position and time, were manually transferred onto topographic maps using a flight pattern data-collection-point overlay. Contours were then manually analysed and smoothed at intervals of $5ms^{-1}$ and $2^{o}C$. SST's were digitised at significant intervals from the strip chart and transferred, in a similar manner, onto a standardised base map for contouring every $2^{o}C$.

The alongshore data resolution had an impact on the interpolation and mapping of parameter fields, particularly SST. A 10-20km resolution gave more confidence to the detailed analysis of microscale circulations and topographic-induced perturbations. Coarse 50km resolutions inhibited confidence in the precise description of complex SST patterns. The greater alongshore spacings, however, enabled 40 $000km^2$ areas to be synoptically monitored and proved useful in describing the alongshore extent of topographic and thermal influences.

Transect and vertical profile data were similarly analysed with position/height/time references, transferred onto

expanded height scale graphs and manually contoured and smoothed. A dense temperature data resolution was achieved during vertical profiling. Unfortunately, only sparse wind data resolutions were available during spiral ascents due to the manual observation methodology and computational limitations.

DIGITAL PROCESSING

In the analysis of 152m level wind data the centered differencing technique, employed in the macroscale investigations, was found to be a suitable computational scheme for solving the wind stress curl equation 6. Employing aerial survey techniques, an observational data base was formed to resolve the 152m wind field into a 10km matrix array using a positive N and E coordinate system. Virtual wind stress components were then computed using the formulae:

$$\tau_x = \rho C_D U (U \cos (\theta - 270)) \qquad \text{[Eq.7]}$$

$$\tau_y = \rho C_D U (U \cos (\theta - 180)) \qquad \text{[Eq.8]}$$

where

U = wind speed ms^{-1}

θ = wind direction ^{o}true

ρC_D = air density and drag coefficient

= constant of $1.58 (10^{-6}) gcm^{-3}$ *

---

* The choice of this constant (used by Bakun off California) is justified by the similiarity of meteorological conditions and for the sake of comparison with other data sets. Although the constant could not be calculated from available data, its application is valid over the range of wind speeds and air densities found locally [9,62].

The numbers 270 and 180 in equations 7 and 8 refer to orthogonal directions, however along the coast from Cape Hangklip to Cape Columbine the local coastline orientation is rotated by approximately 20°:

$\tau_N : (\theta - 250)$ $\tau_T : (\theta - 160)$

For the application of centered differencing techniques wind stress components from equations 7 and 8 were matrix resolved. Curl values could then be computed for each 20km square using the equations and format:

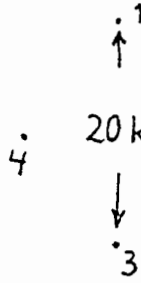

$$\frac{\partial \tau_y}{\partial x} - \frac{\partial \tau_x}{\partial y} = \tau_{curl}\ (10^{-7})\ \text{dynes cm}^{-3} \quad \text{[Eq.9]}$$

$$\frac{\tau_{y2} - \tau_{y4}}{\Delta x} - \frac{\tau_{x1} - \tau_{x3}}{\Delta y}$$

The convention for the southern hemisphere was adopted for the computation of wind stress curl: anticyclonic wind stress curl = + (downwelling - producing) and cyclonic = - (upwelling - producing). These solutions were then utilized in the field application which is chronologically summarized as follows.

Horizontal flight wind maps were matrix-resolved by assigning discrete vectors on a 10km square grid overlay. This procedure was undertaken by an independent and unbiased interpolator using a matrix overlay on the original data plot. The wind vector matrices (included in the Appendix)

were then used as input to a computer program developed in previous research by the author (50). The program calculates over the input data matrix the alongshore V_T and crosshore V_N wind components, the shear, vorticity, and divergence of the wind and the wind stress adjusted to a surface estimate. A contouring and smoothing computer graphics program SACLANT was then used to generate parameter maps to a one in one million scale with a topographic overlay completing the aerial survey data analysis scheme.

SURFACE DATA

Surface, vertical profile and background meteorological data were used to discriminate the horizontal case study results and to relate the various scales of atmospheric and oceanic response. Of importance were the Aanderaa meteorological data records which were digitally processed by the SFRI for time series graphic displays. From SA Weather Bureau publications (80,81) synoptic weather charts were extracted. These charts are based on a rather sparce marine data network supplemented by remotely sensed information. The DF Malan Airport radiosonde profile data played a critical role in the determination of vertical wind shear and thus, in the selection of case studies from the available data. Radiosonde wind and temperature information were analysed against height and time, portraying the cyclic development of thermal inversion layers. Vertical wind shear structures were described by separating the U and V wind components and

vertically differentiating at 200m intervals.

D. A GUIDE TO DATA INTERPRETATIONS

Certain spatially recognisable patterns were found in a cursory review of the wind and thermal parameter contour maps. Using the following guidelines applied to each parameter field, case studies were subjectively discriminated from the aerial survey data base (shown in the following table). Particular attention was given to the contrasting of horizontal wind shear patterns under differing flow depths and to sequential case study analyses.

WIND FIELDS

The 152m wind vector maps compiled from aircraft drift measurements, were inspected for topographic conformity or deflection. Homogeneous flow was more in evidence with increasing depth, while during shallow wind cases topographic obstruction created alongshore and crosshore contrasts. The V_N crosshore wind component was utilized extensively to discriminate flow deflections which occur seawards of the coastal mountains. During seabreeze conditions, inspection of the V_N component highlighted streamline curvatures and entrainment off the landward side of the coastal wind jet.

WIND VORTICITY

Vorticity within the local wind field was used as a measure of topographic shearing and curvature along the SW tip of

Africa. From the matrix computation results standing vorticities were noted leewards of Cape Hangklip, Cape Columbine and the Cape Peninsula. According to theories developed in Chapter 1, upwelling should become focused at the expense of surrounding areas under the influence of cyclonic vorticity. Vorticity was then used as an indicator of differentially forced upwelling.

The vorticity calculation employed a 20km centered difference enabling an accurate description of wind field perturbations in the 10 to 100km range. Using a subjective pattern recognition, areas of cyclonic (-) vorticity were found to be limited in spatial extent and well correlated topographically.

WIND STRESS

The estimation of surface wind stress utilized a wind profile coefficient (.7) empirically derived from a local PIBAL study (50). to scale down flight level winds. The wind stress field was then incorporated in the subjective review to highlight horizontal contrasts in oceanic Ekman transport. Wind stress fields were unrealis- tically smoothed by the homogeneous application of a constantair density, drag coefficient and vertical wind profile across the data input matrix. The wind stress was computed in proportion to the square of the flight wind speed. This simplified approach neglects the possibility that turbulence in the lee of the coastal mountains could

enhance surface wind stress.

WIND STRESS CURL

From the alongshore and crosshore components of the wind stress, the curl or vorticity was calculated using the 20km centered difference. Stress curl fields were manually contoured and used as an indicator of areas where rotational momentum is transferred. In chapter 1 this parameter was equated with oceanic divergence and localised upwelling. A pattern similar to vorticity emerged from the stress curl field with a limited horizontal extent and excellent topographic correlation.

SEA SURFACE TEMPERATURES

Interpretation of the SST contour maps was relatively simple utilizing significant isotherms. Active upwelling plumes were defined by the 12^{o}C isotherm which often extended seawards in a tongue from the coastal headlands. Surface circulations were estimated through a persistence of anomalous SST structures. Nearshore countercurrents were delimited by SST's of greater than 16^{o}C along the west coast, usually resulting from a sudden relaxation of upwelling. Instability in the oceanic thermal front (OTF) often initiated a shorewards entrainment of warmer water in the more sheltered bays.

AIR TEMPERATURES

The air temperature patterns were reviewed for crosshore

contrasts and deviations from coastal alignment. Upwind from the 3 capes convergent motions and atmospheric cooling was often seen while leewards, a horizontally divergent wind flow was compensated by warming. The resultant pattern was that of a tilted "S" in the thermal front centered over each of the capes. The growth of a thermal low over the Berg River Valley was evident during shallow wind cases.

TRANSECT DATA

Vertical transect data were interpreted with reference to upwind topography and inversion layers. Through a vertical differentiation of V_T, wind shear transitions described the lateral and vertical extent of the longshore jet core. In combination with the horizontal wind data, the transects complete a three dimensional view.

SUMMARY

The relationship between vertical and horizontal wind shear was found to have an impact on differential upwelling patterns. The relationship determines whether the meteorological forcing functions at the air-sea interface act homogeneously or in sheared contrast. The hypothesis may be quantified simply: with vertical shears of $-2\ (10^{-2})\ s^{-1}$, horizontal vorticities in equatorward winds exceed a cyclonic $-6\ (10^{-4})\ s^{-1}$ due to topographic friction. The vorticity in the wind stress activates intense upwelling seawards of the coastal mountains, leading to alongshore SST differences of

greater than $1^{o}C\ (10km)^{-1}$. Chapter 2 has outlined the field application of theories developed in the first chapter. Aerial survey has been shown to be a most useful tool in developing a synopsis of wind and sea temperature fields. The mesoscale data gathering techniques were reviewed in detail. Flight grid resolutions were varied in this study according to the scales of motion and proved to be an important factor in describing the sequential development of standing wind vorticies, cold upwelling plumes, and warm nearshore countercurrents. Data processing techniques were outlined and weaknesses in the manual compilation and interpolation scheme were highlighted. A guide to the interpretation of mesoscale data fields was given together with the physical significance of the parameter fields and anomalies.

In the following chapter the mesoscale interaction of wind shear and differential upwelling along the SW tip of Africa is described in 6 case study situations.

LOCATION AND TYPE OF SURVEY	EQUATORWARD WINDS DEEP	EQUATORWARD WINDS SHALLOW	POLEWARD WINDS
CAPE PENINSULA SEQUENCE AND CROSS SECTIONS (medium grid) CASE STUDY A	15 Nov. 79 16 Nov. 79 17 Nov. 79* 18 Nov. 79* 21 Nov. 79 22 Nov. 79* 23 Nov. 79*	19 Nov. 79* 24 Nov. 79* 25 Nov. 79*	12 Nov. 79 26 Nov. 79*
CAPE PENINSULA SEQUENCE (fine grid)	6 Dec. 79 7 Dec. 79 10 Dec. 79 11 Dec. 79	5 Dec. 79 12 Dec. 79	
CAPE PENINSULA SEQUENCE (medium grid)	9 Jan. 80 10 Jan. 80 12 Jan. 80	7 Jan. 80 8 Jan. 80 11 Jan. 80	
SW CAPE COAST (coarse grid) CASE STUDY C	22 Jan. 80* 23 Jan. 80 24 Jan. 80	25 Jan. 80* 26 Jan. 80	
CAPE PENINSULA (fine grid)	7 Feb. 80 8 Feb. 80	6 Feb. 80	9 Feb. 80
CAPE COLUMBINE SEQUENCE AND CROSS SECTIONS (medium grid)	12 Feb. 80 13 Feb. 80 14 Feb. 80 16 Feb. 80		15 Feb. 80
WALKER BAY (medium grid)	18 Feb. 80	17 Feb. 80	
CAPE PENINSULA SEQUENCE (fine grid) CASE STUDIES E & F	20 Feb. 80*	19 Feb. 80* 21 Feb. 80* 23 Feb. 80* 25 Feb. 80*	22 Feb. 80 24 Feb. 80 26 Feb. 80
NAMAQUALAND AND CAPE COLUMBINE (coarse grid) CASE STUDY D	20 Oct. 80 24 Oct. 80 30 Oct. 80 7 Nov. 80	27 Oct. 80 29 Oct. 80 1 Nov. 80* 10 Nov. 80	21 Oct. 80
CAPE PENINSULA AND WALKER BAY (coarse grid)			18 Nov. 80 19 Nov. 80
NAMAQUALAND & CAPE COLUMBINE (medium grid) CASE STUDY D	23 Nov. 80* 24 Nov. 80	22 Nov. 80	29 Nov. 80
COMPOSITE SW CAPE SEQUENCE (medium grid) CASE STUDY D	2 Dec. 80* 3 Dec. 80* 4 Dec. 80* 5 Dec. 80*		
NAMAQUALAND & CAPE COLUMBINE (medium grid)	6 Dec. 80 8 Dec. 80 10 Dec. 80		
FALSE BAY SEQUENCE (fine grid) CASE STUDIES B & E	19 Jan. 81* 20 Jan. 81* 21 Jan. 81 22 Jan. 81 23 Jan. 81 24 Jan. 81 25 Jan. 81 28 Jan. 81 30 Jan. 81 31 Jan. 81 4 Feb. 81* 5 Feb. 81*	29 Jan. 81* 1 Feb. 81* 2 Feb. 81* 3 Feb. 81*	26 Jan. 81

Out of a total of 94 aerial surveys 29 were selected (*) via pattern recognition for case study analysis.

CHAPTER 3 : CASE STUDY RESULTS

INTRODUCTION

An effective means of spatially correlating wind shear and differential coastal upwelling is by the comparison of selected case study results. In chapter three, 6 case studies are presented which describe this relationship along the SW tip of Africa. A variety of data resolutions and geographic settings were chosen to illustrate the interplay of synoptic, mesoscale and microscale meteorological forces.

The combination of a negative vertical wind shear layer and topography was thought to enhance horizontal wind vorticity and differential coastal upwelling. These phenomena are described a 11 day wind/upwelling cycle lasting 11 days in the first case study (A). The growth and decay of a cold plume to the W of the Cape Peninsula was monitored in a sequential analysis of mesoscale aerial survey data. With the addition of a third dimension by means of transect data, a negative wind shear layer below the elevation of the coastal mountain ridges imposed a differential wind stress on the leewards sea surface.

The second case study (B) focuses on False Bay during another 11 day equatorward wind event. A fine resolution flight grid enabled the description of upwelling plumes and adjacent warm currents in the bay. Wind flow channelling by the upwind

topography produced a shear boundary with wind acceleration and wake areas in spatial correlation to SST's across the predominantly warm water, semi-enclosed bay.

A comparison of two equatorward wind flow trajectories with differing vertical wind and thermal characteristics is made in the third case study (C). Thermal fronts deviated from coastal alignment in the shallow wind field due to the enhancement of surface friction in the vicinity of the three capes along the SW tip of Africa.

A second comparison of deep and shallow wind flow fields is made over the smoother headland of Cape Columbine in the fourth case study (D). The shallow case was characterised by a leewards wake extending across St. Helena Bay. During the case study period, persistent cut-off low pressure cells created a calm wind wake and the formation of a warm nearshore countercurrent.

During periods of weak surface pressure gradients, the coastal atmosphere along the SW tip of Africa responds to land-sea temperature contrasts. The resultant seabreezes and convergence zones are described and compared in the fifth case study (E). A cyclonic streamline confluence was noted during the light wind conditions and the rate of upwelling was found to be considerably diminished.

Utilizing surface and marine based data sources, a time series analysis in the sixth case study (F) indicates a nocturnal pulsing of winds and upwelling at Oudekraal. The site-specific noturnal wind acceleration was further studied using a buoy array which delimited the extent of the turbulent downslope jet. The diurnal rise and fall of an inversion layer was linked to a similar cycle in SST's measured at Oudekraal.

The following table summarises the case study locations, time scales, spatial resolutions, central themes and supporting observations.

CASE STUDY SUMMARY

	LOCATION	TIME SCALE	SPATIAL RESOLUTION	CENTRAL THEME AND SUPPORTING OBSERVATIONS
A	Upwelling plume to the W of the Cape Peninsula	11 day sequence	20-40km horizontal 100m vertical	A sequential description of a wind/upwelling event cycle. Equatorward winds intensified then abated while an upwelling plume expanded and contracted in sympathy. Vertical shear was enhanced by topography.
B	False Bay and vicinity	11 day sequence	10-20km	A sequential view of wind and upwelling patterns in the semi-enclosed bay. An upwind mountain ridge imposed a sheared wind field across False Bay leading to differential upwelling.
C	SW tip of Africa: Danger Point to Cape Columbine	2 days out of a 4 day cycle	50-100km	A large scale comparison of deep and shallow equatorward wind flow fields. Topographic deflections caused perturbations in atmospheric and oceanic thermal fronts along the SW tip of Africa.
D	Cape Columbine St. Helena Bay and Namaqualand	2 days out of a month background	20-40km	A comparison of deep and shallow southerly winds and differential upwelling patterns. Cold plumes off Cape Columbine were seen in contrast with warm currents in St. Helena Bay.
E	Cape Peninsula and adjacent coastline	5 hours in a 24 hour cycle	10-20km	A study of seabreeze circulations which curve clockwise around the Cape Peninsula. Warm water entrainment and upwelling relaxation coincided with the seabreezes.
F	Oudekraal area to the W of Table Mountain	12 hour cycles in a day	1-10 km	A boundary layer study of the nocturnal downslope jet off Oudekraal. Winds and upwelling activity peaked at mid-night due to a thermal interface near Table Mountain.

A. A CYCLE OF THE CAPE PENINSULA UPWELLING PLUME

GENERAL SETTING

The Cape Peninsula at 34°S lies to the NW of a significant mountain ridge and, extending seawards some 40km, lies directly in the path of coast-parallel winds. A shallow equatorward wind "jet", driven by the South Atlantic Anticyclone (SAA), is often channelled and deflected by the Cape Peninsula. Interactions between the SAA and transient mid-latitude wave cyclones modulate the coastal gradient winds (50,62). One such wind cycle is illustrated by mesoscale aerial survey data in this case study. A map of the area showing the geographic complexities which surround the Cape Peninsula is presented in Fig.2. The case study flight plan, 152m level data collection points, place names and 300m topography are included on the map.

CASE STUDY DATA

During the period 15-26 November 1979 a wind cycle caused the growth and decay cycle of an upwelling plume off the Cape Peninsula. Aerial survey-derived wind and thermal data were available for the entire period and provide a "moving-picture" of transient wind shear and differential upwelling patterns. The equatorward wind cycle is defined in the time series data given as background continuity to the aerial view.

Hourly averaged wind vectors at two points along the coast were compared with the atmospheric thermal structure from a nearby radiosonde profile. A differing response to coastal winds can be seen in the Oudekraal (ODK) and Olifantsbos (OFB) stick vectors in Fig.3. These sites are 30km apart along the Peninsula's western shore and experience different mean winds through the cycle. Gusty and variable winds at ODK can be attributed to turbulence in the lee of a mountain. At OFB, peninsula buffering effects may be inferred in the more consistent directions. Winds from the SE sector began on 15 November, abated somewhat during the 19th and reversed abruptly on the 25th.

The vertical thermal structure given in the lower portion of Fig.3 reveals the presence of a temperature discontinuity in the 850-950mb layer. When this layer descended on the 19th and 25th, surface winds became deflected offshore. Coastal winds appeared to diminish in sympathy with the height of the inverted temperature layer. The air in this layer is sinking and places an effective "lid" on equatorward winds.

GROWTH PHASE OF CYCLE

The period 16-18 November 1979 was characterised by increasing SE winds and the growth of a distinct upwelling plume off the Cape Peninsula. A mesoscale description was made from 152m wind vectors and SST's collected over the aerial grid shown in Fig.2. At selected data points the wind

vectors are represented for the 3 day period in Fig.4. While SE winds remained steady across the southern area, leewards of the Cape Peninsula a gradual offshore veering and increase in speed was found from the 16th to the 18th. The sheltered "wake" of Table Mountain (enclosed by the dashed area), shrank under deepening SE gradient winds.

Mesoscale flow perturbations were highlighted by the analysis of the vorticity and normal wind components for 18 November. Embedded within the $20ms^{-1}$ flow, an area of intense cyclonic vorticity prevailed directly over the Cape Peninsula as seen in Fig.5a. A divergent wind flow trajectory was interpreted in the normal component analysis (Fig.5b). An inland component of $+4ms^{-1}$ was contrasted with predominantly offshore flow ($-8ms^{-1}$, shaded) to the W of the Peninsula. The combined effects of cyclonic vorticity and offshore accelerations caused a localising of Ekman divergence in the oceanic surface layer. This led towards the sudden growth of the Cape Peninsula upwelling plume.

The growth phase of a distinct upwelling plume is shown in the SST pattern in Fig.6a, b, and c. The plume core (less than $12^{o}C$, represented in blue) spread over a $400km^{2}$ area during the 3 day period. Meanwhile only slight changes in the Oceanic Thermal Front (OTF, red shaded band) occurred. In the sheltered "wake" of Table Mountain, a small passive area remained throughout the growth phase (yellow shaded patch) as

shown in Fig. 6c. The differential nature of wind-activated upwelling plume formation featured prominently during this period.

DECAY PHASE OF CYCLE

From 24-26 November 1979 a slackening of surface pressure gradients and upwelling-favourable wind stress was observed. From the mesoscale aerial survey data, 152m wind vectors are represented during the decay phase of the cycle in Fig.7 Equatorward wind flow on the 24th was replaced by light and variable seabreezes. With a cold front approaching, NW winds strengthened by the 26th in a complete flow reversal. The vorticity field, which had remained cyclonic over the Peninsula during the equatorward winds, gradually changed to anticyclonic (+) by the 26th as sequentially illustrated by Fig. 8a, b, and c. This led to Ekman convergence and downwelling activity along the western shore of the Cape Peninsula.

A quick oceanic response to wind stress reversal is documented for the decay phase by the SST distributions shown in Fig. 9a, b, and c. On the 24th active upwelling was found W of the Peninsula and to the N of Cape Town. The relaxation of upwelling began with a large pool of warmer water entraining shorewards and spreading to the S on the 25th (red shaded area, greater than 16^{o}C). The deteriorating upwelling plume was compressed against the SW tip of the Peninsula with

the cold core detached from the coast by the 26th.

The case study description moves from sequential wind and upwelling patterns to a matrix-averaging analysis in order to emphasise the persistent differential nature of upwelling throughout the lifecycle.

DIFFERENTIAL UPWELLING

Matrix resolved SST's during the active upwelling period of 15-25 November were used in an analysis of crosshore and alongshore SST contrasts independent of time. A mean SST field was averaged over the cycle and differential features were then brought out by centered differencing of the SST's in both x and y directions. These results are contoured and displayed in Fig. 10a and b.

In the offshore direction (dx) SST's increased at greater than 2^{o}C per 10km to the N of Cape Town and W of Olifantsbos. This represents the outer edges of the upwelling centres and the OTF respectively. The negative areas may be contrasted in Fig.10a with a decrease in SST's offshore in the sheltered wake of Table Mountain.

Due to the topographic shearing of winds, the alongshore change in SST's was equal in magnitude to the offshore increase. Along the northern half of the Peninsula positive alongshore values describe the equatorward edge of a cold

plume. On either side of the wind activated plume axis (defined by the zero line bisecting the Peninsula), SST's declined. South of the Peninsula, warm oceanic water skirted the coast strengthening the differential features.

The alongshore and crosshore SST gradients result from differential coastal upwelling whose origins lie in the manner in which shallow equatorward winds are topographically sheared. The controlling mechanism for wind shear production is the depth of flow. This variable is given attention in the following section.

VERTICAL SHEAR ENCHANCEMENT LEEWARDS OF TWO CAPES

Factors which control the topographic shearing of horizontal flow are described by the analysis of aerial survey vertical transect wind data. A third dimension is added leewards of the mountain ridges of the Cape Peninsula and Cape Hangklip in two transect sequences from 17-19 and 22-24 November 1979. The transect sequences were flown concurrently with the preceding horizontal grids and support a link between vertical atmospheric stratification, topographic shearing and differential upwelling.

Background data, providing time series continuity to the transect sequences, were available from an instrumented tower along the coast to the N of Cape Town and from the DF Malan airport radiosonde. A comparison of the two data sets is

presented in Fig.11. A negative wind shear layer of $-2(10^{-2})s^{-1}$ was present in the 900-950mb layer on 17-19 and 22-24 November. The tower data show that equatorward winds prevailed, but that thermal contrasts caused a diurnal modulation in flow originating from the Cape Flats. Atmospheric conditions, as parameterised in the vertical temperature difference, tended towards instability except on days when land-seabreezes occurred on 19 and 25 November. Distinct atmospheric thermal inversion and wind shear conditions coincided with the passage of coastal lows on those two days. It can be inferred that the two transect sequences took place during negative wind shear periods with increasing low-level stratification.

In order to quantify the effect of topographic barriers on the longshore wind jet, transect lines were chosen immediately downwind from the mountainous coastal promentaries of the SW tip of Africa as shown in Fig.12a. Observation levels were selected at 150, 490 and 1160m based on local wind profile climatology. The topographic features upwind from the 2 transect lines are similar in their complexity and vertical extent as schematically viewed in Fig. 12b and c. Upwind from transect 1 features consist of the N-S oriented Cape Flats valley and a pronounced orographic barrier in the Cape Peninsula, split by a narrow gap separating Constantiaberg from Table Mountain. Upwind from transect 2, the Hottentots Holland mountain ridge

extends to Cape Hangklip with a gap at Sir Lowry's Pass and a major coastal peak in Kogëlberg.

TRANSECT 1

Vertical transect data, collected from 0 to 90km offshore at levels of 150, 490 and 1160m along line 1 from 17-19 November 1979, show an accelerated core of longshore winds over the Cape Peninsula gradually shifting offshore and diminishing in vertical extent (Fig.13a, b and c). During the sequence a thermal "lid" decended (refer to Fig.3) causing accelerations to be replaced by horizontal deflections. The two $15ms^{-1}$ jet cores on the 18th were diverted offshore by the 19th forming a substantial wind wake in the "shadow" of Table Mountain. In compensation, a reversed flow inversion layer descended from aloft as shown by the area of less than $-5\ ms^{-1}$ in Fig.14c.

The vertical shear of the longshore wind component was calculated by matrix differencing with height and is displayed for transect 1 in Fig.14a, b, and c*. Positive shear below 500m was replaced by a negative shear layer above the alongshore core on the 18th and 19th. The negative shear layer grew in strength between 200 and 500m (shaded) seawards

---

* The subjective analysis of V_T wind components may have created certain inaccuracies in the computation of vertical shear. Consequently, the shear patterns are qualitatively highlighted in this description.

of the Cape Peninsula mountains. The enhancement of vertical shear is attributed to the channelling of the shallow longshore wind "jet" and to atmospheric subsidence and thermal stratification in the lee of the coastal mountains.

TRANSECT 2

The second transect sequence obtained from data collected from 10-80km offshore at the standard heights and shown in Fig.15a, b, and c for 22-24 November, was characterised by a longshore wind core rounding Cape Hangklip and a secondary maxima over Sir Lowry's Pass. In similarity with the transect 1 sequence, the jet became flattened by a descending thermal inversion layer. Increasing synoptic pressure gradients and topographic deflections caused the jet to gather in strength on the 23rd while an anticyclone ridged to the S of the area. By the 24th the wind jet had split into two cores under the thermal "lid".

A gradual descent of a negative shear layer was documented in the vertical shear analysis for transect 2 in Fig. 16a, b, and c. The shear layer dropped from 700m on the 22nd to 400m on the 24th. A shorewards tilt and increase in the shear layer was observed on the 23rd. By the 24th negative shear maxima were found over the Sir Lowry's Pass and Cape Hangklip wind cores due to downslope funnelling along the subsidence inversion.

THREE DIMENSIONAL COMPARISONS

From a comparison of horizontal and vertical wind shear patterns in the survey and transect case studies, there appears to be a significant interrelation. Vertical shears of $-2\ (10^{-2})\ s^{-1}$ below the 500m level were translated into horizontal wind vorticity via topographic friction. Along the sides of the leeward wakes the additional wind stress curl served to intensify local upwelling. The presence of negative vertical wind shear was therefore a key factor in the production of a differential upwelling circulation along the SW tip of Africa. The "wake capture" areas extending downwind from the coastal mountains led to diminished upwelling activity, a prerequisite to the formation of warm nearshore countercurrents.

Through topographic wind shear, the shorewards edge of the Benguela current becomes perturbed, spinning off unstable eddies and gyres which advect along the OTF. The alongshore and temporal changes in wind stress produce a mixing of upwelled and oceanic water. The entrainment of the two water masses assists the biological productivity essential to the renewability of fisheries stocks along the SW tip of Africa.

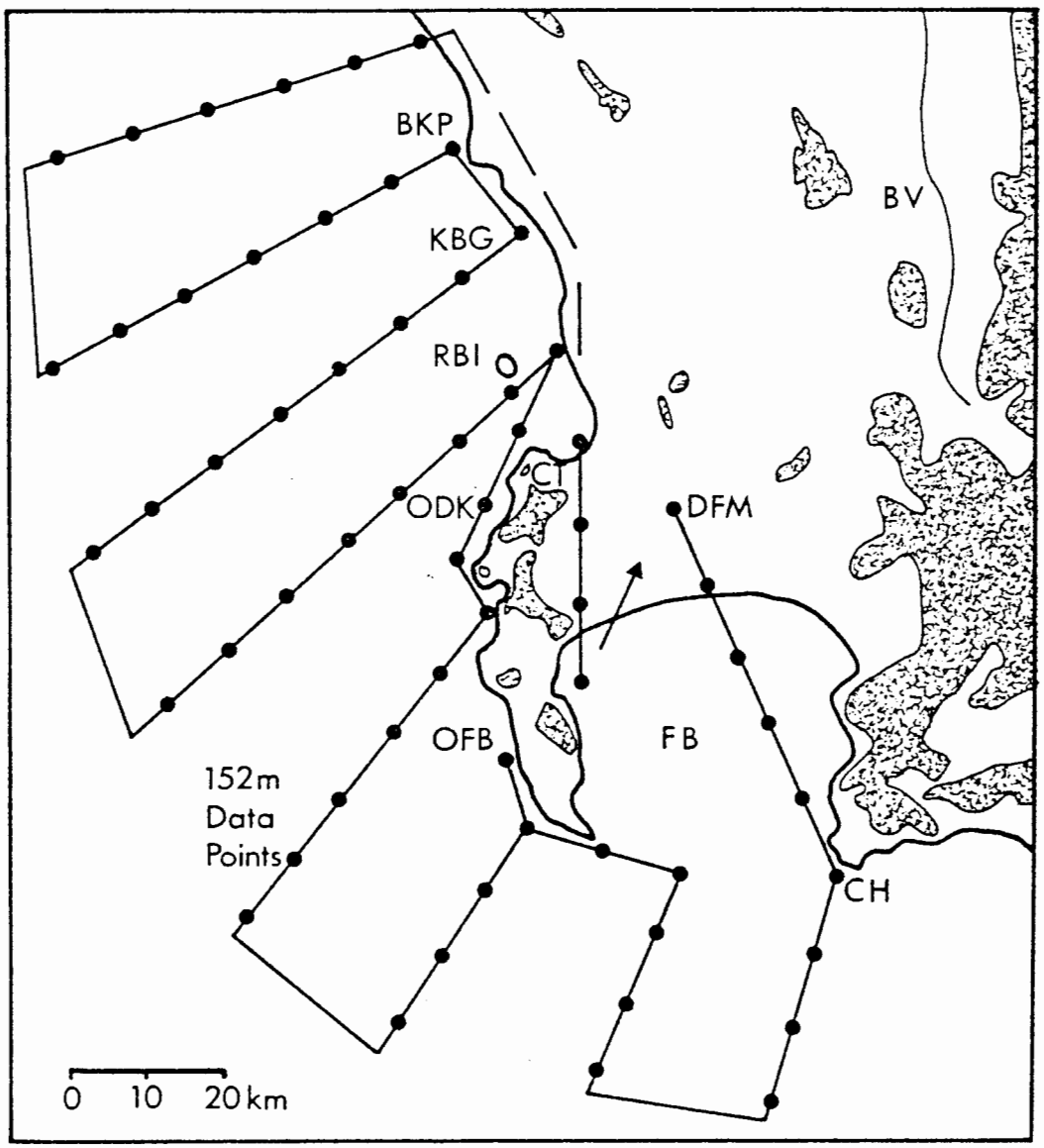

Fig.2 : A mesoscale topographic map of the Cape Peninsula area with elevations greater than 300m shaded. The 152m aerial survey grid is superimposed. Data collection points are shown by dots. Abbreviations are as follows: BKP Bokpoint, KBG Koeberg, RBI Robben Island, ODK Oudekraal, OFB Olifantsbos, BV Berg River Valley, DFM DF Malan Airport, FB False Bay, and CH Cape Hangklip.

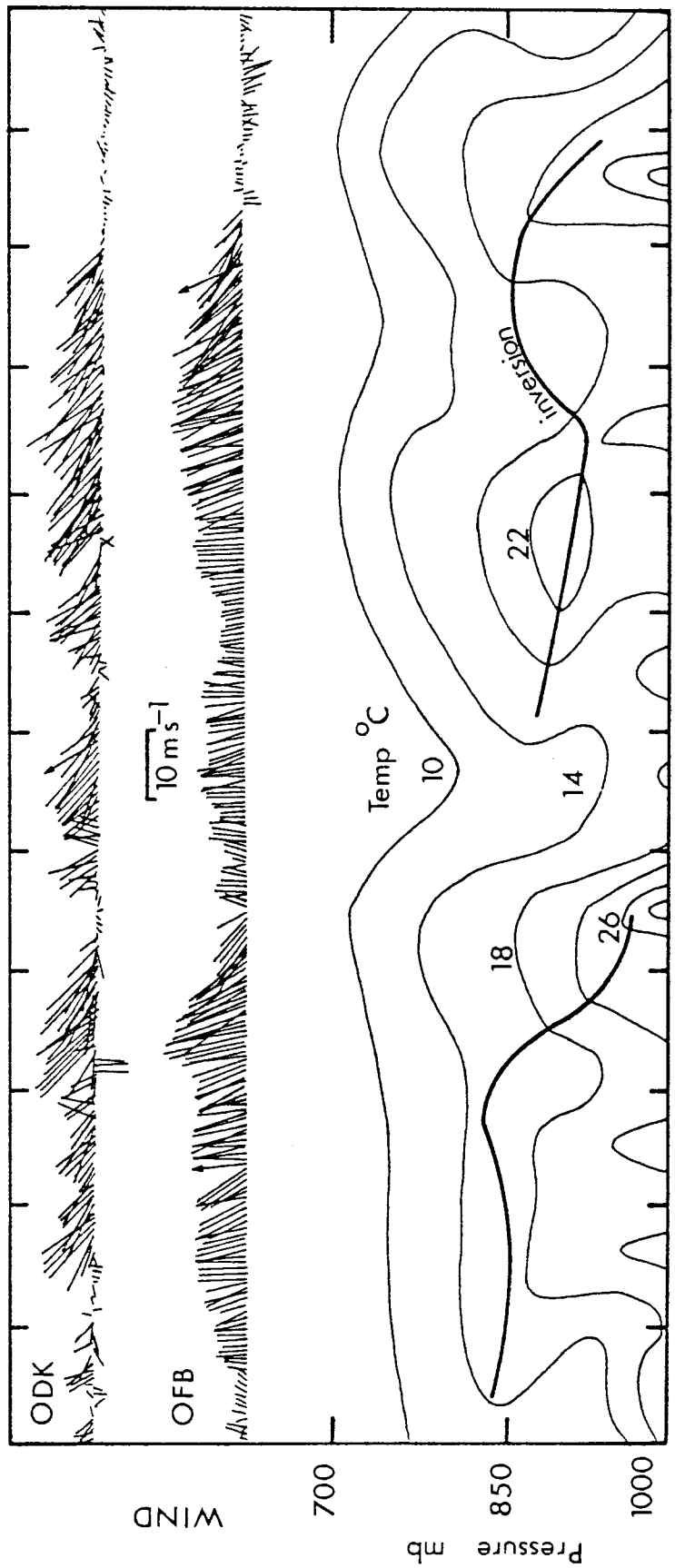

Fig. 3 : A comparison of hourly wind vectors and atmospheric thermal structures for the period 15 to 26 November 1979. Oudekraal shows a more variable flow than Olifantsbos due to the presence of an inversion layer and marked upwind topography. The thermal inversion (bold) is seen to descend twice during the case study period in response to the ridging of a transient anticyclone.

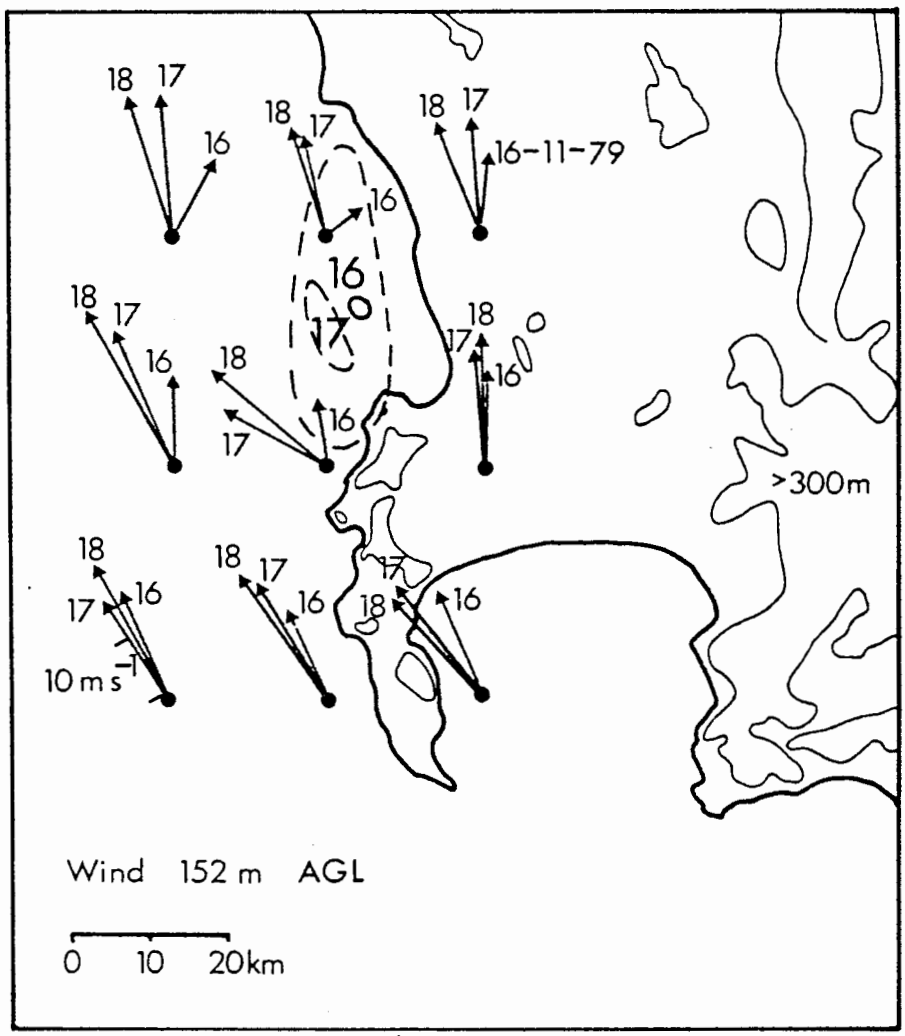

Fig. 4 : A 3 day representation of 152m wind vectors at selected locations around the Cape Peninsula, 16, 17 and 18 November 1979. A counter-clockwise rotation and increase in speed is observed. The wake of Table Mountain is shown for 16 and 17 November by the dashed area.

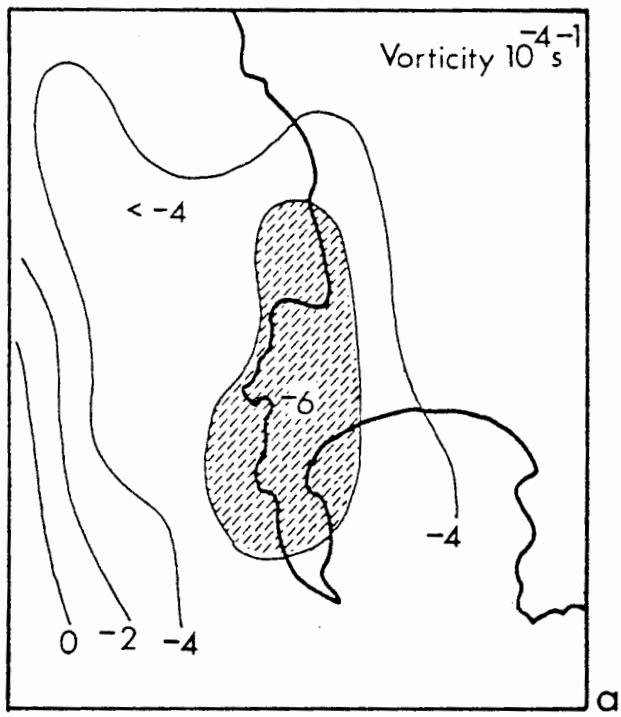

18-11-79

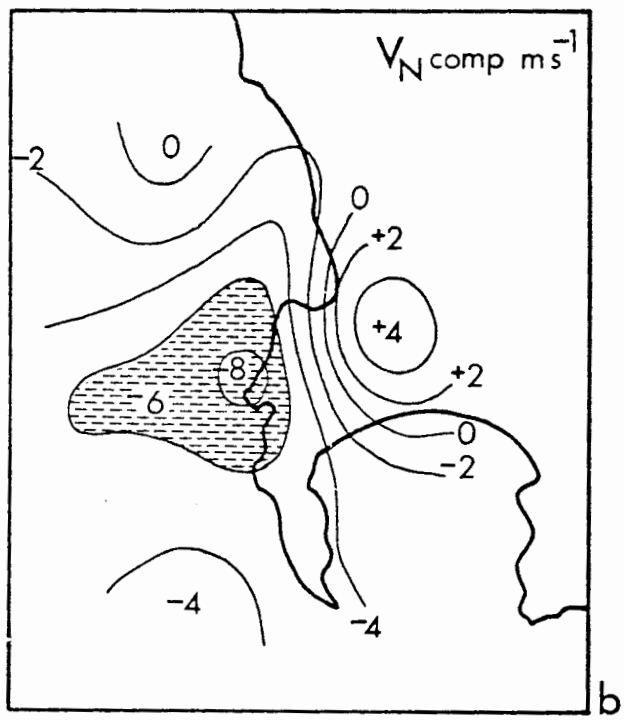

Fig. 5a: The wind vorticity field on 18 November 1979. The shaded area distinguishes a cyclonic rotation and frictional shearing of winds by the local topography.

Fig. 5b: The normal wind component field on 18 November 1979. The shaded area indicates where offshore deflections occur. A diffluence of flow is infered with onshore components further inland.

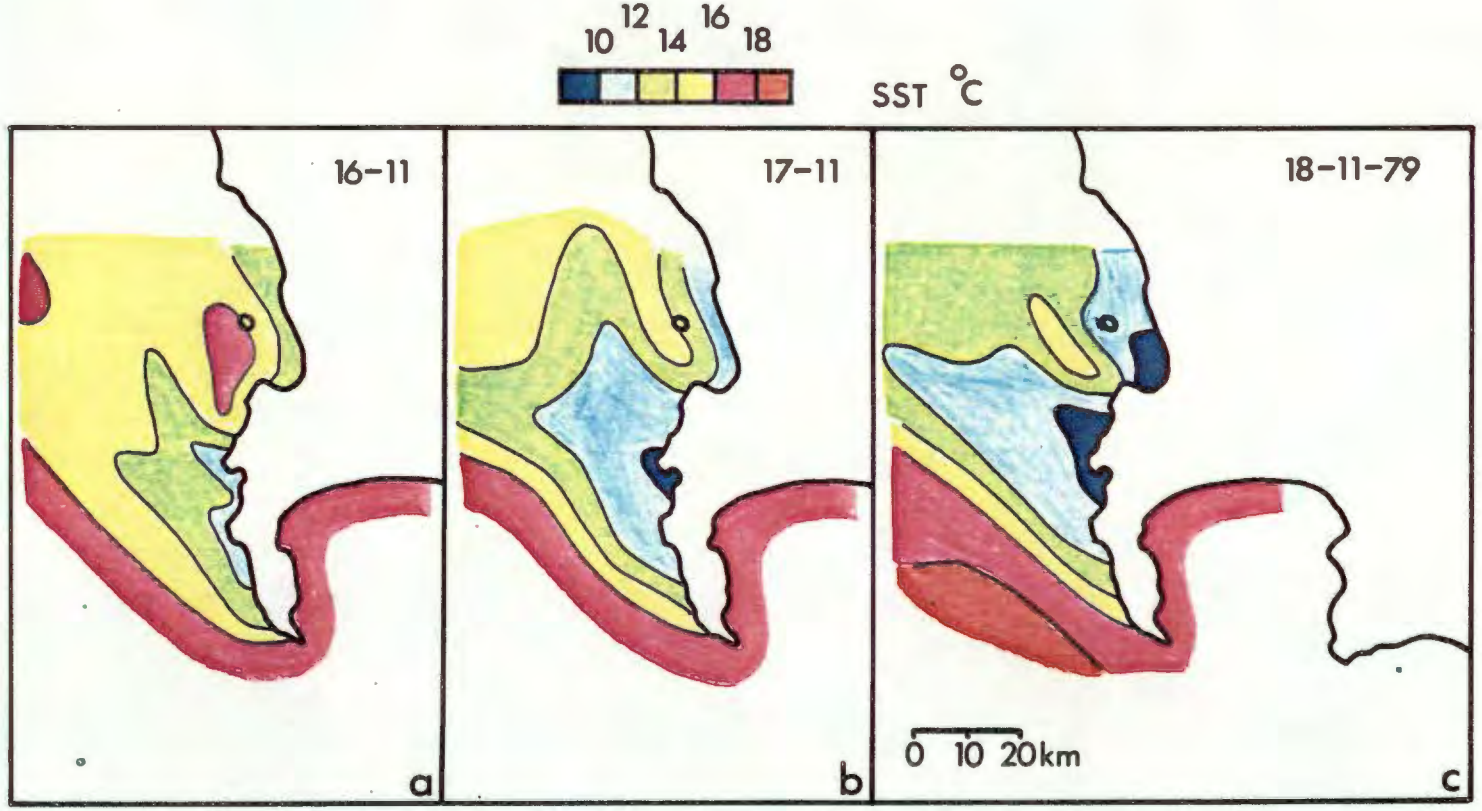

Fig. 6a, b, c: The SST distribution in a 3 day sequence representing the growth phase of the upwelling cycle. A sudden growth of the plume (green and blue shaded areas) is evident to the W of the Peninsula. Warm SST's persist in the lee of Table Mountain where a relatively calm, mesoscale eddy has developed.

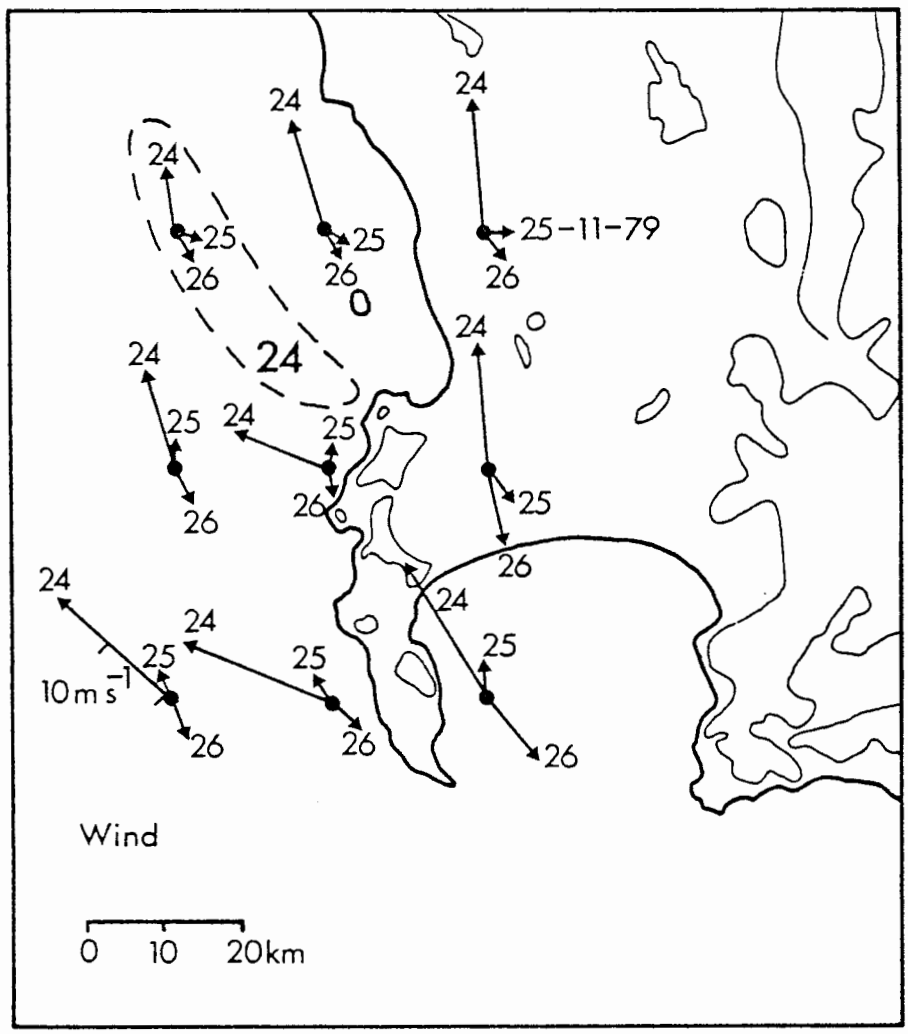

Fig. 7 : A 3 day representation of 152m wind vectors at selected locations around the Cape Peninsula, 24, 25 and 26 November 1979. A clockwise reversal of wind flow is noted. The 24 November wake area in the shadow of Table Mountain is dashed.

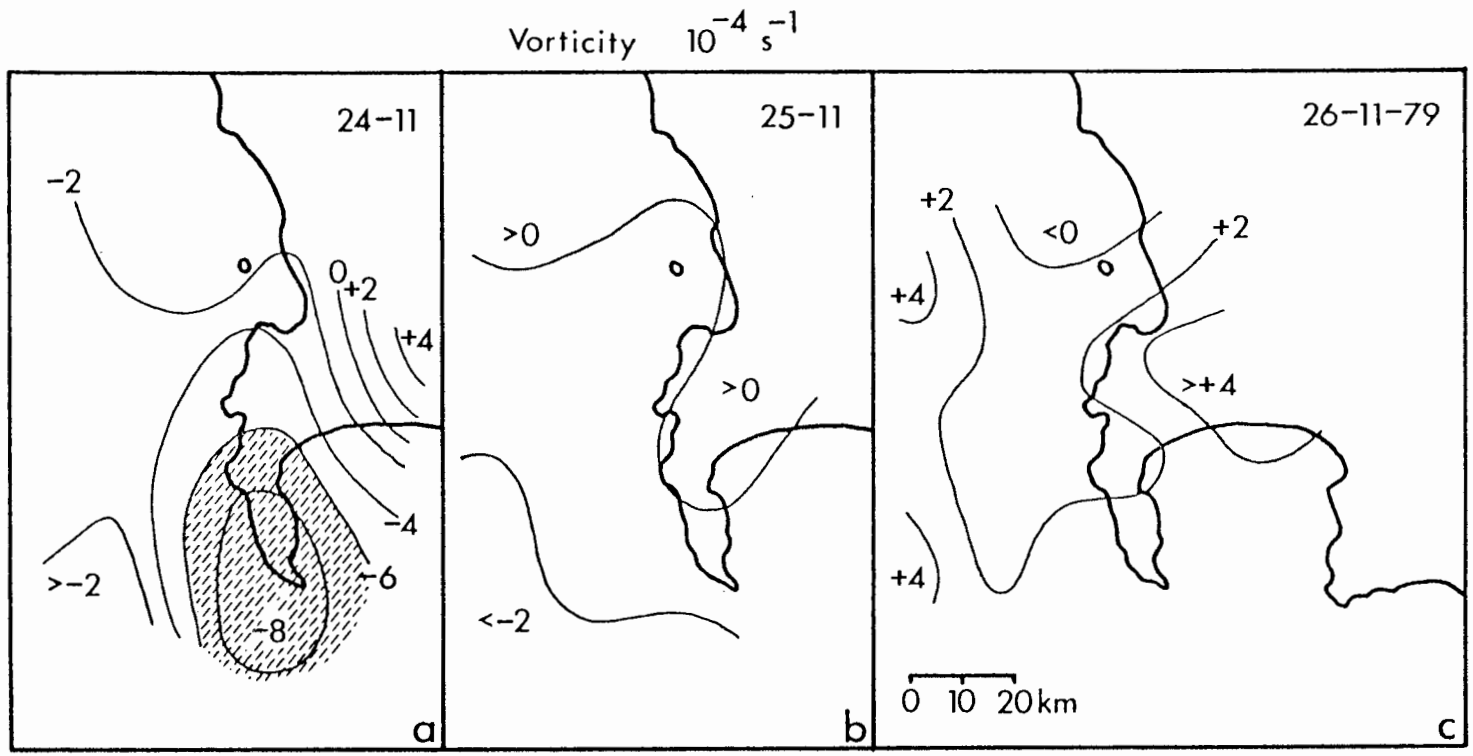

Fig. 8a,b,c: The wind vorticity field in a 3 day sequence, 24 to 26 November 1979. The wind reversal produces a change in sign of the vorticity. Cyclonic rotation and frictional shearing on the 24th (shaded) is gradually replaced by anticyclonic values during the period.

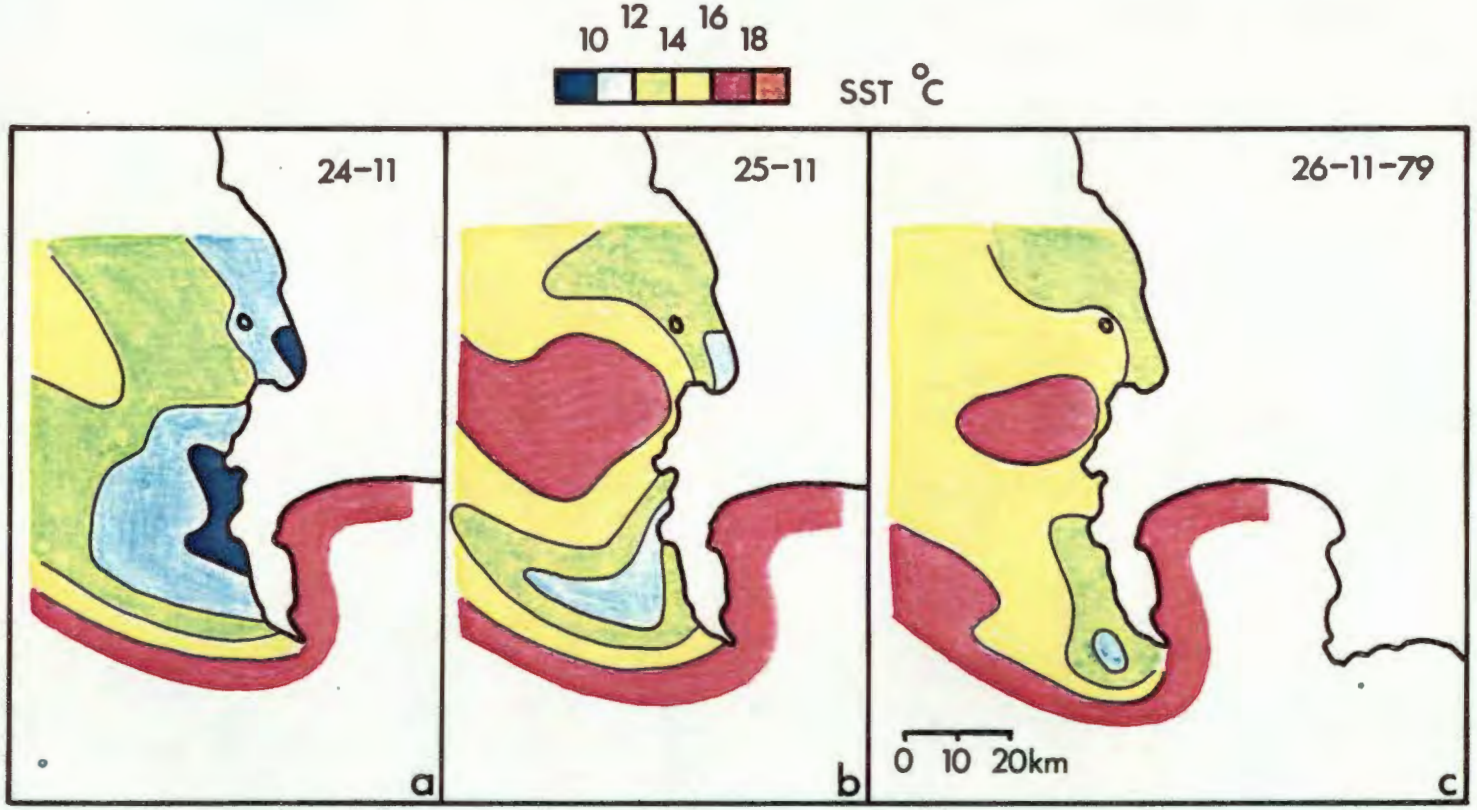

Fig. 9a,b,c: The SST distribution in a 3 day sequence representing the decay phase of the upwelling cycle. A marked deterioration of the plume (green and blue shaded areas) is evident. By the 26th warm water has pushed shorewards at Oudekraal. The remaints of the plume are detached from the coast near Cape Point.

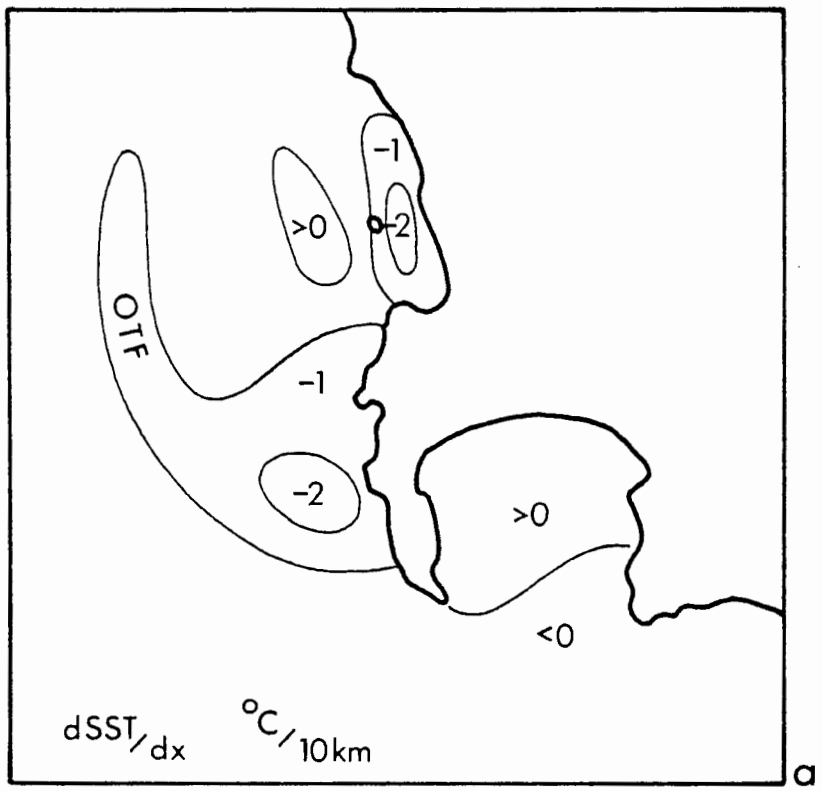

Averaged 15 to 25-11-79

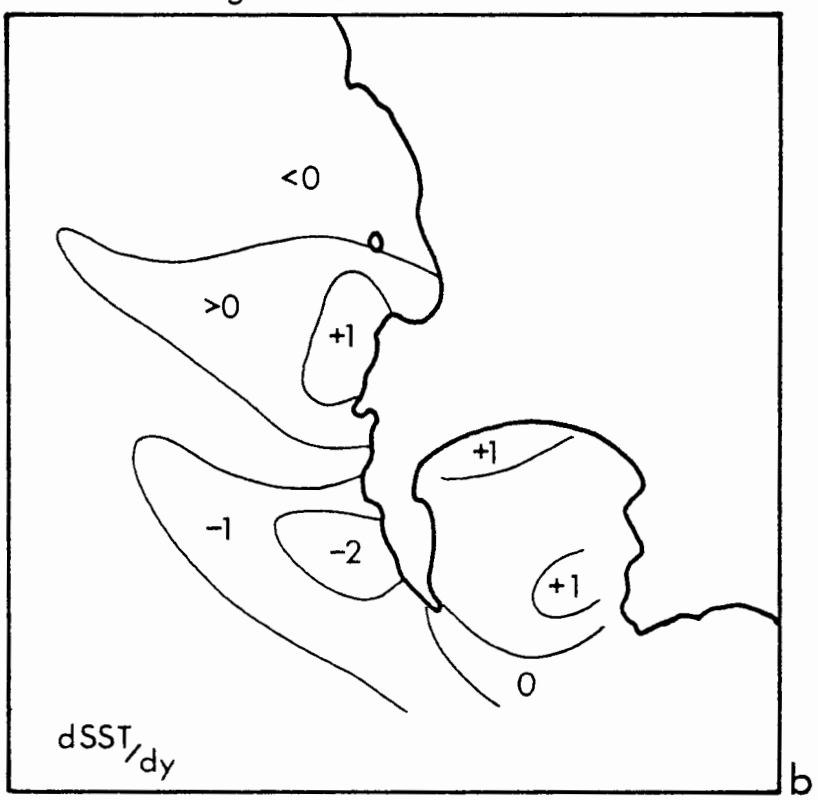

Fig. 10a: The crosshore shear of SST's matrix averaged over the period 15-25 November 1979. The OTF (Oceanic Thermal Front) is shown extending to the NW of the Peninsula.

Fig. 10b: The alongshore shear of SST's matrix averaged over the period. Values are of opposite signs on either side of the plume. Alongshore and crosshore shears are of the same order of magnitude by comparison.

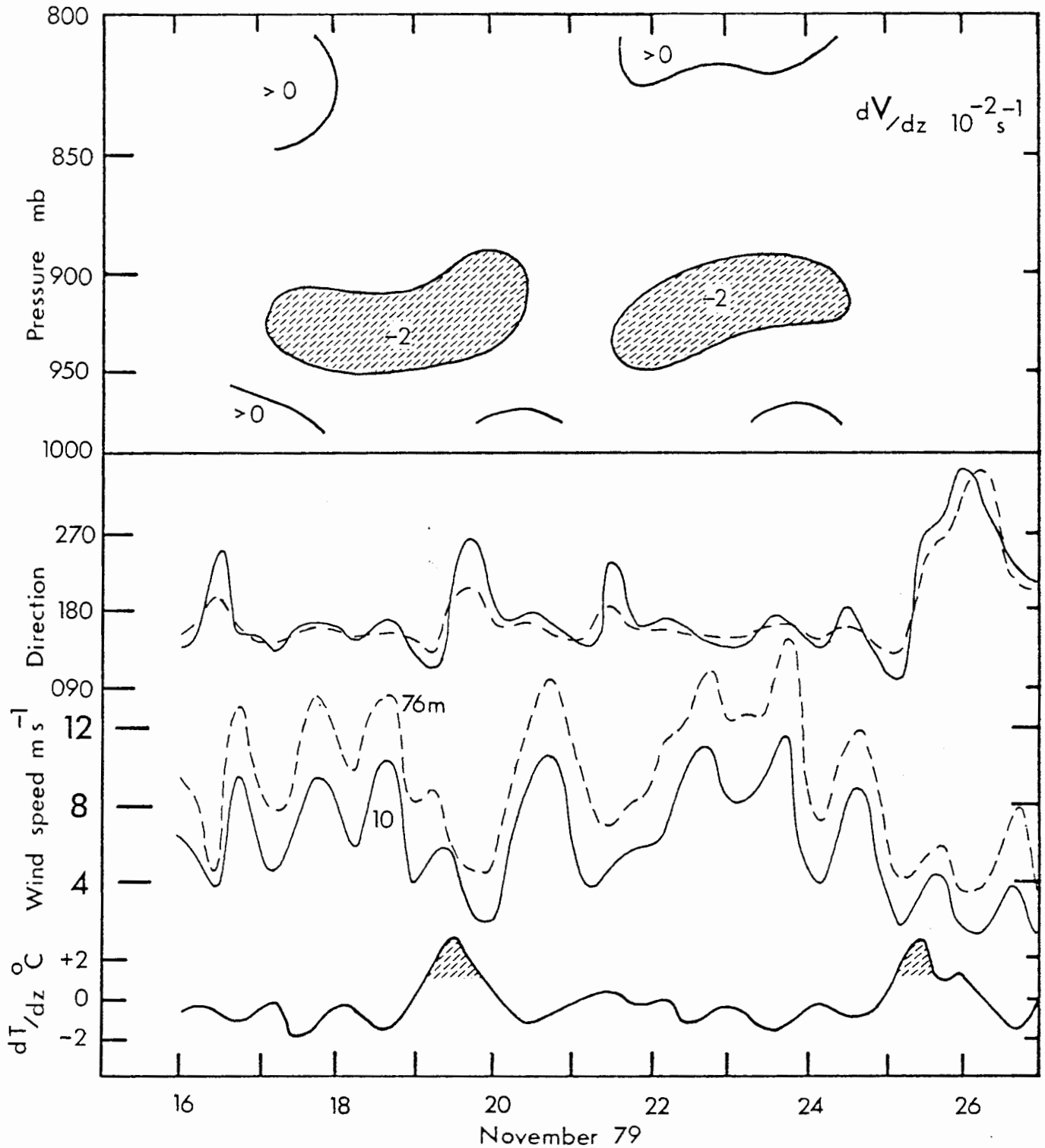

Fig. 11: A time series comparison of radiosonde and instrumented tower derived vertical wind shear data (top and bottom respectively) for the period 16-26 November 1979. Land-seabreezes and stable stratification (seen in the curves in the bottom diagram) are temporally correlated with negative wind shears in the 900-950mb layer (shaded area in the top diagram).

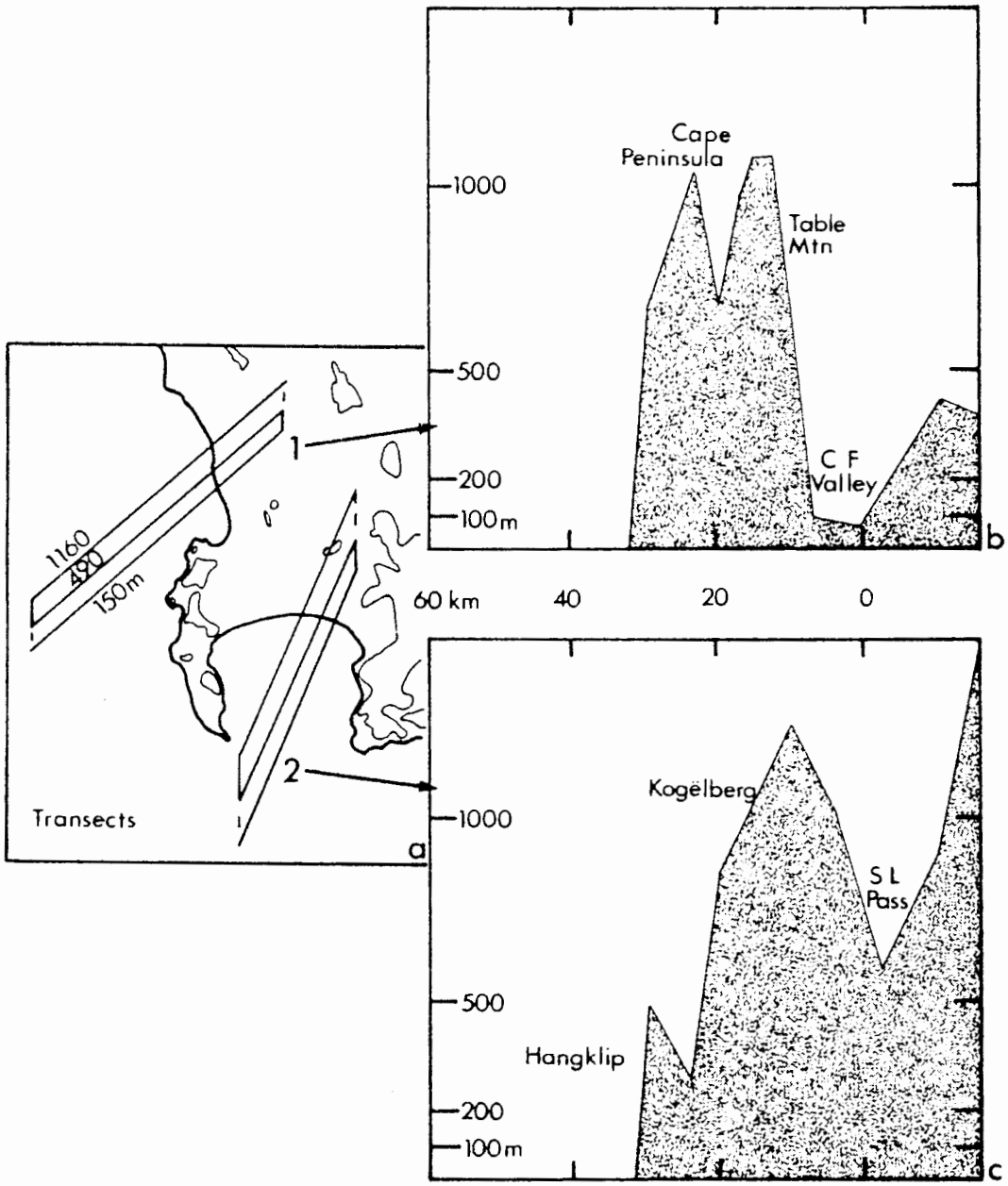

Fig. 12a: A reference map showing cross section/transect line locations and altitudes.

12b: A schematic view of topography upwind from Transect 1 including the Cape Peninsula, Table Mountain and the CF (Cape Flats) Valley.

12c: A schematic view of topography upwind from Transect 2 including Cape Hangklip, Kogëlberg and SL (Sir Lowry's) Pass.

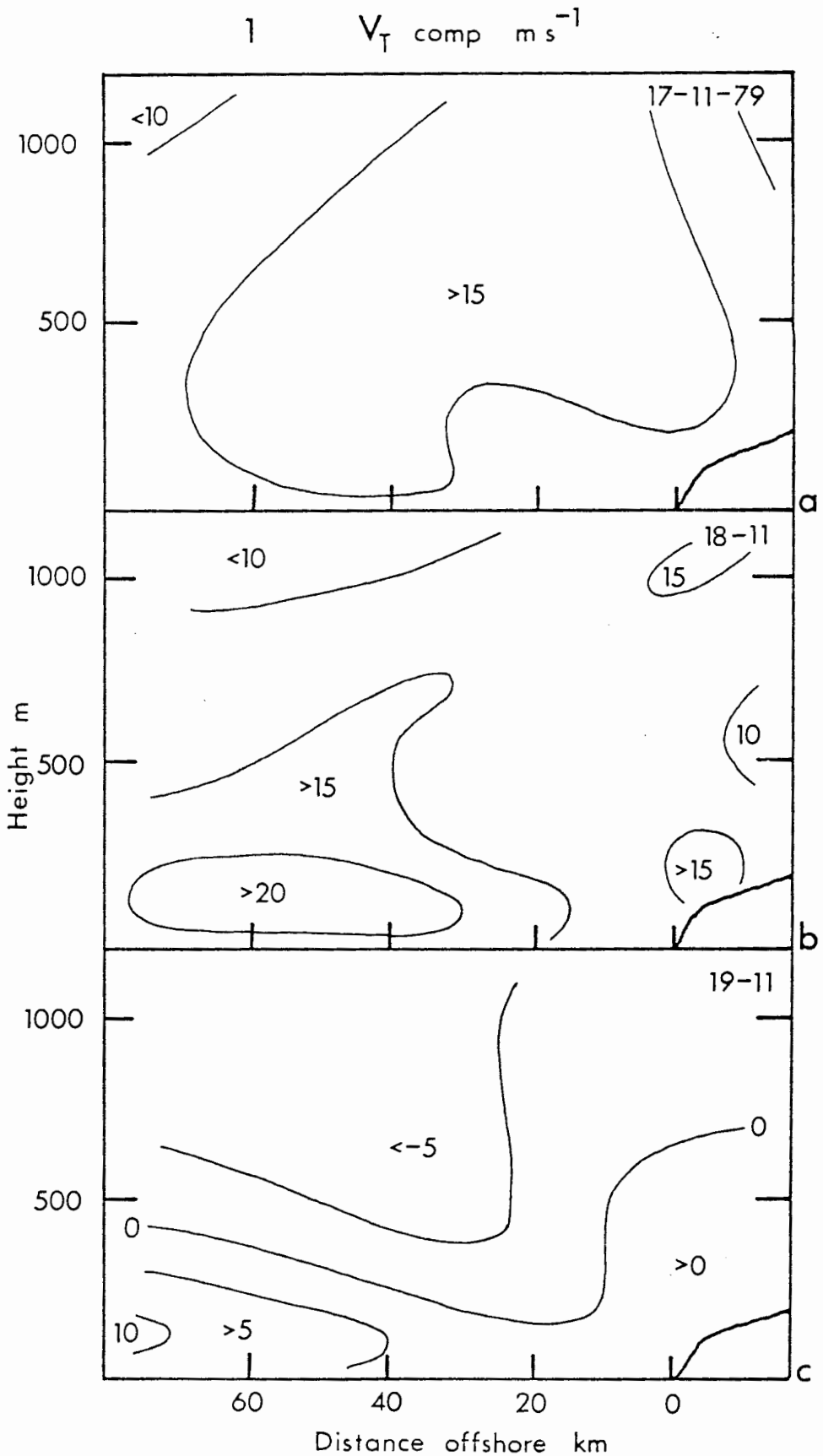

Fig. 13a,b,c: A height-distance sequence on Transect 1 of the alongshore V_T wind component, 17, 18 and 19 November 1979. The equatorward wind jet core 15ms^{-1} is seen to flatten while moving offshore. Reversed flow aloft is evident on the 19th.

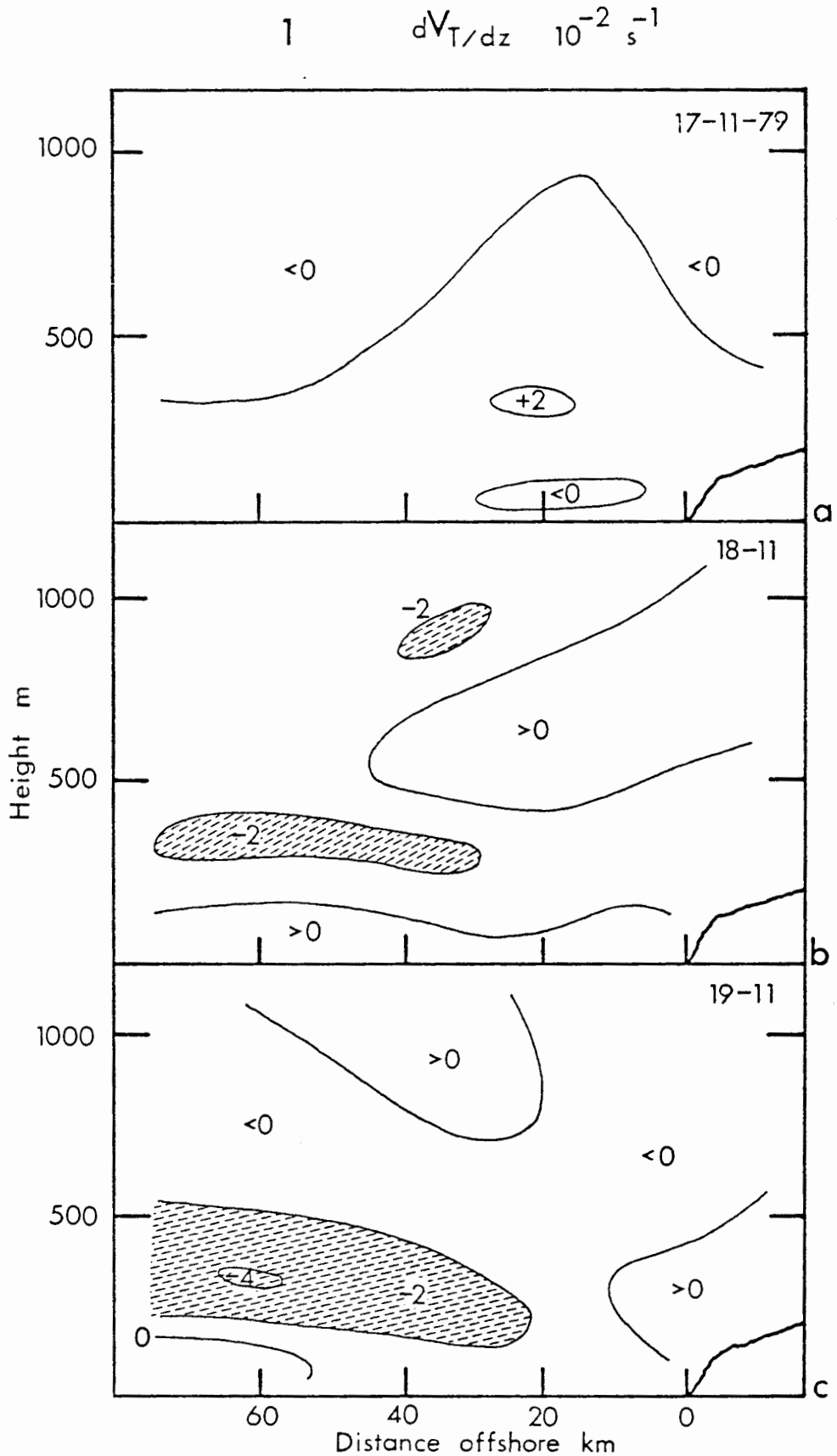

Fig. 14a,b,c: A height-distance sequence on Transect 1 of the vertical shear of the V_T wind component, 17, 18 and 19 November 1979. A negative shear layer grows above the jet core in response to a descending thermal inversion.

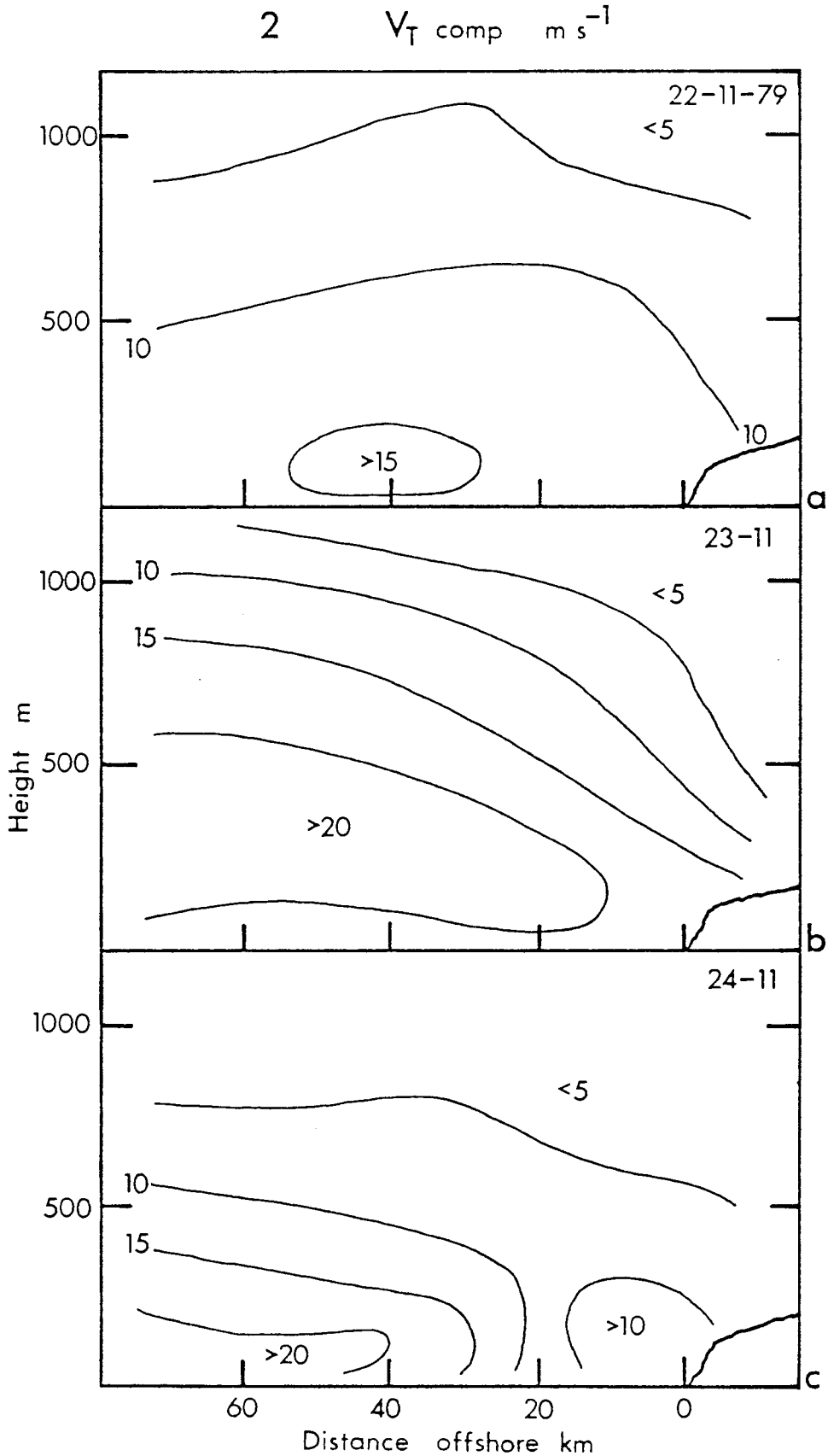

Fig. 15a,b,c: A height-distance sequence on Transect 2 of the alongshore V_T wind component, 22, 23 and 24 November 1979. A wide equatorward wind jet intensifies, becoming channelled by the upwind topography.

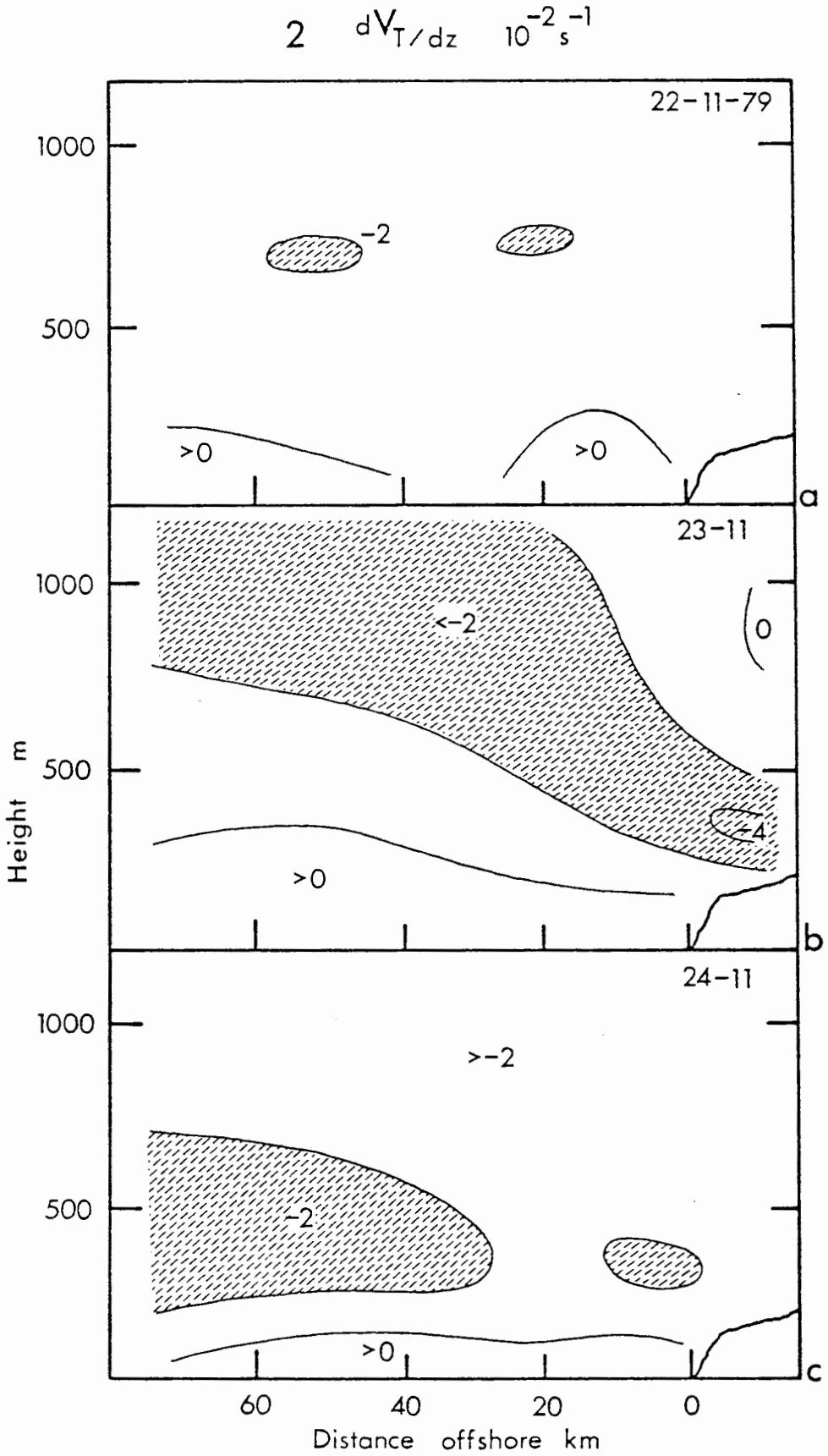

Fig. 16a,b,c: A height-distance sequence on Transect 2 of the vertical shear of the V_T wind component, 22, 23 and 24 November 1979. A marked negative shear layer slopes down towards the coast on the 23rd due to a feedback of orographic subsidence.

B. WIND SHEAR AND UPWELLING IN FALSE BAY

Topographic channelling of a wind axis over False Bay was investigated during the period 19 January to 4 February 1981 using sequential, fine grid aerial survey data. Low level SE wind flow exceeded 1km in depth throughout the case study period. The atmosphere was characterised by cool temperatures aloft and unstable, turbulent conditions. A meteorological background is provided by progressive wind vector data from Olifantsbos and Oudekraal as illustrated in Fig.17. At Olifantsbos winds flowed in a coastal alignment responding to the local pressure gradient. Wind directions at Oudekraal were offshore and more perpendicular to the coast, being forced to rise over Table Mountain before descending along the steep slopes at Oudekraal. From the 23rd to the 26th a lee vortex from winds "overshooting" the mountain resulted in an apparent return flow. Equatorwards flowing winds appear to have converged to the W of the Peninsula from the crossing of vector paths.

FLIGHT DATA

Selected stages during the case study upwelling cycle were contoured as two day composite maps for improved mesoscale SST resolution in False Bay. Wind maps are shown for individual days in Fig. 18a, b and c. The Cape Flats wind axis (represented by the area exceeding $15ms^{-1}$) was activated by 30 January. Originating from compression at Cape Hangklip,

the jet of wind swept northwards across False Bay and the southern Cape Flats, losing strength N of Table Bay along the coast (Fig. 18a). The 3 February 1981 wind field, represented by vector arrows in Fig.18b, was distinguished by streamline confluence across False Bay and difluence over the Cape Flats valley and Table Mountain. Return flow was observed just to the N of the Peninsula.

An analysis of stress curl indicated a sharp boundary on either side of the wind axis (zero curl line) in Fig.18c. Anticyclonic (+) stress curl was found over the SW quadrant of False Bay and over Table Bay. A predominant feature was the intense cyclonic curl area over the NE quadrant of False Bay (shaded area). The development of a differential upwelling pattern in the semi-enclosed bay is linked to these curl areas and to the wind deflections imposed by topography. These may be described in more detail by analysing wind vector components.

V and U wind components were calculated over a 10km square grid matrix and then manually contoured without smoothing for representation in Fig.19a and b. Positive V wind components prevailed along an axis from Cape Hangklip to Table Bay, in contrast to lower values leewards of Kogëlberg and in the "wake capture" (-V) return flow area behind Table Mountain. A degree of complexity was noted in the U wind component pattern on 3 February 1981. Generally offshore (-U) flow was

seen to the W of Cape Hangklip and the Cape Peninsula due to offshore deflections. Over the southern Cape Flats a pronounced onshore flow area (+4) was due to the curvature of winds around Kogëlberg and to seabreeze-thermal entrainment influences.

SST PATTERNS

A sequence of composite SST maps (Fig.20a, b, and c) describes the development of small scale upwelling within False Bay. On 19 and 20 January a small plume was found NW of the Peninsula with nearly homogeneous 18-20°C SST's in False Bay. Following a period of gale force equatorward wind stress a differential SST pattern had developed. By the 1st and 2nd of February a cold plume from Cape Hangklip had penetrated into the middle of False Bay with a considerable SST gradient along its NE edge. A separate tongue of upwelled water at Gordon's Bay was separated from the main plume by a warm band of water residing in the sheltered wake of Kogëlberg Mountain. Concurrently the plume to the NW of Cape Town spread seawards pushing the OTF into a zonal alignment. By the 4th and 5th a compensating warm current was inferred from the SST distribution. Warm water circulated from the northern False Bay coast into the Kogëlberg wake. The Cape Hangklip plume had changed direction towards Cape Point while weak upwelling activity continued at Gordon's Bay. Warm water persisted along the western and northern coasts of False Bay due to onshore winds and the restricting coastal geometry.

DIFFERENTIAL UPWELLING

Derivatives of the spatially averaged SST fields of the 31st, 2nd and 4th were calculated in E-W and N-S directions by matrix subtraction. The results, displayed in Fig.21a and b, are dominated by a marked positive SST shear axis diagonally bisecting False Bay. From these features it is postulated that cold plumes were activated in close proximity to a warm countercurrent which flowed from the central False Bay coast towards Koëlbaai. The cold plume from Cape Hangklip persisted alongside the warm water through geographic constraints imposed on the Cape Flats wind axis.

OVERVIEW OF SEQUENTIAL CASE STUDIES

The sequential case studies A and B emphasise that wind shear and differential upwelling are present throughout the cyclic modulation of coastal wind flow. Time scales of weeks are common for the repeat of mesoscale patterns. Both case studies followed coastal upwelling developments over a wind event with a time scale of 11 days. The growth and decay of cold plumes along Cape Hangklip and the Cape Peninsula were shown to be a direct response to surface wind stress. The shear or vorticity in the wind stress field imposed an alongshore variability which, over a period of days, led to the development of warm nearshore countercurrents. The importance of vertical wind shear was further highlighted in a sequential analysis of transect data. An increase in

negative vertical shear meant that the wind axis was more susceptible to topographic deflection. The wind shadow created by individual coastal mountains was found to be a major cause of differential upwelling on time scales of days to weeks.

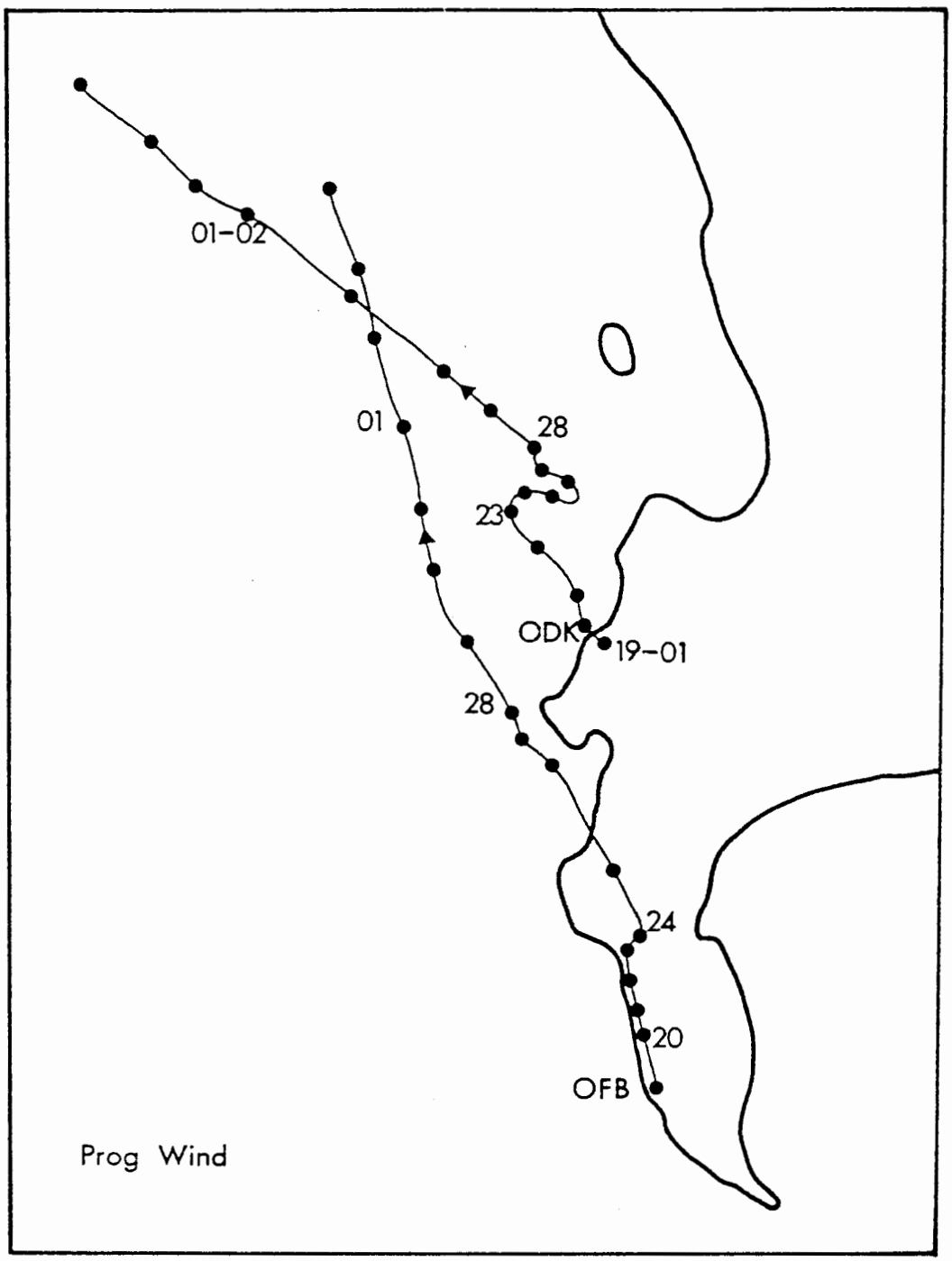

Fig. 17: A progressive wind vector diagram for the period 19 January to 4 February 1981 from data collected at OFB (Olifantsbos) and ODK (Oudekraal). A mean flow convergence is inferred by the crossing of vector paths in the wake of the Peninsula's mountains.

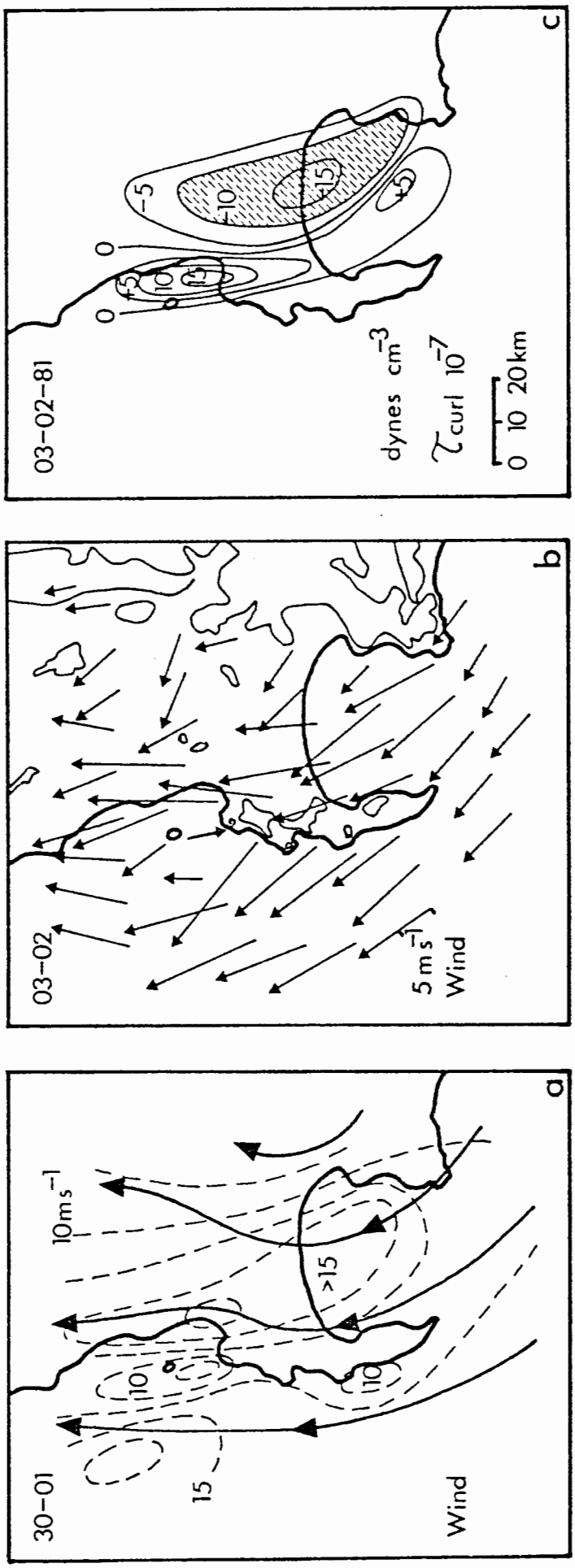

Fig. 18a: The wind field on 30 January 1981 represented by streamlines and isotachs. The Cape Flats Jet axis is evident (15 ms^{-1}).

18b: A wind vector representation for 3 February 1981. Alongshore flow is deflected, becoming reversed in the lee of Table Mountain.

18c: The wind stress curl distribution for 3 February showing a marked cyclonic area (shaded) over False Bay and an anticyclonic area over Table Bay to the NW.

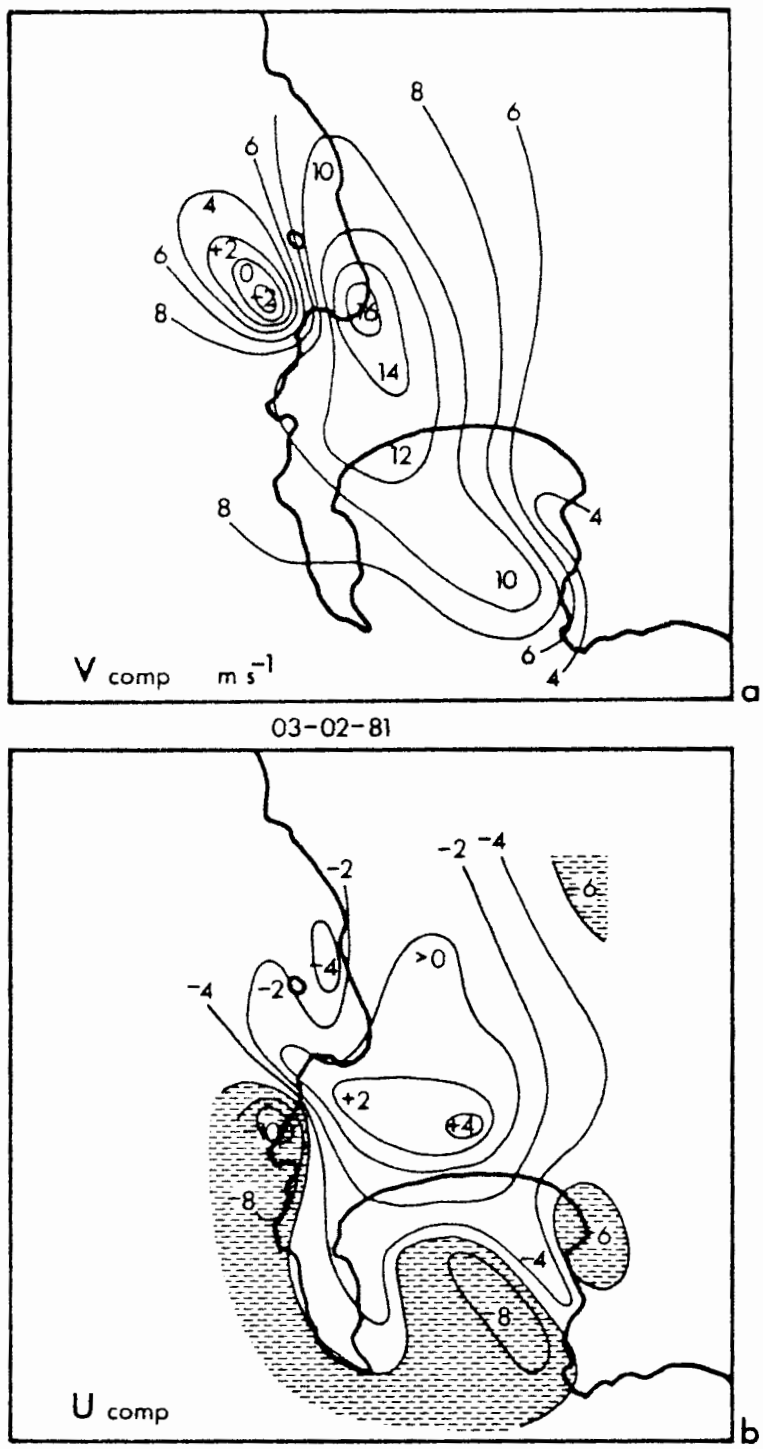

Fig. 19a: The V wind component distribution on 3 February 1981. An accelerated axis extends from Cape Hangklip to Table Bay. Reversed wind flow is found in the lee of Table Mountain.

19b: The U wind component distribution on 3 February 1981. Offshore deflections (shaded) predominate along the west shores of Cape Hangklip and the Cape Peninsula. Onshore flow is seen over the Cape Flats due to seabreeze influences.

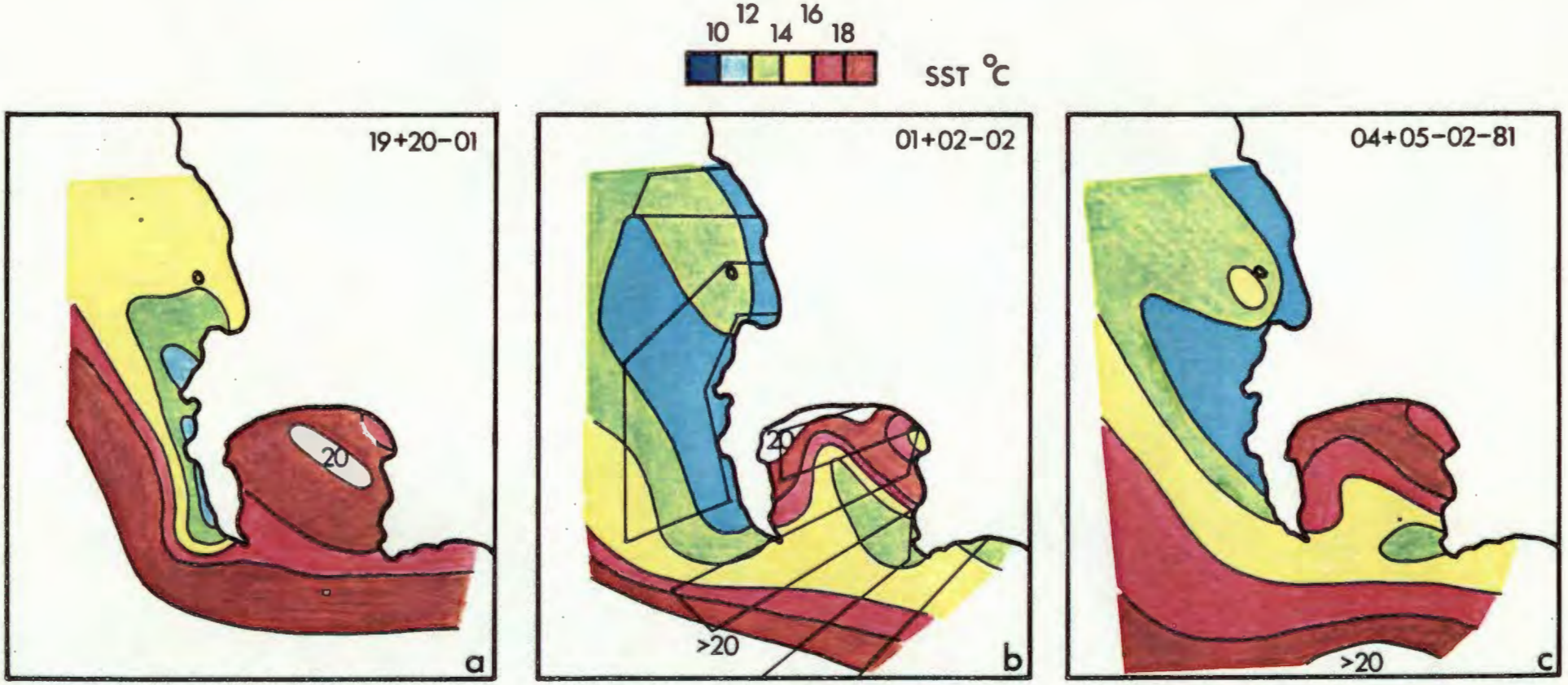

Fig. 20a,b,c: A composite SST distribution sequence for the period 19 January to 5 February 1981. Homogeneous SST's in False Bay change to a differential upwelling pattern during the wind event. The flight grid is shown in 20b.

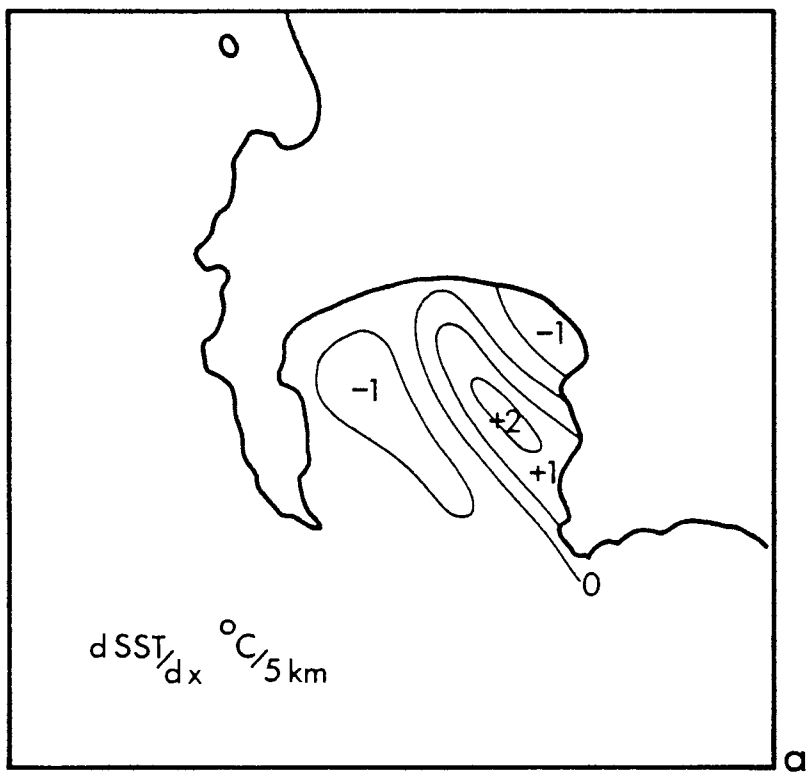

Averaged 31-01 to 04-02-81

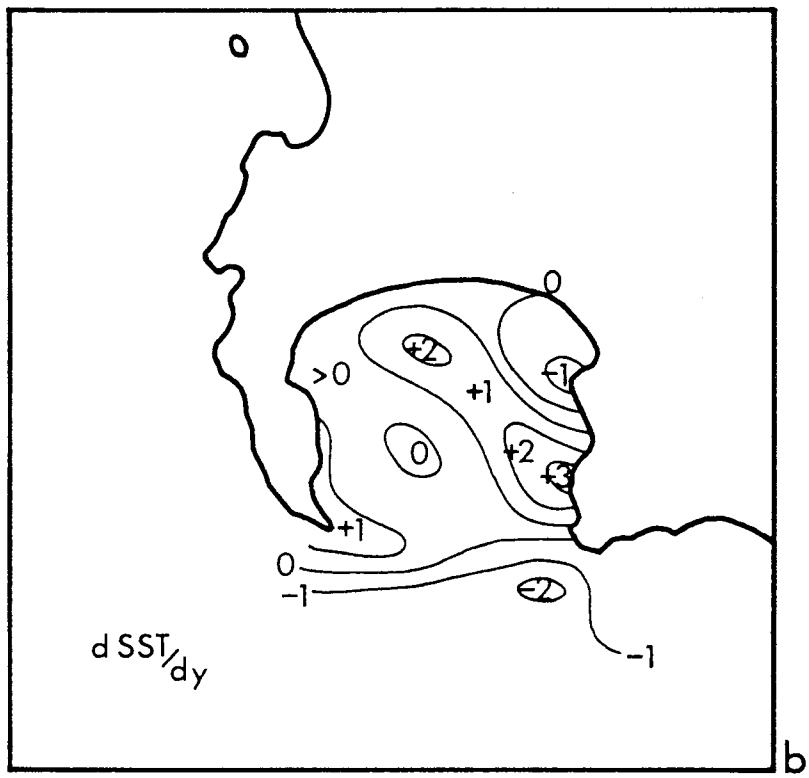

Fig. 21a: The crosshore shear of SST's matrix averaged over the period 31 January to 4 February 1981. A positive shear axis stretches across False Bay in the lee of Kogëlberg.

21b: The alongshore shear of SST's matrix averaged over the period 31 January to 4 February 1981. A similiar positive shear axis is seen. Negative shears are noted on either side of the axis. Alongshore and crosshore shears are of the same order of magnitude by comparison.

C. A COMPARISON OF THERMAL FIELDS IN DEEP AND SHALLOW EQUATORWARD WIND FLOW

Over the period 21-26 January 1980 the SW tip of Africa was surveyed on a different scale using a coarse sampling grid. A comparison between deep and shallow flow fields was made by selecting results for individual case study days on the 22nd and 25th of January.

A time series comparison of surface and upper air data was made as an observational foundation. During this time an anticyclone ridged to the S of the study area coincident with the progressive descent of a warm atmospheric layer. Accompanying the shifting of the high pressure cell, a coastal low moved southwards along the coast. Surface and upper air winds and temperatures responded to these macroscale influences as seen in Fig.22. Alongshore wind components of $12ms^{-1}$ persisted over Olifantsbos. At Oudekraal the proximity of horizontal and vertical thermal constraints imposed a diurnal oscillation. Winds in the 850-900mb layer became easterly as seen in the local airport radiosonde analysis at the bottom of Fig.22. The descent of air in this layer resulted in a subsidence inversion and a "capping" effect over gradient winds. Oudekraal winds accelerated to an offshore peak during the latter portion of the 25th.

FLIGHT DATA

Wind shear patterns along the SW tip of Africa were described with an alongshore aerial survey resolution of 50km, allowing a 40 000km^2 area to be covered. The V_T wind component field, shown in Fig.23a, revealed a broad maxima to the SW of Cape Columbine during the deep flow of the 22nd. An axis of onshore $+V_N$ components was observed along the coast from Cape Columbine to False Bay, the result of seabreeze influences. An offshore deflected $-V_N$ area was seen to the W of the Peninsula in Fig. 23b.

Intense upwelling plumes emanating from Oudekraal and Table Bay dominated the SST distribution on the 22nd as illustrated in Fig.24a. A narrow band of upwelled water was observed along the west coast to Cape Columbine. The OTF appeared to be well defined (red shaded strip), paralleling the coast at offshore distances of 10km in the S to 40km in the N. With onshore wind forcing in False Bay, little upwelling activity was noted and SST's rose above 18^{o}C.

The 152m air temperature field Fig.24b contained only weak contrasts due to the deep and turbulent wind flow on the 22nd. The upper Berg River Valley warmed to 26^{o}C while on the following days an increasing negative vertical wind shear caused thermal contrasts to grow considerably.

As the depth of flow diminished on the 25th, the alongshore

wind axis was prevented from rising over the coastal mountains as inferred from Fig.25a. Instead the winds became accelerated to the W of Cape Hangklip and deflected away from the coast N of Cape Town. The wind shadow of Table Mountain extended far downwind. A strong V_T shear line (along the $14ms^{-1}$ isotach) separated the accelerated and obstructed areas, having an impact on the OTF. The flow deflections on the 25th were highlighted by variations in the V_N component field (Fig.25b). Onshore and offshore areas coexisted to the E and W of Cape Town, respectively. An offshore deflected axis extended to the S of Cape Point (shaded) and along the western side of the Peninsula where downslope winds reinforced the topographic deflections.

A more differential and unstable upwelling pattern was evident on the 25th under the influence of a shallow wind field. Distinct cold plumes (dark blue) were observed seawards of Cape Columbine, the Cape Peninsula and Walker Bay, as well as from Cape Hangklip and Gordon's Bay as shown in Fig.26a. Tongues of warm water spread shorewards in the orographically sheltered areas of St. Helena Bay and Robben Island. The OTF (red strip) appeared to meander in an unstable fashion, compacting SST gradients differentially. This meandering often leads to eddy formations, a phenomenon which anticipates the upwelling relaxation phase.

In the atmosphere, thermal contrasts extended seawards under

the capping thermal discontinuity on the 25th. As marine winds were deflected seawards by the mountains, the Berg Valley Thermal Low (30°C) expanded across the northern Cape Flats. The mid-day peak in crosshore temperature gradients activated a seabreeze along the N coast of False Bay. A seawards perturbation of the thermal front leewards of Table Mountain was attributed to divergence-compensating subsidence. The thermal front provides impetus to downslope winds which "pour" off the coastal mountains as the subsiding layer consolidates late in the evening.

STRESS AND VORTICITY COMPARISONS

A comparison of wind stress fields for the deep and shallow cases emphasises the interaction of negative vertical shear layers and topography. A more homogeneous stress was exerted on the sea surface during the deep case of the 22nd as depicted in Fig.27a and b. Three days later in the cycle, Cape effects were maximized with wind stress enhancement from 2 to 6 dynes cm^{-2} off the Peninsula. The stress maxima shifted southwards over 100km from the 22nd to the 25th of January, precipitating the instabilities in the OTF. Flow trajectories were quite similar in both cases and differences arose from the decrease in flow depth and subsequent increase in wind vorticity.

A standing vortex was found over the Cape Peninsula in a comparative analysis of wind vorticity for the two cases in

Fig.28a and b. Cyclonic vorticities grew in strength and areal distribution from the 22nd to the 25th. Values of $-6\ (10^{-4})\ s^{-1}$ were found over the Peninsula during the shallow flow. The descent of a negative wind shear layer translated into cyclonic wind vorticities, perturbing the atmospheric and oceanic thermal fronts along the SW tip of Africa.

INTERCOMPARISONS

The major difference between the case study observations lies in the thermal perturbations. Flow depth was initially quantified by the local radiosonde temperature discontinuity and wind profile. By selecting deep and shallow flow cases separated by 3 days, an instantaneous view of the wind-induced thermal perturbations was formulated. Upwelling was coast-parallel when deep flow passed over the orographic obstacles. Major changes occurred thereafter as cold plumes grew only along the headlands. Atmospheric thermal perturbations were documented with increasing complexity under the inversion layer. It appeared that topographic wind deflections were carried further seawards by perturbations in the atmospheric thermal front. In response, the oceanic front became perturbed and unstable particularly to the W of the Cape Peninsula and Cape Columbine.

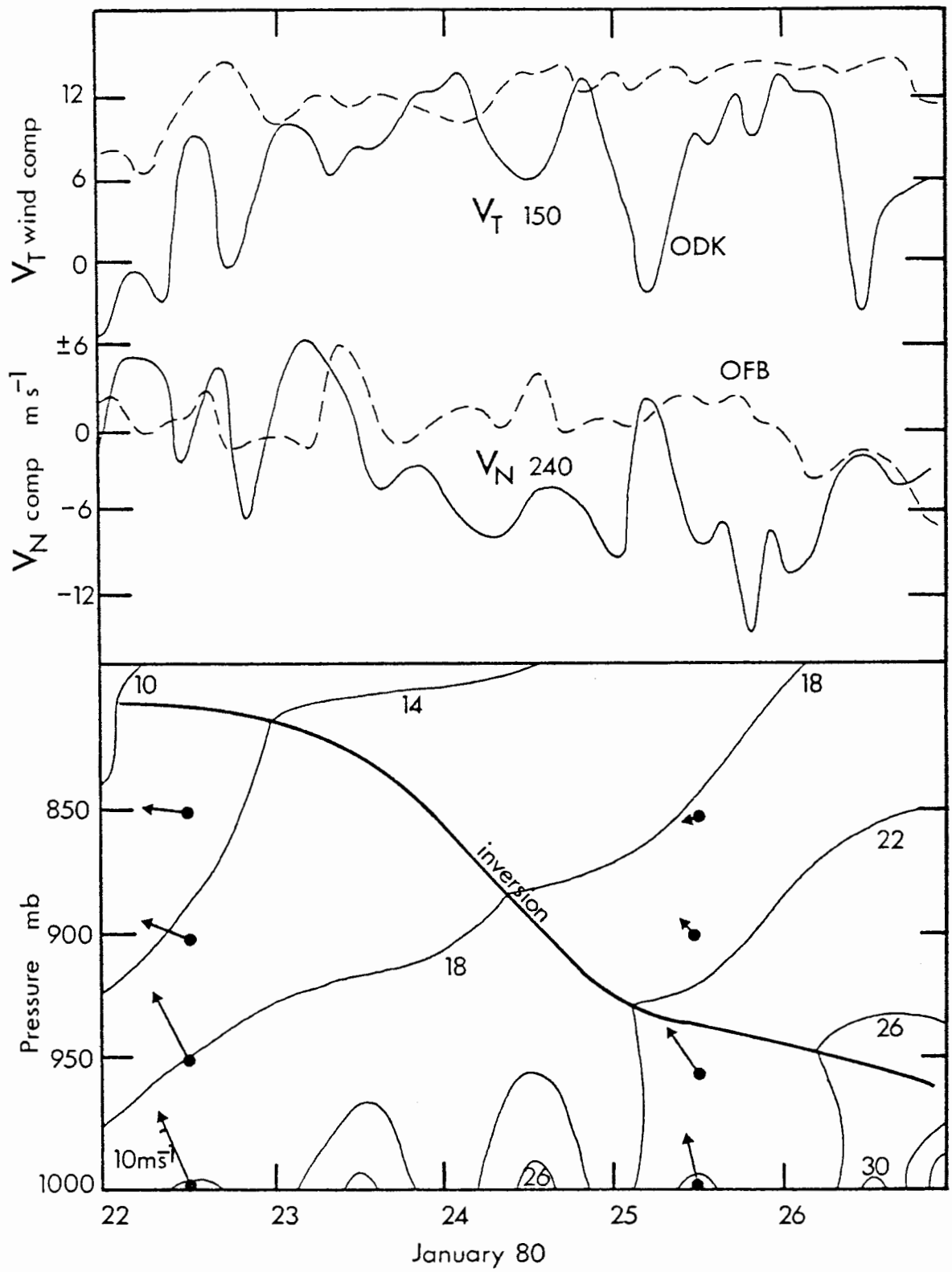

Fig. 22: A comparison of V_T and V_N wind components at Oudekraal and Olifantsbos with the radiosonde temperature time series for the period 22 to 26 January 1980. A descending inversion layer caps alongshore wind flow. Oudekraal, in Table Mountain's lee, shows diurnal cycles beneath the inversion. Winds at Olifantsbos are less affected by topographic and thermal effects.

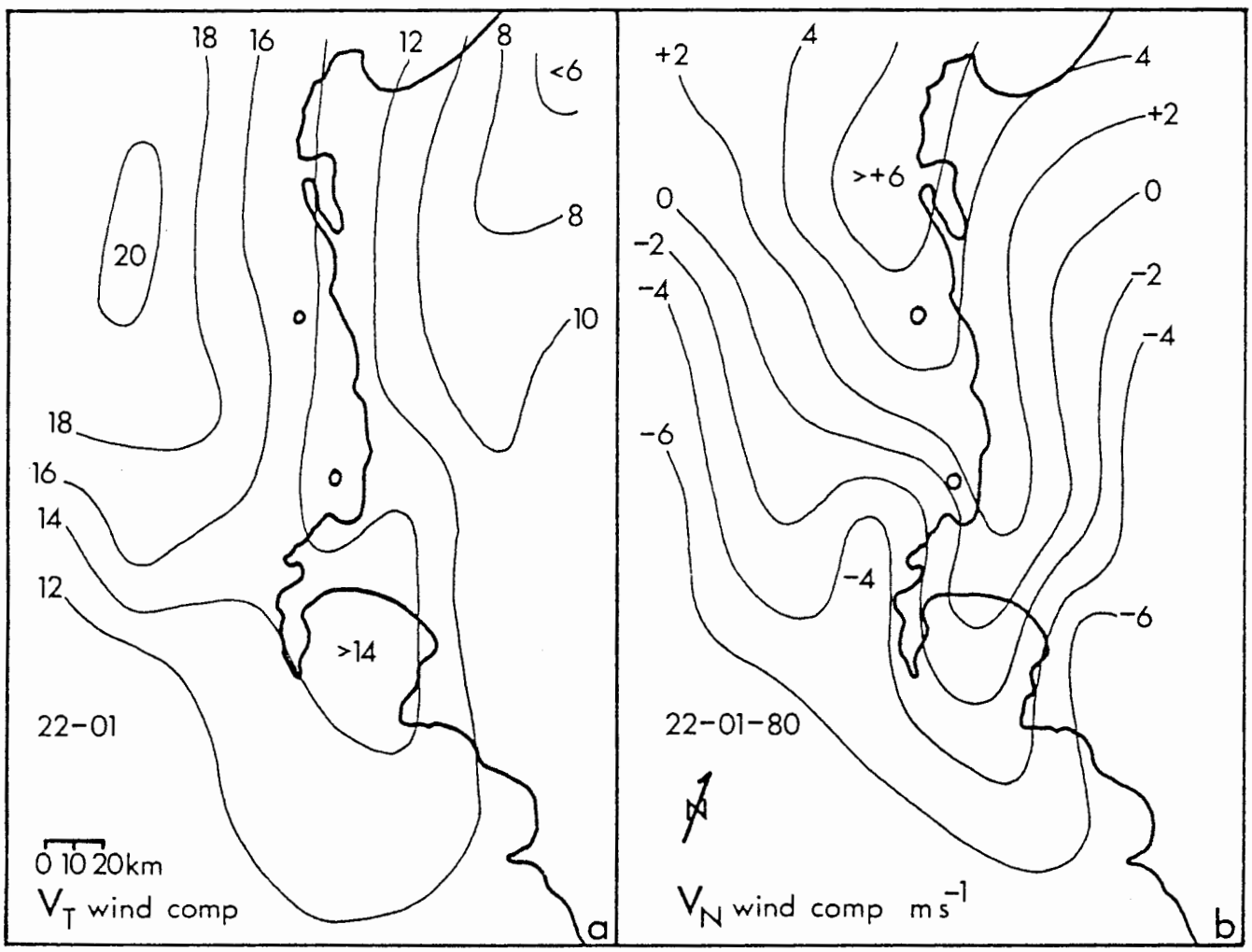

Fig. 23a: The alongshore V_T wind component distribution for the deep flow case study 22 January 1980. An axis of accelerated wind extends to the NW of the Peninsula.

23b: The crosshore V_N wind component distribution for the deep flow case study 22 January. Offshore deflections to the SW are contrasted with a line of onshore flow along the northern portion of the west coast due to thermal contrasts and subsequent seabreeze circulations.

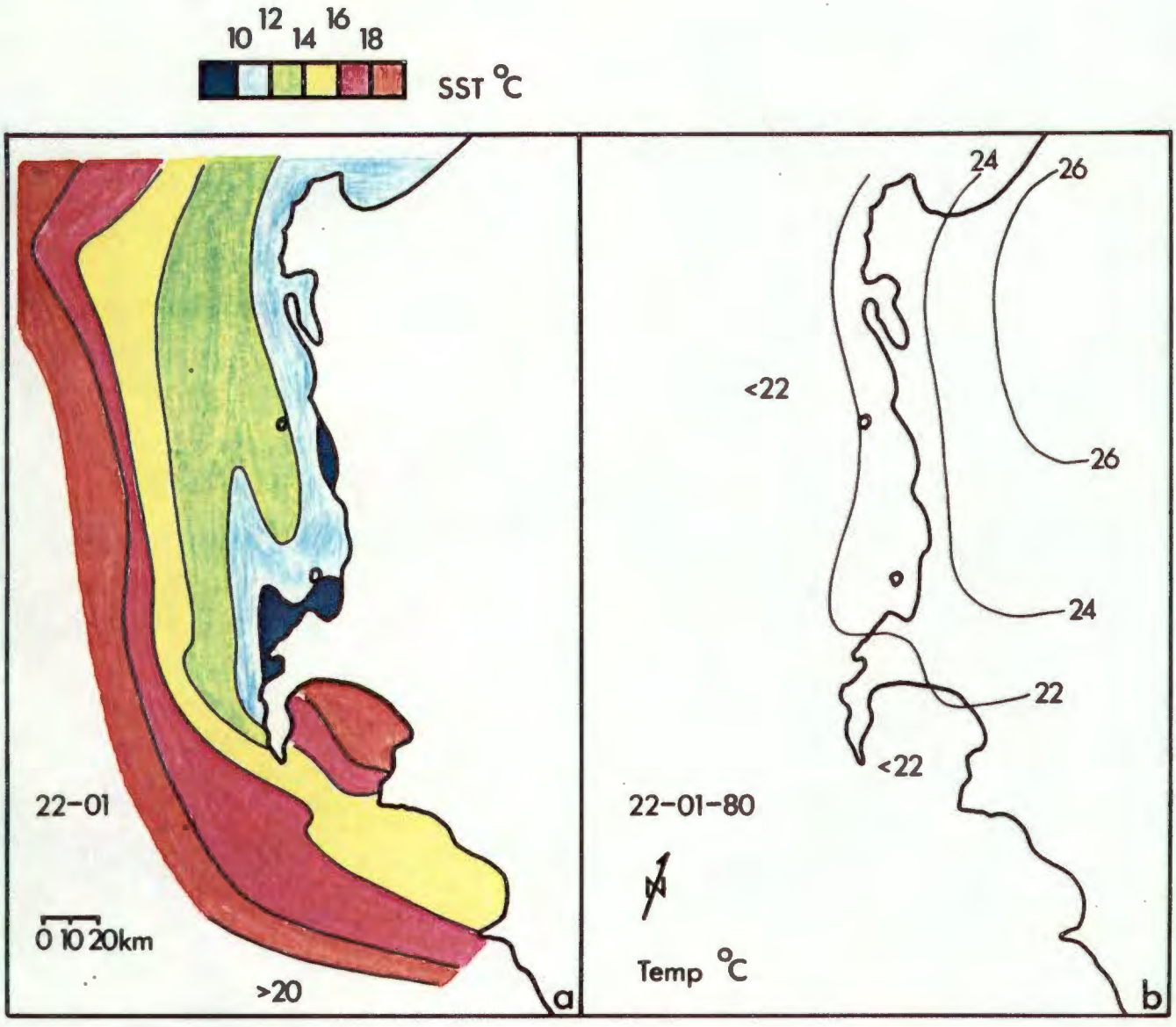

Fig. 24a: The SST distribution for the deep flow case study, 22 January 1980. An intense upwelling plume extends to the NW of the Peninsula. Upwelling is somewhat coast-parallel.

24b: The air temperature distribution for the deep flow case, 22 January. Weak crosshore gradients are observed in the turbulent, unstable conditions.

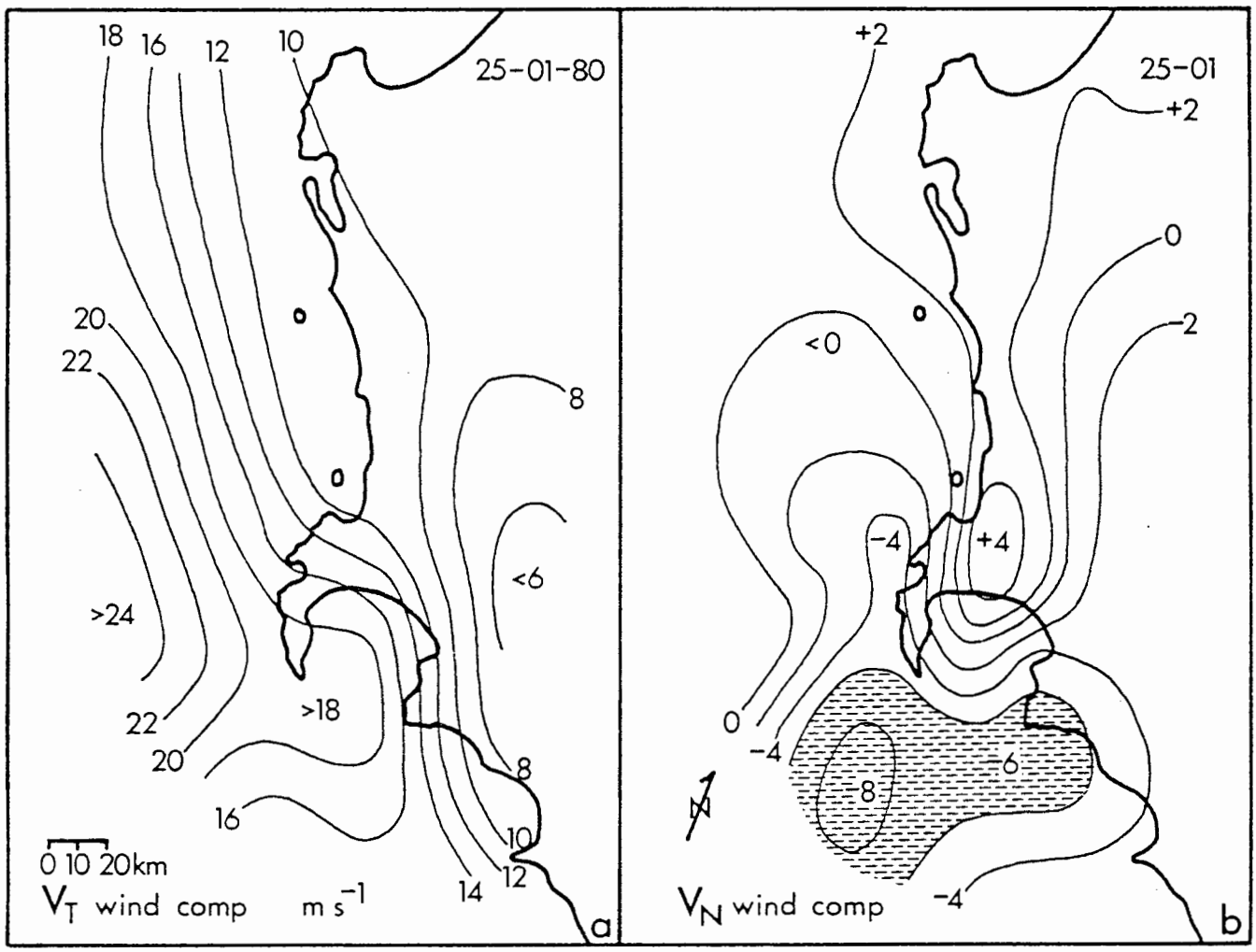

Fig. 25a: The alongshore V_T wind component distribution for the shallow flow case study, 25 January 1980. The accelerated axis shifts southwards by comparison, extending west from Cape Hangklip 18ms^{-1}.

25b: The crosshore V_N wind component distribution for the shallow flow case study, 25 January. Offshore deflections (shaded) are found SW of Cape Hangklip. Wind flow bends onshore (+4) over the Cape Flats as a result of the leewards wake of Kogëlberg.

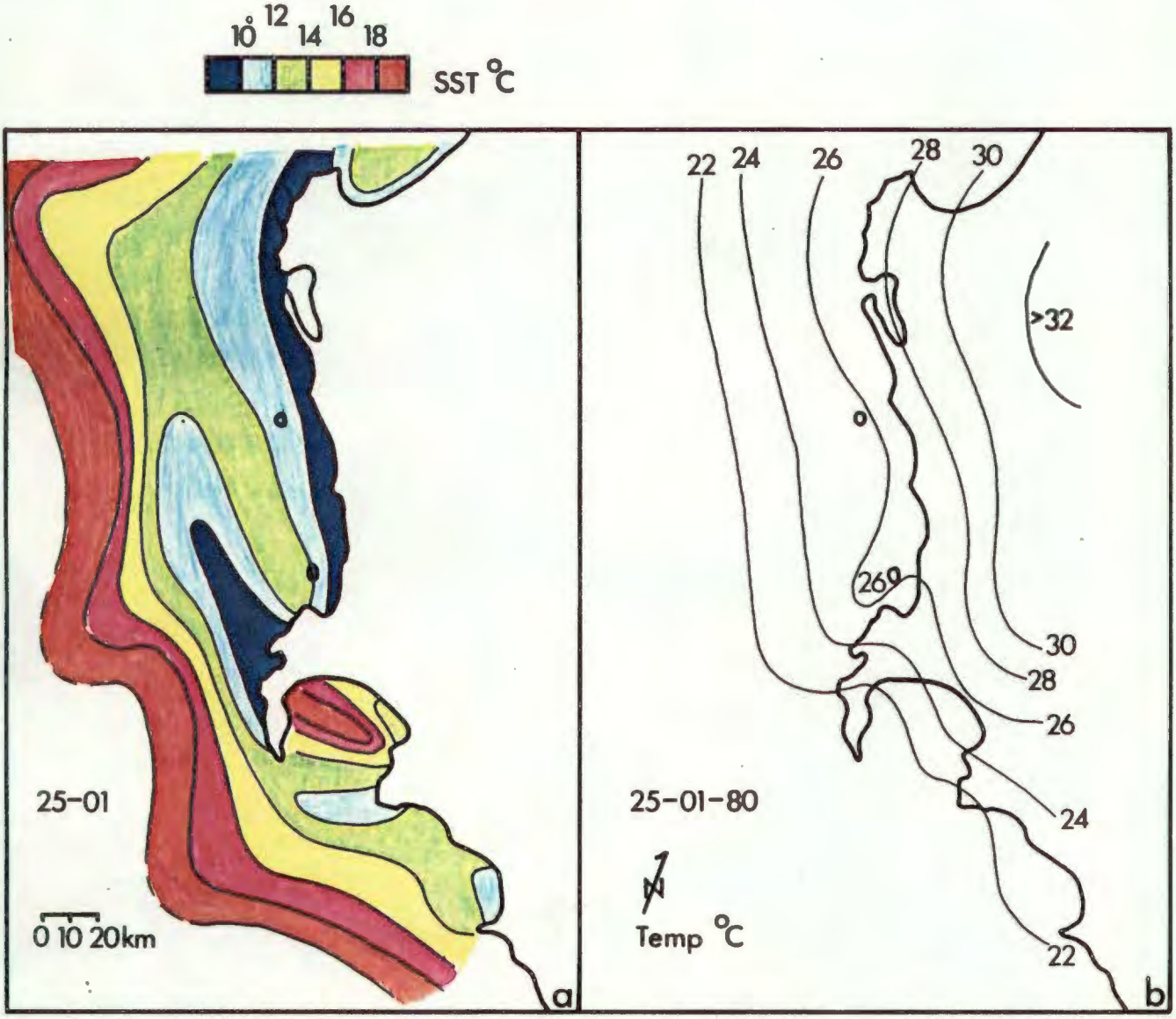

Fig. 26a: The SST distribution for the shallow flow case study, 25 January 1980. The Cape Peninsula upwelling plume is fully developed. Secondary plumes at the coastal headlands cause perturbations in the Oceanic Thermal Front (OTF).

26b: The air temperature distribution for the shallow case, 25 January. Beneath the capping inversion a thermal low has developed in the Berg River Valley. Consequently a sharp thermal front is noted along the coast.

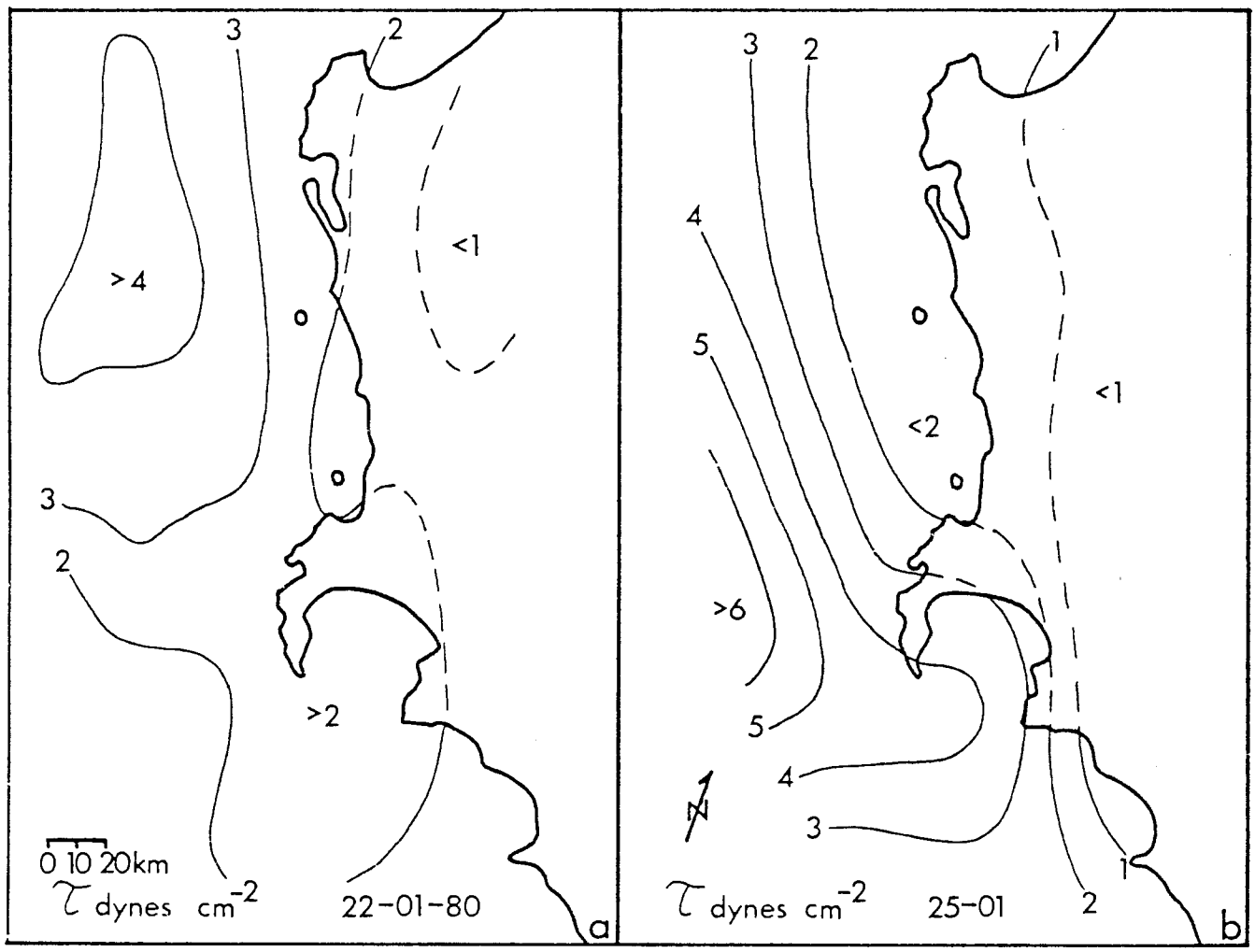

Fig. 27a,b: A comparison of estimated surface wind stress distributions for the deep and shallow case studies, 22 and 25 January 1980. The stress maximum shifts southwards and intensifies in Cape effect as the capping inversion descends.

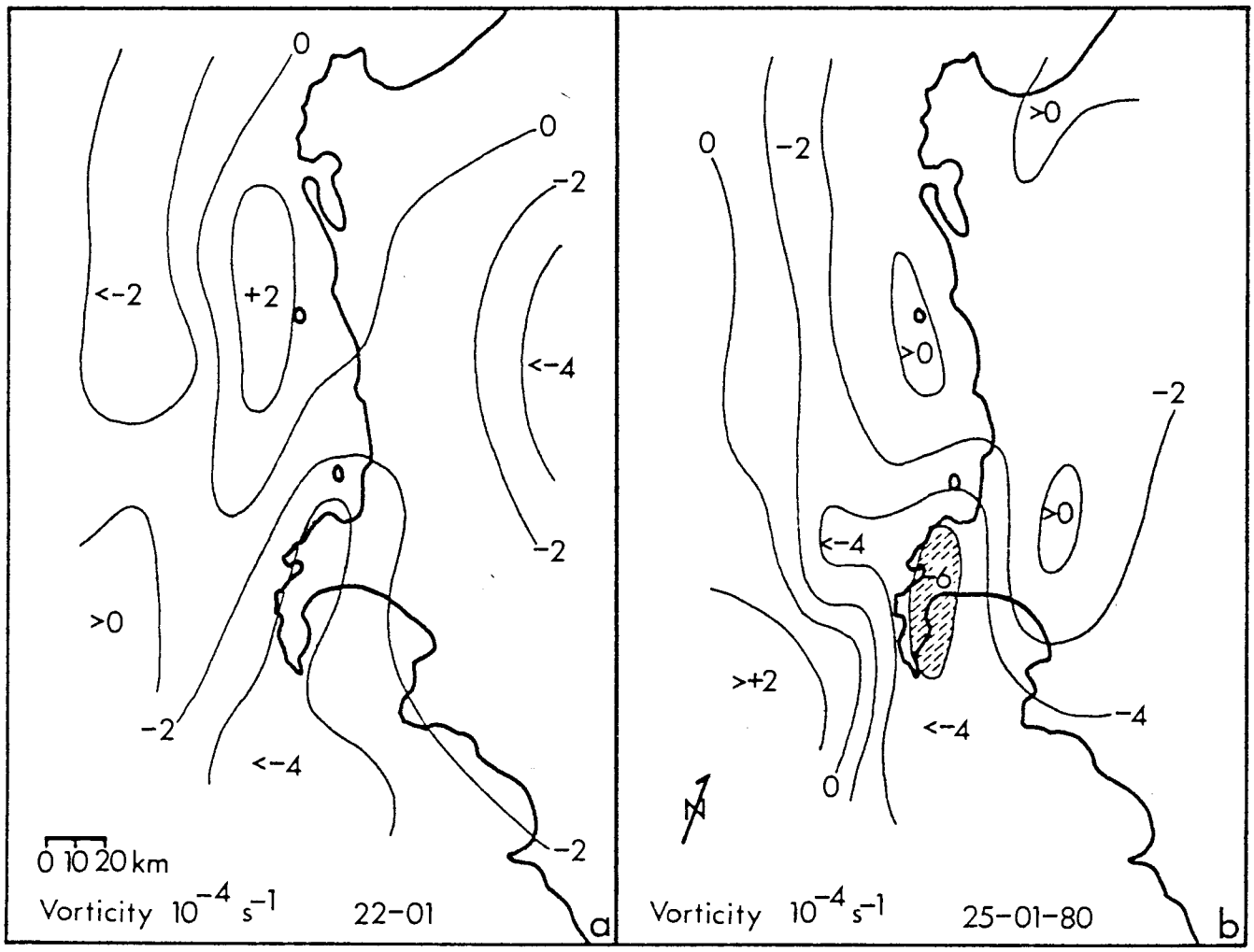

Fig. 28a,b: A comparison of wind vorticity fields for the deep and shallow case studies, 22 and 25 January 1980. The cyclonic vorticity maximum intensifies over the Cape Pensinsula as the inversion descends.

D. WIND SHEAR AND COUNTERCURRENTS LEEWARDS OF CAPE COLUMBINE

Cape Columbine is a headland extending seawards at 33°S consisting of low smooth hills rising to about 250m. Because of its position downwind from the Cape Peninsula upwelling plume, the coastal wind axis is cooled from below and a warm subsiding layer forms above the Benguela-modified air. As a result, alongshore equatorward winds become shallow and more prone to horizontal compression by the Cape Columbine headland. The leewards coast bends away into the wide sweeping bay of St. Helena, an area which is usually protected from summer winds. Seasonal trends often prevail over synoptic cycles along the stretch of coast to the N of Cape Columbine.

In comparing wind shear and differential upwelling in the lee of Cape Columbine, two particular case study days were selected from the available data base. The results for 1 and 23 November best illustrate the effects of variable flow depth. Contrasting atmospheric thermal structures were evident from vertical profile data collected 5km to the W of Lamberts Bay and displayed in Fig.29a. A 10°C inversion between 60-300m was observed on the 1st while much cooler temperatures were capped by an elevated 350-500m inversion of 5°C on the 23rd. The horizontal temperature pattern, shown in Fig. 29b and c, appeared relatively similar on both days as the coastal headland caused a leewards bulge in the thermal

front. Lower temperatures were recorded on the 23rd and the isotherms curved more shorewards, particularly in the deep convergent flow over the Olifants River Mouth (ORM). On the 1st, continental air became entrained over the marine layer causing isotherms to bend offshore. With the presence of a strong low-level inversion, the deflecting effects of the Cape Columbine headland were carried further downstream.

The influence of topography on deep and shallow flow fields was highlighted in a comparison of wind vectors for 1 and 23 November in Fig.30a and b. A distinct leewards wake and cyclonic curvature of flow was noted on the 1st. Shallow winds from the Berg River Valley were entrained into a vortex over St. Helena Bay. During the deep flow of the 23rd, onshore curvature was aided by the geometry of Cape Columbine and to seabreezes near the ORM. In both cases alongshore winds accelerated over the sea to the W of the headland. Peak velocities were found to shift to the N in deep cases and SW'wards during shallow flow.

An analysis of wind stress curl for the deep and shallow flow fields is presented in Fig.31a and b. An intense cyclonic area was found to be associated with the headland in both flow depths (shaded area). The leewards extension of this cyclonic wind stress curl area was restricted by topographic deflection on the 1st. However on the 23rd under deep southerly flow, the curl area penetrated downstream along the

coast to the N of St. Helena Bay. The distribution of stress curl affected local upwelling activity as illustrated in the SST maps in Fig. 31c and d.

Along the coast to the N of St. Helena Bay scant upwelling activity was observed on the 1st due to the leewards wake vortex and anticyclonic stress curl. On the other hand, marked coastal upwelling was present on the 23rd as alongshore winds and cyclonic stress curl extended further downstream from the Cape Columbine headland. Similarities were noted in the distinct cold plume emanating northwards from the headland and in the warm water pocket (red shaded) near the wind-sheltered Berg River Mouth. The juxtaposition and cyclonic circulation of cold and warm water currents is thought to create conditions favouring marine bioproductivity in St. Helena Bay.

COUNTERCURRENT VIEWED BY COMPOSITE ANALYSIS

A composite picture of wind shear and differential upwelling features along the entire SW tip of Africa was developed over the period 2 to 5 December 1980. Four flight grids were flown sequentially between 30° and 35°S latitude and from 10km inland to about 60km offshore. This 4 day period was characterised by steady equatorward flow following an unseasonal lull in winds and coastal upwelling.

A broad wind maxima appeared NW of Cape Columbine between the 2nd and 5th as shown in the composite streamline-isotach analysis Fig.32. Both topographic and pressure gradient effects reduced wind speeds along the Namaqualand coast. Diminished velocities extended downstream from the Cape Columbine headland for over 200km. Weak pressure gradients and low inversions along the coast favoured the development of seabreezes. At 34°S winds accelerated across False Bay and the Cape Flats Valley and a wind wake formed leewards of Table Mountain in response to topographic deflections.

The composite SST distribution revealed distinct upwelling plumes off the Cape Peninsula, Table Bay and Cape Columbine as illustrated in Fig.33. A strip of coastal upwelled water was seen at 30°S, however further south at 32° warmer water was observed. The warm SST band coincided with the light wind zone along the coast between the Olifants River Mouth and St. Helena Bay. It is inferred that a nearshore countercurrent had formed there due to the persistently calm conditions. Temporal cycles were investigated to further describe the mechanisms leading to the formation of this countercurrent.

A series of 3 wind reversals took place prior to the composite mapping period, as displayed by Hondeklip Bay progressive wind vectors in Fig.34a. NW winds from 3-7 November were followed by light onshore winds from the 11th to the 20th. Strong SE winds and upwelling were observed

from 20-26 November, returning again to NW from the 27th to 1 December. It is likely that residual downwelling following the 3rd wind reversal enhanced the nearshore countercurrent to the S of the Olifants River Mouth. The duration of unseasonal poleward wind events, combined with the Cape Columbine wind shadow, could underlie the formation of warm coastal currents and red tide outbreaks in the southern Benguela region.

The November 1980 wind reversals over Namaqualand were induced by a persistent mid-level trough as described by the 700mb pressure anomaly chart, Fig.34b. The development of 3 cut-off lows interrupted the early summer equatorward wind stress pattern. In moving the pressure gradient further offshore, the leewards wake of Cape Columbine became enlarged. The vast horizontal extent of the headland's wake was made possible through the low inversion layers which accompany cut-off coastal lows. The warm countercurrent highlights the roles which vertical and horizontal wind shear play in producing differential upwelling along the SW tip of Africa.

OVERVIEW OF CASE STUDY FLOW DEPTH INTERCOMPARISONS

The comparisons which underlie case studies C and D may be likened to two instant frames of a cyclical moving picture. The frames are selected in order to contrast mesoscale spatial variations in two depths of flow. Macroscale weather

patterns provide the ingredients of horizontal pressure gradients and vertical thermal/wind constraints. The local topography along the SW tip of Africa then provides the variable friction and horizontal thermal gradients. In the deep flow cases a more homogeneous flow accelerates over the coastal mountains producing additional wind stress for upwelling. As the cycle progresses an inversion limits vertical atmospheric movement and the local topography then acts to deflect the shallow wind flow. Leewards wakes, cyclonic vorticity, and differential upwelling characterise the shallow cases. Warm nearshore countercurrents appear to seek out the mountain wind shadows when macroscale ingredients permit.

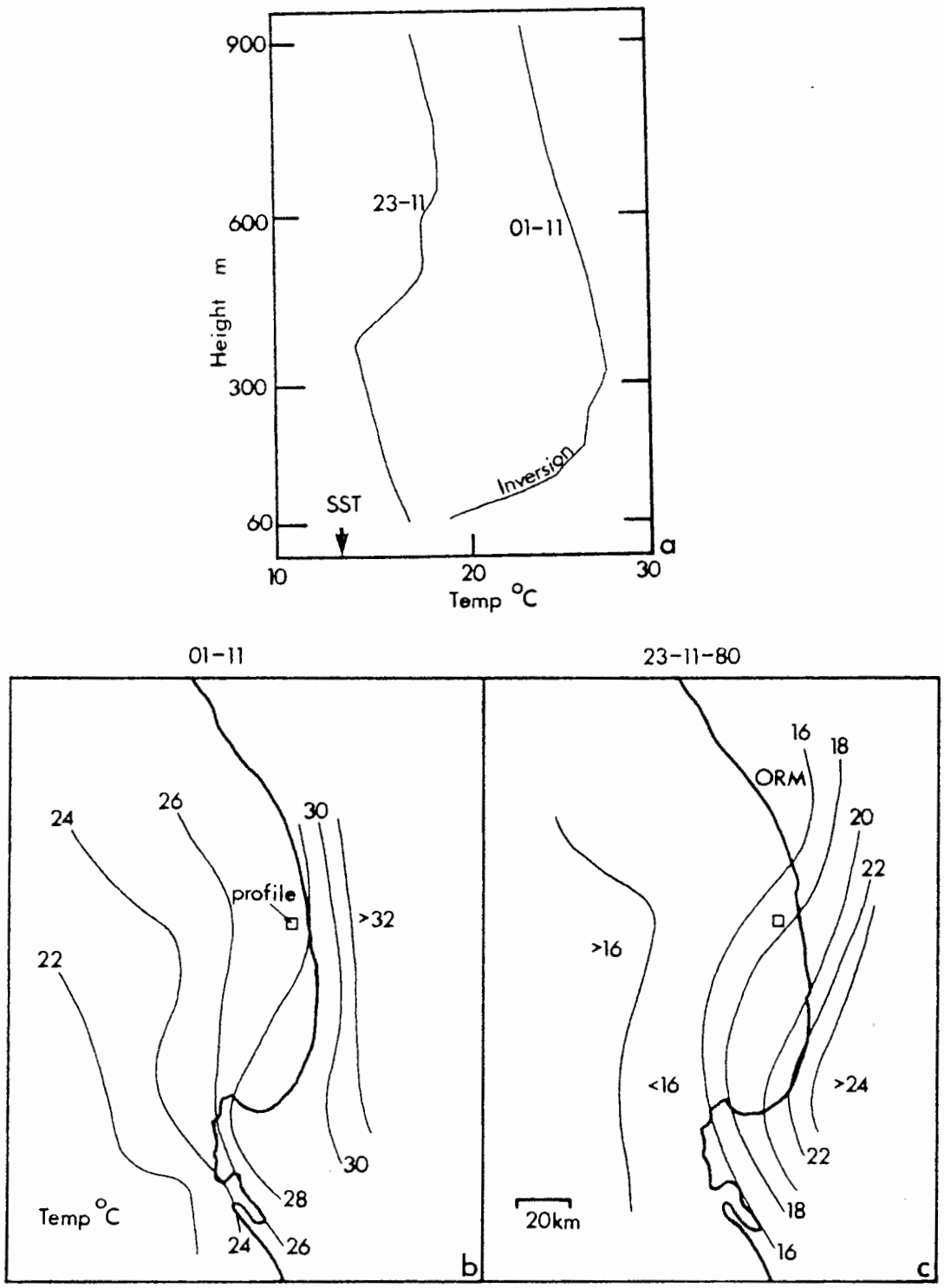

Fig. 29a : Vertical temperature profiles for the shallow and deep wind flow case studies. A pronounced low level inversion is seen on 1 November. Cooler temperatures aloft characterise the deep flow case.

29b,c: Comparison of horizontal temperature fields for shallow (1 November, left) and deep (23 November, right) case studies in the lee of Cape Columbine. In the shallow case warm air extends further offshore. The deep case is characterised by cooler air, particularly near the Olifants River Mouth (ORM).

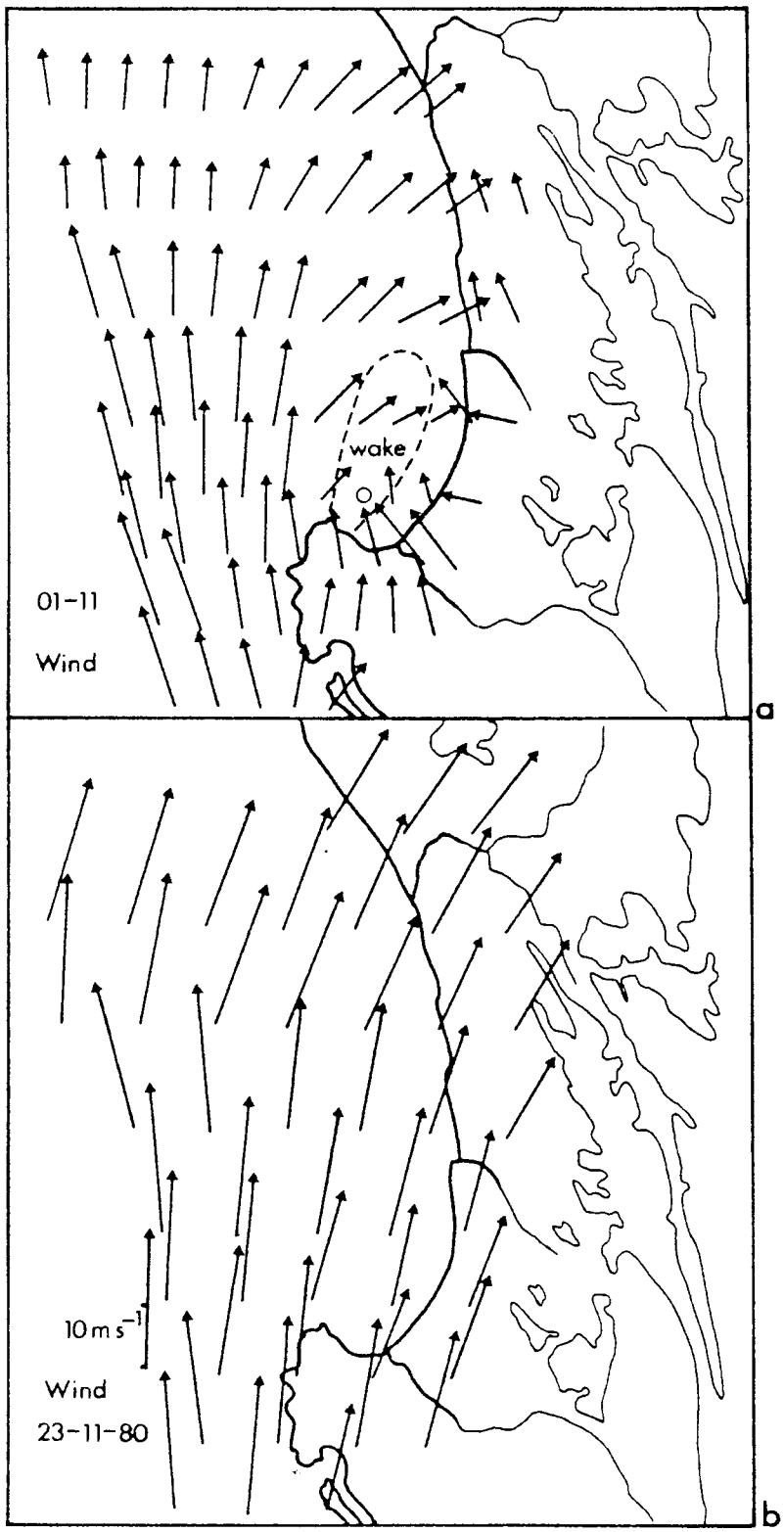

Fig. 30a,b: A comparison of shallow and deep case study wind vectors in the lee of Cape Columbine, 1 and 23 November 1980. A cyclonically curving wake shadow is cast by the headland in the shallow case. In the deep case study a more uniform flow is noted.

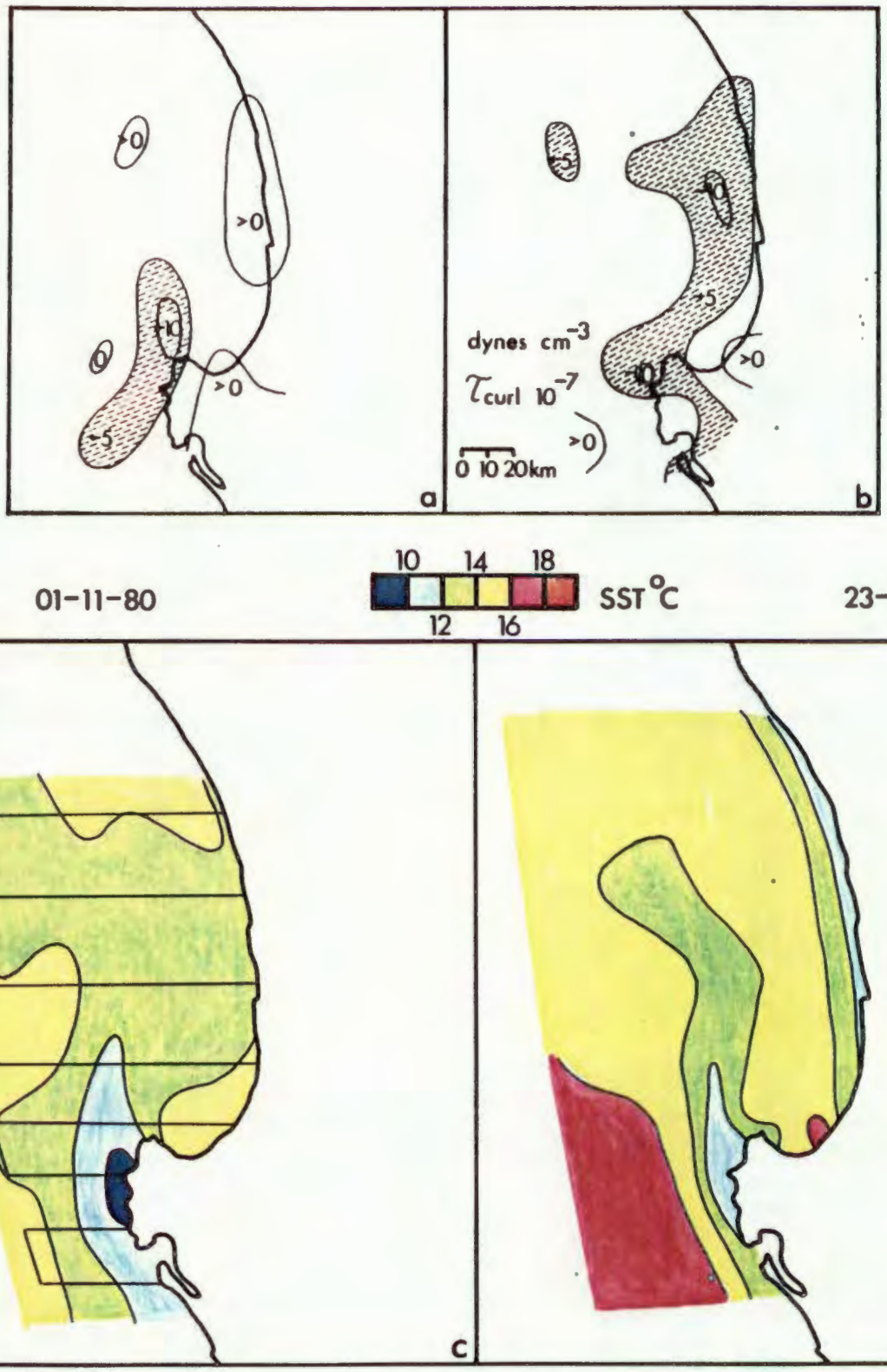

Fig. 31a,b: A comparison of shallow and deep flow wind stress curl distributions, 1 and 23 November 1980. Cyclonic curl is present over the headland in both cases. In the shallow case anticyclonic curl is found on the leewards coast due to topographic deflections.

31c,d: A comparison of SST distributions for shallow and deep flow cases, 1 and 23 November 1980. An upwelling plume persists at Cape Columbine. In St. Helena Bay upwelling activity occurs only during deep flow.

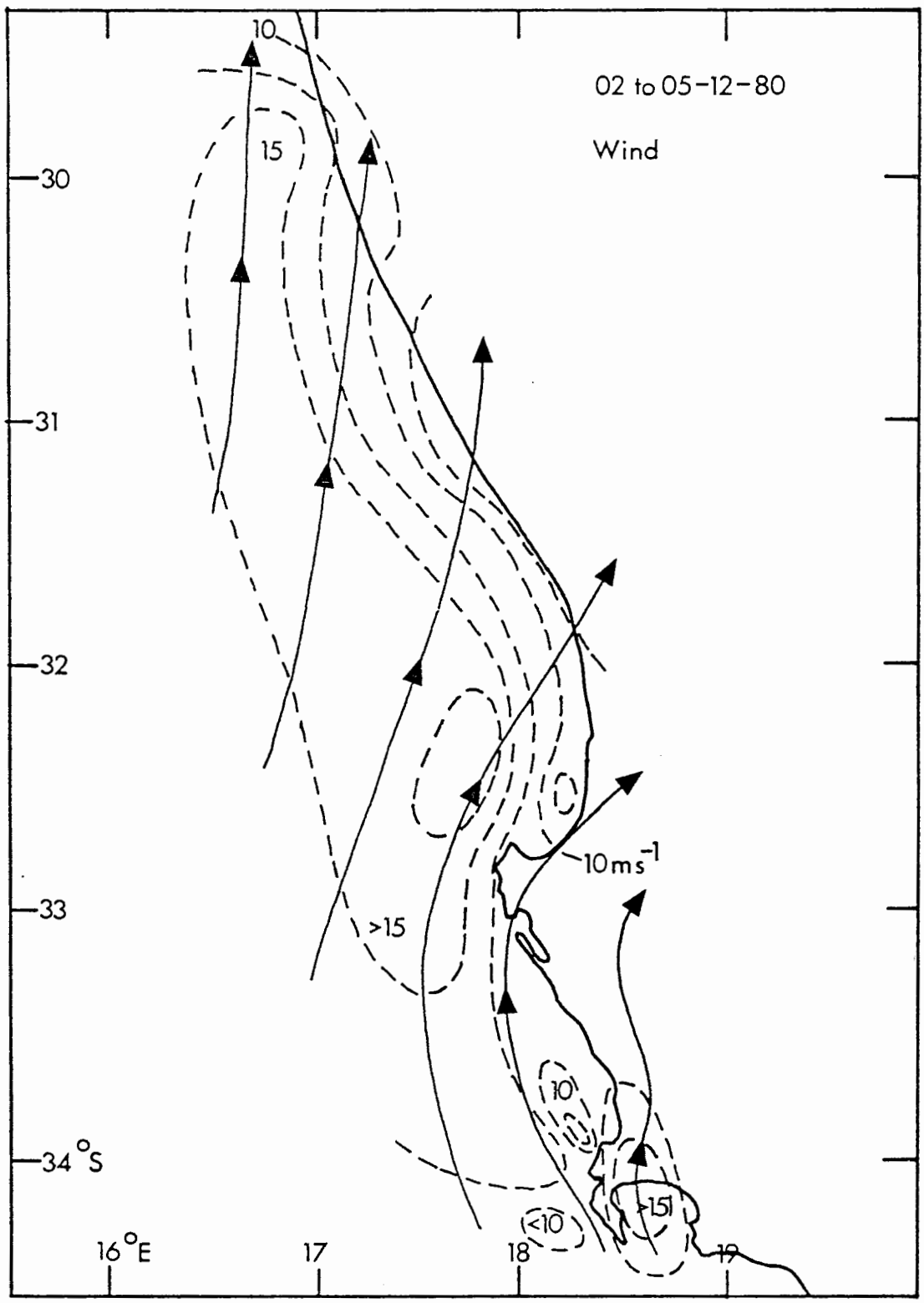

Fig. 32: A composite map of wind flow represented by streamlines and isotachs along the SW tip of Africa for the period 2 to 5 December 1980. Wind accelerations occur over False Bay and to the NW of Cape Columbine. A downwind wake extends northwards along the coast from St. Helena Bay.

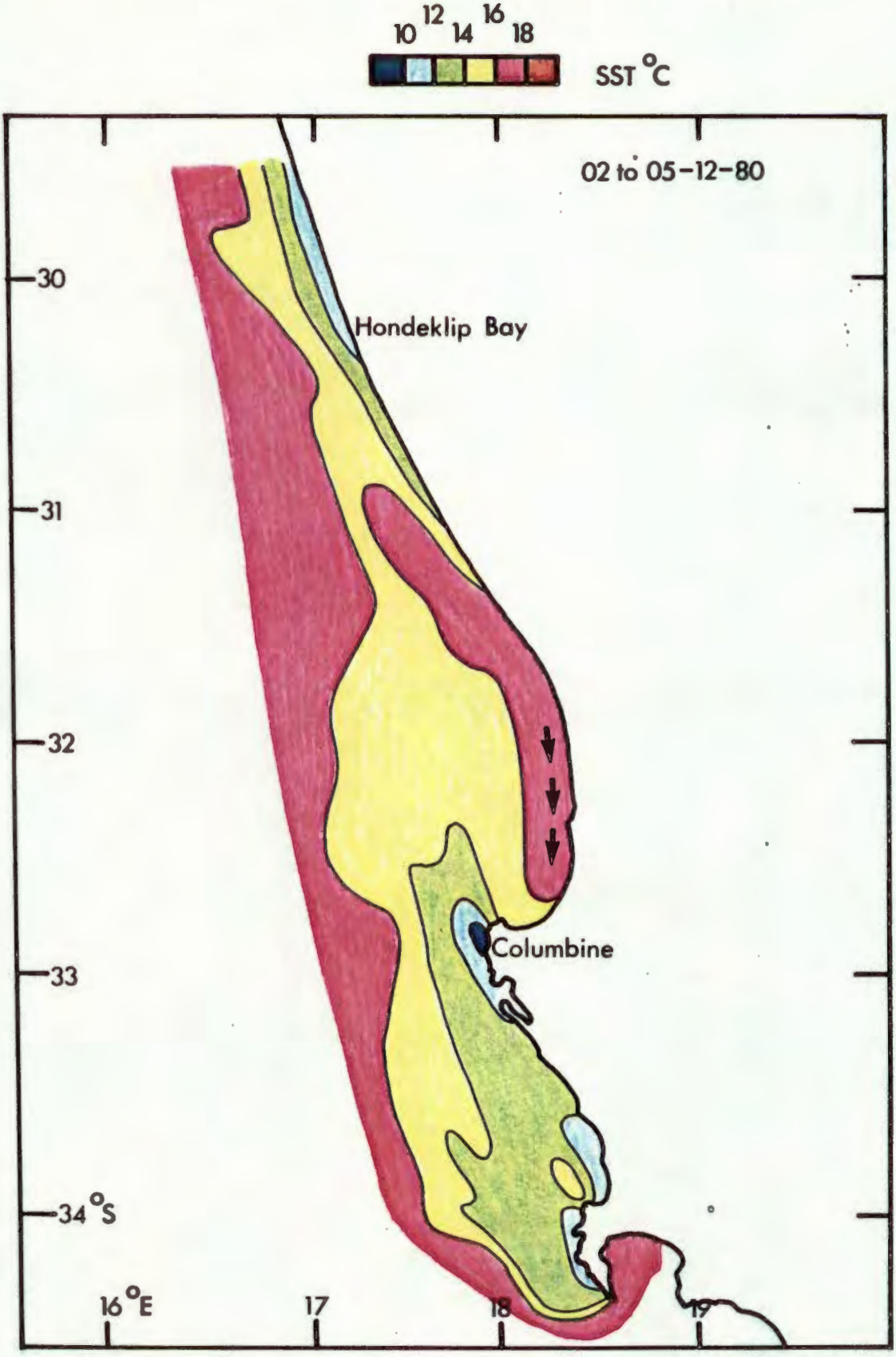

Fig. 33: A composite map of SST's along the SW tip of Africa for the period 2 to 5 December 1980. Upwelling activity is found along the Cape Peninsula, Cape Columbine and further north at Hondeklip Bay. A warm nearshore countercurrent persists along the coast north of St. Helena Bay due to the light wind wake.

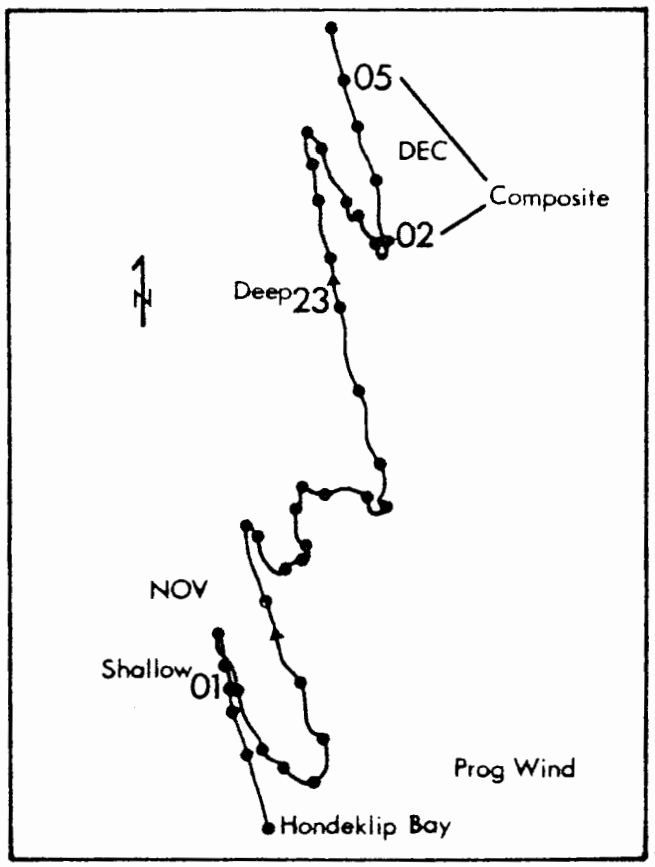

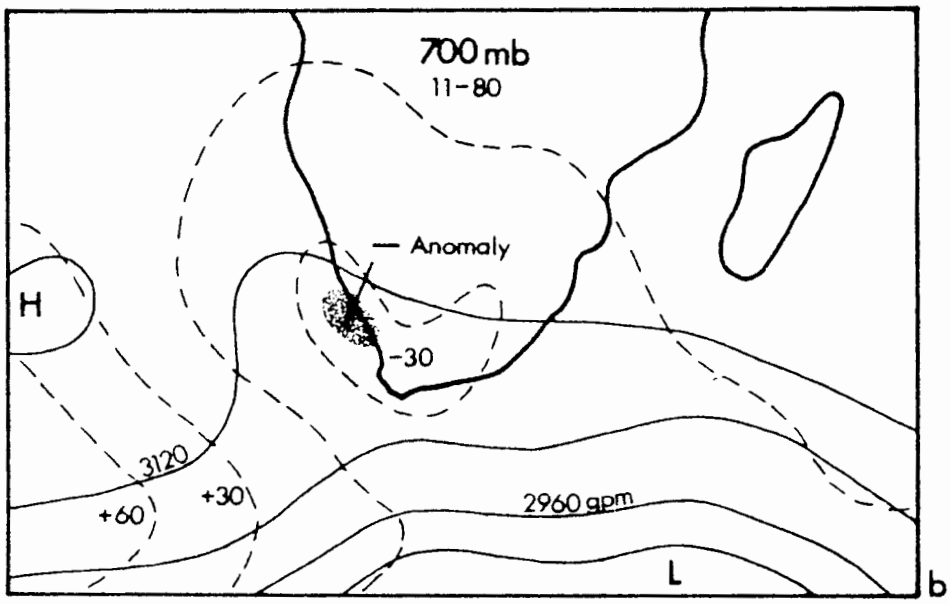

Fig. 34a: A progressive wind vector diagram from Hondeklip Bay for the period 29 October to 6 December 1980. Three major wind reversals occurred during the early summer.

34b: The 700mb level mean pressure and pressure anomaly chart for November 1980. A sharp negative anomaly is observed along the Namaqualand coast (shaded). The anomaly reflects the persistence of cut-off lows.

E. THERMAL CONTRASTS AND SEABREEZES DURING WEAK PRESSURE GRADIENTS

As the atmospheric pressure gradients relax, local surface friction and thermal contrasts begin to control the coastal wind field. A number of case study results were available during periods of weak pressure gradients which illustrate mesoscale wind eddies, seabreezes and a differential reduction of upwelling activity around the Cape Peninsula.

CASE STUDY OF A MOUNTAIN WAKE

A mesoscale wind eddy was observed on 29 January 1981 as gradient equatorward winds lulled briefly under an inversion layer. A diurnal cycle was observed in the coastal wind data. Seabreezes peaked at mid-day along the coast to the N of Cape Town. These were followed by a return to gradient SSE winds in the late afternoon. Aerial survey data, collected between the hours of 1000 and 1500 SAST, document the flow-deflected seabreezes and their causative mechanisms.

A wave-like perturbation was noted in the alongshore thermal front, Fig. 35a. This perturbation was caused by a convergent axis of marine air which penetrated the western Cape Flats. On either side, orographic deflections led to thermal buildups of warm, dry air leewards of Kogëlberg and Table Mountain.

Due to the atmosphere's vertical stratification, a divergence of wind flow occurred on either side of Table Mountain. This resulted in a downstream eddy, as seen in the wind vector pattern of Fig. 35b. In the wake area (enclosed by the dashed line) subsiding air and wake "capture" produced a reversed NW wind flow. In response to the contrasts in wind stress, the Cape Peninsula upwelling plume was split by warmer water (yellow) beneath Table Mountain's wake as shown in Fig. 35c. A tongue of cold water extended northwards from Table Bay, being driven by the Cape Flats jet. As vertical oceanic mixing is a function of wind speed, interactions across the wake interface were limited. SST gradients were observed to be spatially coincident with variations in wind stress.

The formation of orographically sheltered areas leewards from the coastal mountains is the first step in the downwelling cycle. The wake areas grow under descending inversion layers producing a differential reduction in upwelling. In these conditions thermal contrasts overshadow pressure gradients and seabreezes emerge as the dominant wind circulation.

SEABREEZE CIRCULATIONS

Weak pressure gradients often occur during transitions in synoptic-scale weather patterns along the SW tip of Africa, most notably after the passage of a coastal low and prior to the influences of westerly wave cyclones. During summers crosshore thermal contrasts of up to 10^{o}C per 10km drive a

seabreeze circulation around the Cape Peninsula between the hours of 10h00 and 15h00 SAST (coincident with aerial survey times).

Two seabreeze circulations were observed on 23 and 25 February 1980 resulting from a period of slack pressure gradients. The synoptic weather chart for the 23rd Fig. 36a, indicated that a weak low pressure area was approaching the SW tip of Africa. With the influence of the South Atlantic Anticyclone removed, equatorward winds and coastal upwelling activity were subdued. Vertical profiles during the seabreeze case studies were recorded by the local radiosonde at DFM Airport on the Cape Flats. Light NW flow and cool temperatures aloft characterise the profiles as shown in Fig.36b. Unstable atmospheric conditions with steep near-surface lapse rates could be specific to the radiosonde site landwards of the Cape Flats thermal front.

A cyclonic, clockwise rotation of the flow trajectories was apparent from the wind vector results on the 23rd and 25th (Figs. 36c and 37a respectively). In both cases SE winds of lesser magnitude rounded Cape Hangklip and became entrained into a southerly seabreeze over the western Cape Flats. Downstream from Table Mountain weaker westerly flow was drawn off Table Bay. This cool, westerly seabreeze accelerated on passing the coastline and moved inland towards the Berg Valley Thermal Low.

A distinction is drawn between the two cyclonic circulations by comparison of convergence zones. A line of convergence formed across the Cape Flats where the warm, gradient-assisted False Bay seabreeze over-rode the cool Benguela seabreeze. The convergence line had shifted southwards on the 23rd due to the dominance of the cool, undercutting seabreeze off Table Bay. On the 25th the warm southerly seabreeze off False Bay prevailed, driving the line of convergence northwards. A marked cyclonic curvature of marine wind trajectories summarises the pattern of mid-day seabreezes around the Cape Peninsula and adjacent headlands.

Seabreezes often persist during the late summer with the interior thermal low present and the South Atlantic Anticyclonic receding. In these periods differential upwelling activity diminishes considerably as exemplified by the 25 February SST field Fig. 37b. A weak plume (yellow-shaded) along the SW side of the Peninsula resided under the light equatorward winds. Oceanic inertia and bathymetric uplifting of the coastal water may have prolonged the plume's lifespan. A warm water countercurrent appears to have broken the OTF, entraining an eddy towards Oudekraal. During seabreezes the preferential area for upwelling relaxation is to the SW of Robben Island in the Table Mountain wind wake.

It is apparent from earlier case studies that the link between wind shear and differential upwelling remains

throughout the wind cycle. When cyclic amplitudes diminish, as in extended periods of seabreezes, a cyclonic streamline curvature of wind is observed. Wind shear values weaken but the upwelling plume retains its shape along the southern half of the Peninsula. To the N of Oudekraal cyclonic seabreezes bring warm water shorewards into a gyre which signifies the start of the downwelling cycle of importance to local fisheries.

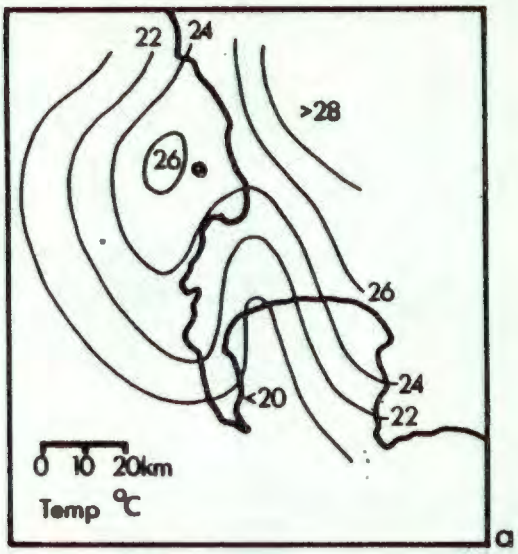

29-01-81

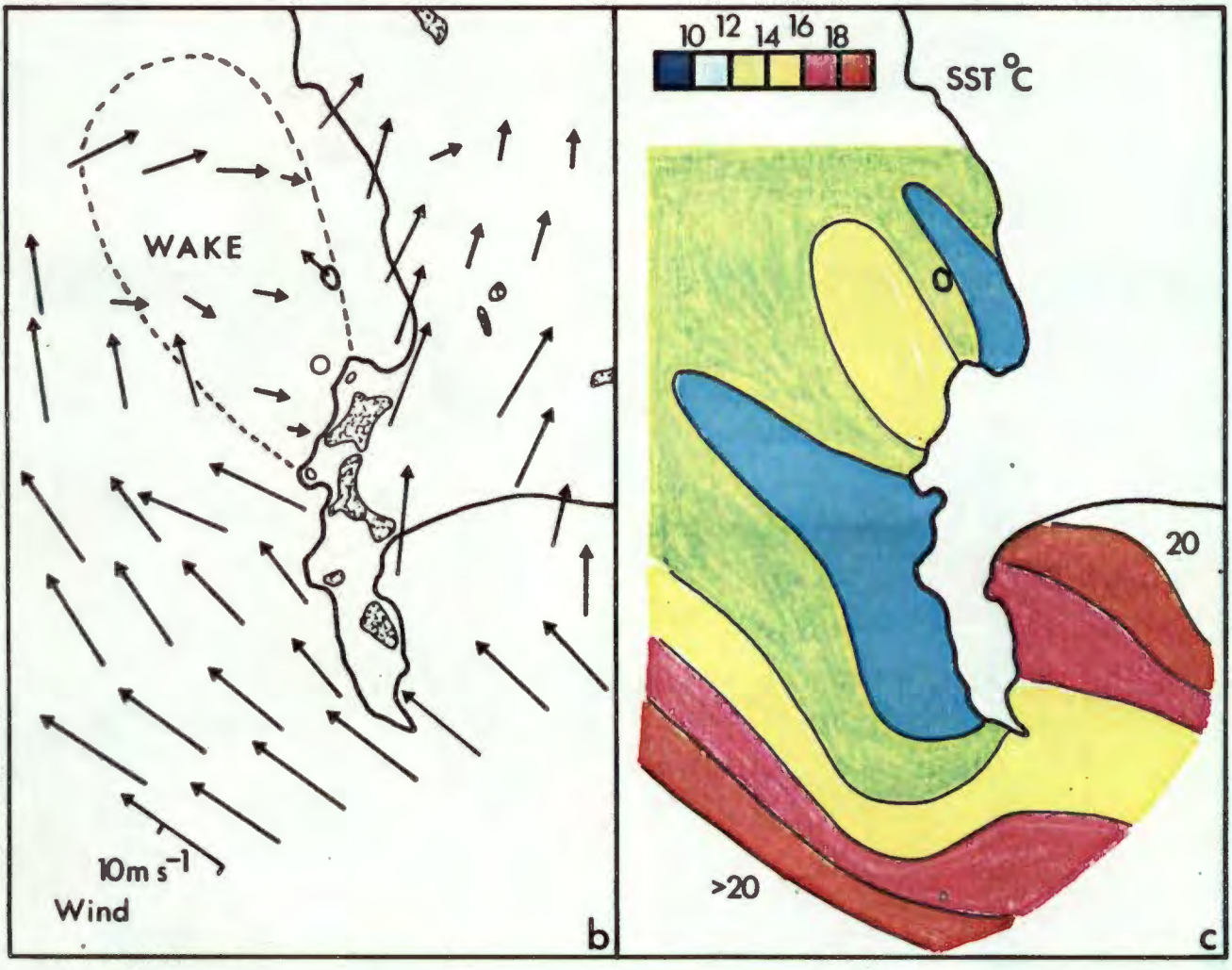

Fig. 35a: The air temperature distribution on 29 January 1981. An offshore perturbation in the thermal front (26°C) is noted leewards from the Peninsula.

35b: The wind vector representation on 29 January. The Peninsula's mountains (shaded) deflect alongshore flow leaving a leeward wake area.

35c: The SST distribution on 29 January. Upwelling plumes are observed off Olifantsbos and Table Bay. In the wind wake area, upwelling is diminished.

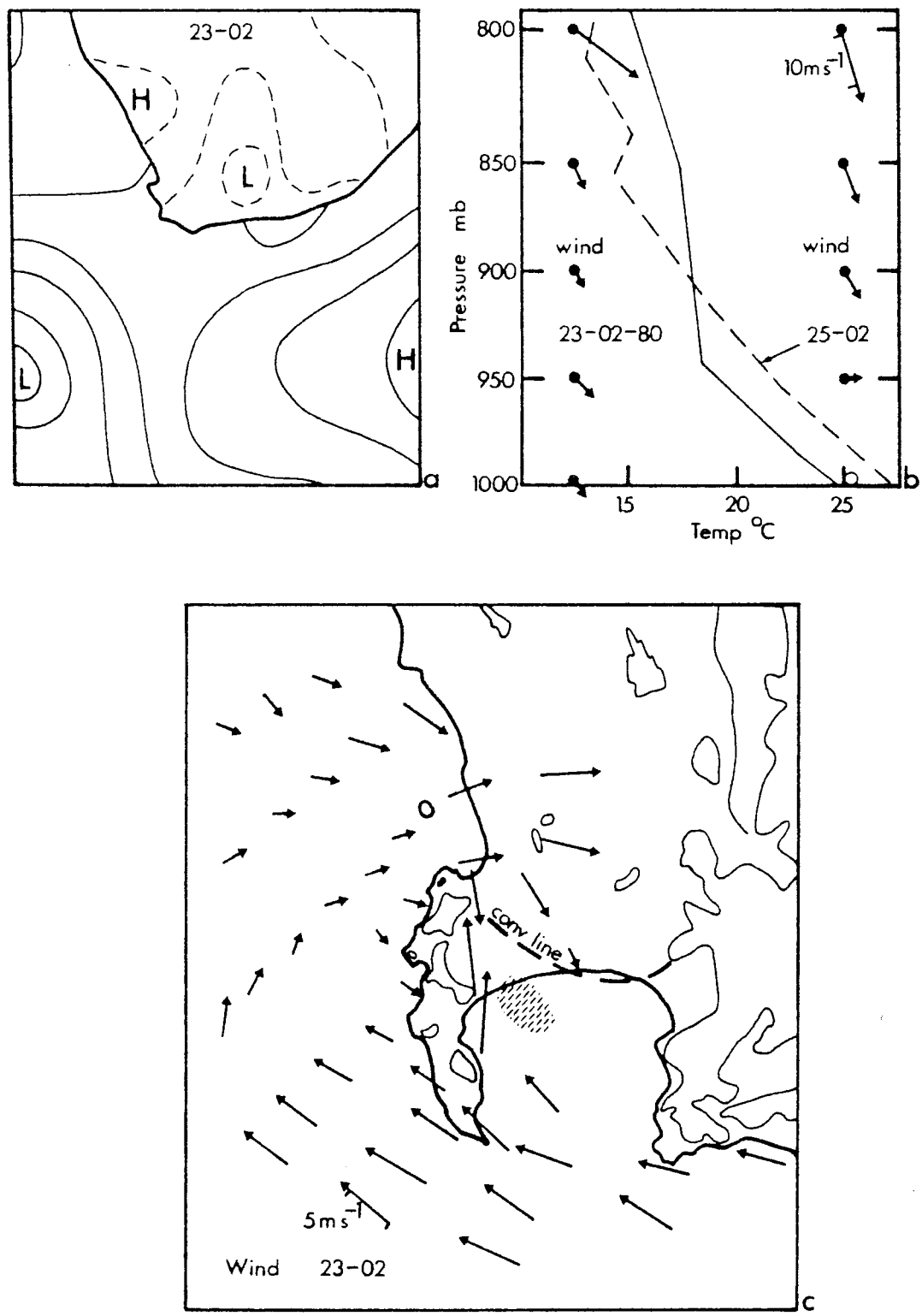

Fig. 36a: The synoptic weather map on 23 February 1980. A transition to an approaching low pressure system causes slackened pressure gradients.

36b: Vertical wind and temperature profiles for seabreeze case studies 23 and 25 February 1980. Cool air and NW winds aloft are typical during seabreeze conditions.

36c: A wind vector representation of a seabreeze on 23 February 1980. A line of convergence separates cool Benguela and warm False Bay seabreezes. The cyclonic vorticity maximum is shaded.

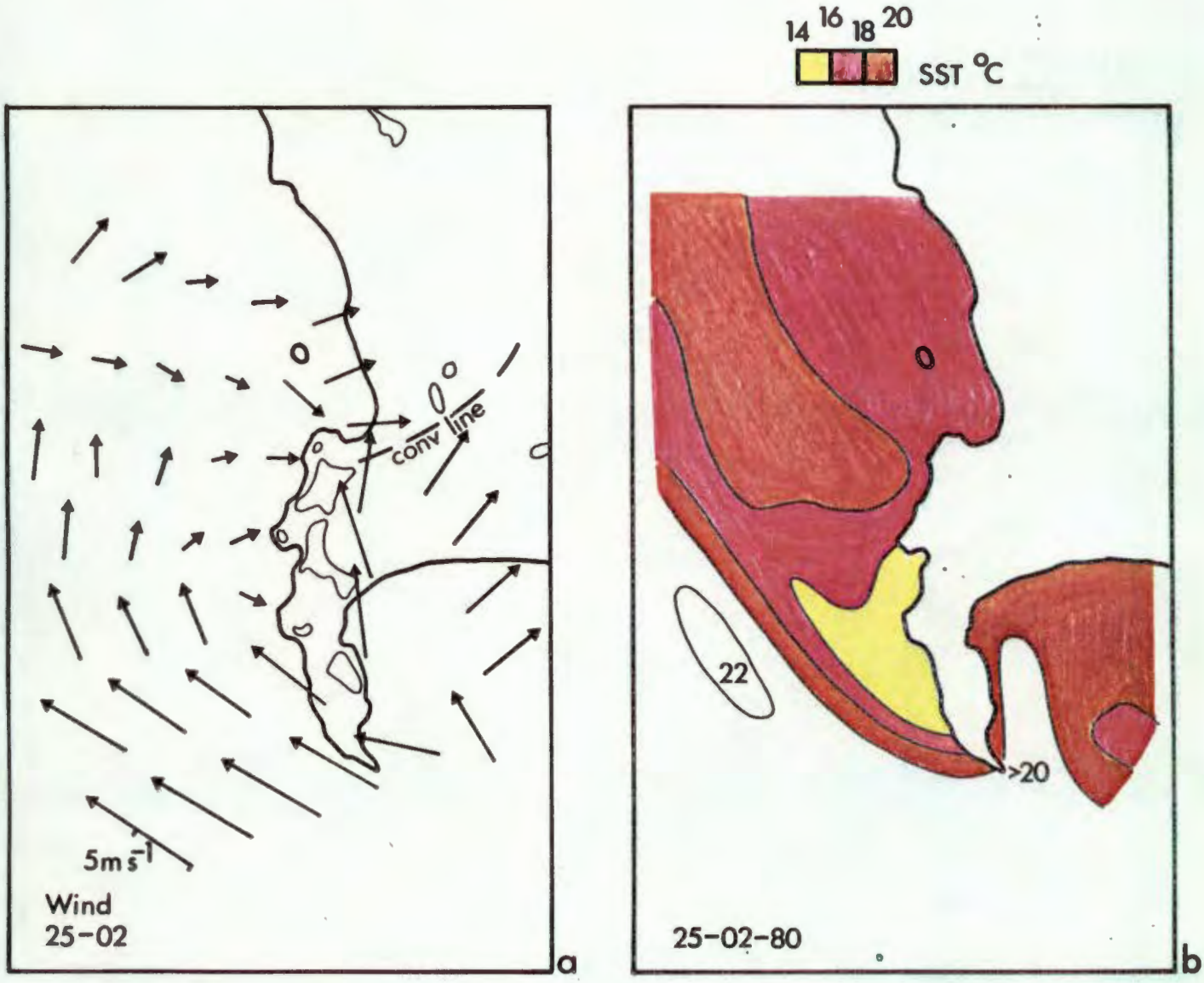

Fig. 37a: A wind vector representation of a seabreeze on 25 February 1980. The convergence line is located further north by comparison, as the False Bay seabreeze intensifies.

37b: The SST distribution on 25 February. During light seabreezes upwelling is diminished. Warm counter-currents move shorewards at Oudekraal and in False Bay.

F. DIURNAL PULSING OF WINDS AND UPWELLING OFF OUDEKRAAL

As part of a boundary layer study along the western side of the Peninsula, the SFRI deployed moored buoys to collect surface wind data in time series. Temporal cycles of wind shear and differential upwelling were investigated from this data base. Diurnal cycles were prevalent during the clear summer weather. In such conditions the downwind wake of Table Mountain was observed to expand and contract in sympathy with the horizontal temperature gradient and vertical inversion layer. Mesoscale wind cycles at Oudekraal, where mid-day breezes become nocturnal gales, were thought to "pulse" the upwelling activity. These interactive phenomena were investigated using an automatic marine meteorological station moored 2km west of Oudekraal during the period 18 to 21 February 1980.

Supporting flight data were gathered throughout the period of buoy deployment. A representative mesoscale meteorological pattern occurred on 19 February and selected parameter fields are discussed with relevance to the 24 hour cycle. Dewpoint temperatures at 152m reflected the sharp contrasts in orographically modified flow as shown in Fig. 38a. Moist air (16^{o}C) was observed along the convergent Cape Flats jet while leewards of Table Mountain a dry, subsidence trough (0^{o}C) indicated a lowering of the inversion layer. The rise and fall of this layer controls the diurnal cycle of

wind-forced upwelling at Oudekraal.

A SE wind "curved" from a 15 ms^{-1} maxima near Cape Point to a light SW seabreeze downstream at Robben Island, as illustrated in the vector map Fig. 38b. The winds on the 19th were shallow and unable to accelerate over Table Mountain. However on the previous night, time series data indicate that a descending inversion and the pressure gradient combined to produce a strong downslope jet. The jet "poured" off the mountain and accelerated along the inversion interface. This mechanism is summarised as follows.

The local orography is responsible for abrupt changes in the compression of the alongshore jet. Combined with these frictional influences is the daily cycle of heating and cooling which affects the thermal "lid". The inversion layer rises and breaks up during daytime heating, allowing wind flow over the coastal mountains with increasing depth but diminished speed. Towards evening the inversion interface descends, compressing flow against the orographic barrier. In this manner an accelerating downslope jet is formed at Oudekraal, triggering intense upwelling activity.

A cold plume was found to the W of the Cape Peninsula from SST data collected on 20 and 21 February 1980 Fig. 39a and b. A marked alongshore SST gradient was observed at the Oudekraal buoy position, along the NE edge of the plume. The

plume responded to the downslope jet by growing on the 20th. However by the 21st the cold plume had contracted under light winds and a warm pocket in Table Mountain's wake began shifting southwards in countercurrent fashion.

Time series information describing the downslope wind jet and upwelling cycles were available from data at the moored automatic weather station positioned off Oudekraal by the SFRI. V_T wind components and SST's for the period 18-21 February 1980 indicate that macroscale weather influences were overwhelmed by diurnal cycles as shown in Fig.39c. Nocturnal pulsing of the downslope jet occurred on the 18th and 20th in a combination of pressure and temperature contrasts. It is postulated that a steady state, finite-amplitude "hydraulic jump" gravitational acceleration further enhanced the downslope jet. SST's declined in sympathy as the cold, well mixed plume expanded over the buoy position. A pressure gradient "collapse" on the 19th and 21st prevented the nocturnal wind and upwelling pulse. Instead, SST's rose by $4^{o}C$ with the formation of a warm, southward flowing, nearshore countercurrent. The 4 hour response lag in SST's is correlated with the nocturnal pulsing of a wind shear axis off Oudekraal.

MICROSCALE WIND FLUCTUATIONS OFF OUDEKRAAL

Wind pulsing off Oudekraal was studied in greater detail by the SFRI using wind speed data from a 4 buoy array over the

period 16-20 March 1981. Equatorward winds were capped by a thermal inversion around 900mb (1000m) as illustrated in the radiosonde temperature analysis Fig. 40a. The level of the inversion remained nearly constant while temperatures aloft increased gradually. Manually observed marine wind speeds from the buoy positions (shown in Fig. 40b) were supplemented by land-based wind data at Oudekraal. A time series graph of the nearshore and offshore buoy wind speeds is compared with the Oudekraal data in Fig. 41a.

The prevailing 135° downslope wind jet was opposed by seabreeze influences between 1200 and 1400 SAST, coinciding with lightest speeds in both coastal and moored data. Wind speeds appeared more constant at the offshore positions while along the coast a nocturnal amplification was observed. It is inferred that the nocturnal downslope jet was limited to the coast to the W of Table Mountain. The limiting mechanism is postulated to be a rapid deceleration of the wind jet as it moves away from the constricting orography. Downslope winds which pour off the mountain deflect and then decelerate along the sea surface.

Average diurnal wind speeds were contrasted for the nearshore, offshore, and coastal positions in Fig. 41b. Marine winds (represented by the offshore buoys) declined to a minimum at 1000 SAST. Thereafter winds built up slowly to a peak during mid-afternoon. In contrast the coastal wind cycle

was phase-shifted 4 hours later. The time delay is attributed to a slow consolidation of the inversion "lid" following mid-day heating. Coastal winds lulled at 1400 SAST and peaked towards midnight. This pulsing enhances differential upwelling features along the boundary of the Table Mountain wake.

OVERVIEW OF SMALLER SCALE STUDIES

On smaller spatial scales the presence of vertical wind shear and orography interact to produce cyclonic wind stress curl and differential upwelling at Oudekraal. These phenomena occur on scales below the observational range of mesoscale aerial survey. Surface based instruments are used to document the abrupt changes near an orographic wake. The downslope wind jet is not an uncommon phenomena and both Kogëlberg, near Cape Hangklip, and Chapman's Peak, to the S of Hout Bay, have downslope jets which operate with identical mechanisms. Atmospheric stratification and an inversion interface were found to be necessary ingredients for the nocturnal jet at Oudekraal. The hydraulic jump theory best fits observational evidence as an explanation for this phenomenon. The jet pours onto the ocean surface along the coast at Oudekraal, enhancing the frictional drag coefficient and local upwelling.

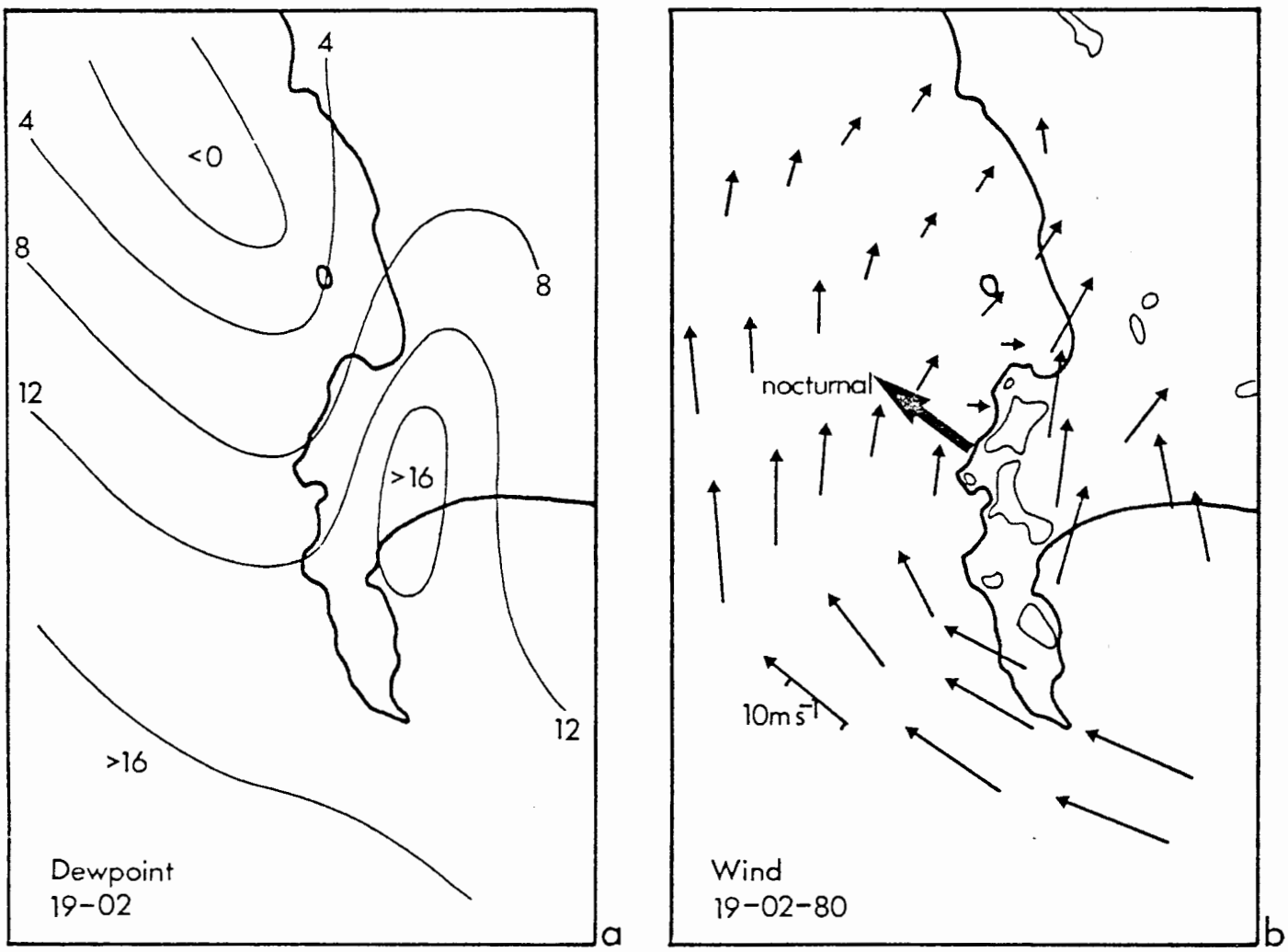

Fig. 38a: The dewpoint temperature distribution on 19 February 1980. Moist convergent air (16°C) in western False Bay is contrasted with dry, subsidence conditions in the lee of Table Mountain.

38b: A wind vector representation on 19 February 1980. Cyclonic curvature of alongshore flow is noted. The nocturnal downslope jet is shown at Oudekraal.

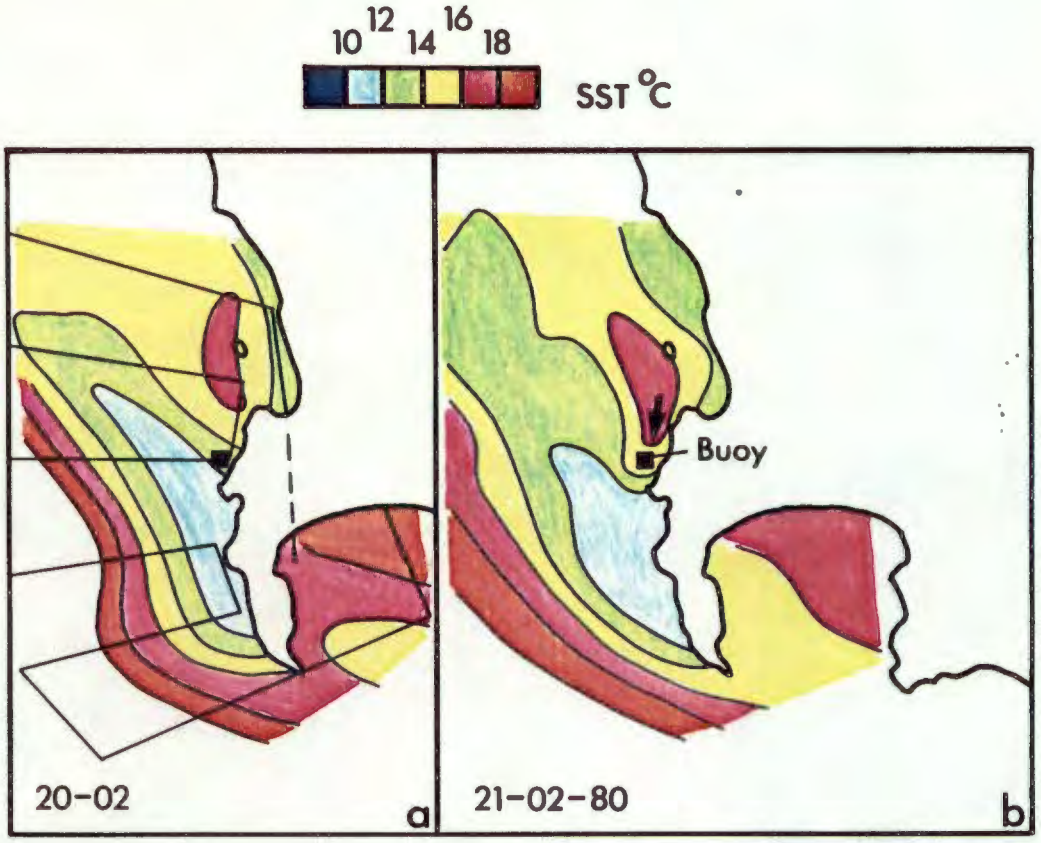

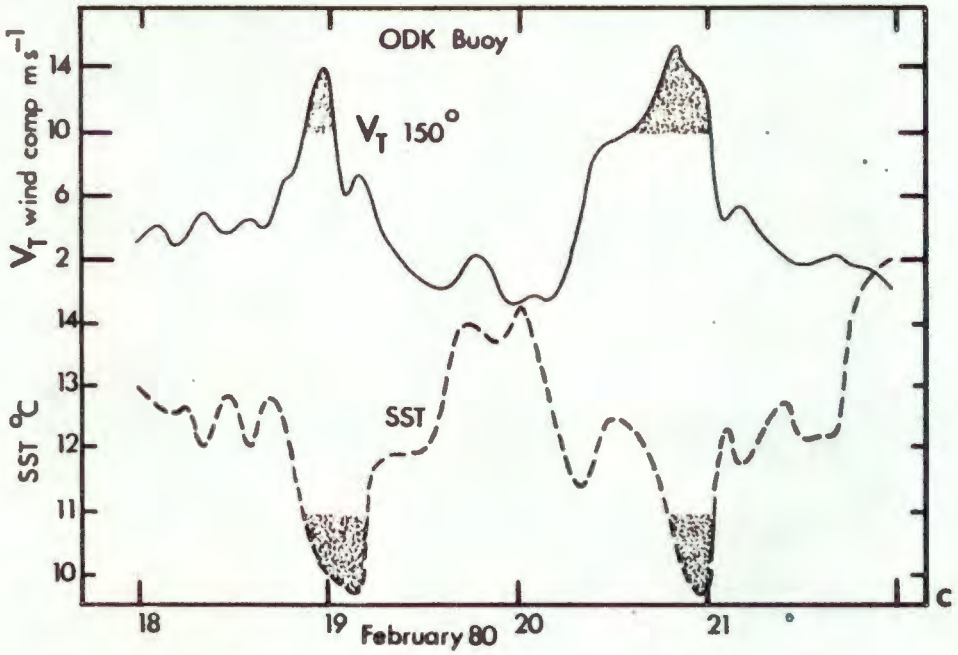

Fig. 39a, b: A SST distribution sequence for 20 and 21 February 1980. The upwelling plume spreads northwards on the 20th. The following day a warm nearshore countercurrent develops at Oudekraal. The flight track and buoy position are shown.

39c: The longshore V_T wind and SST data from the Oudekraal moored buoy for the period 18 to 21 February 1980. A distinct inverse correlation is observed which highlights the quick response of local upwelling to wind forcing.

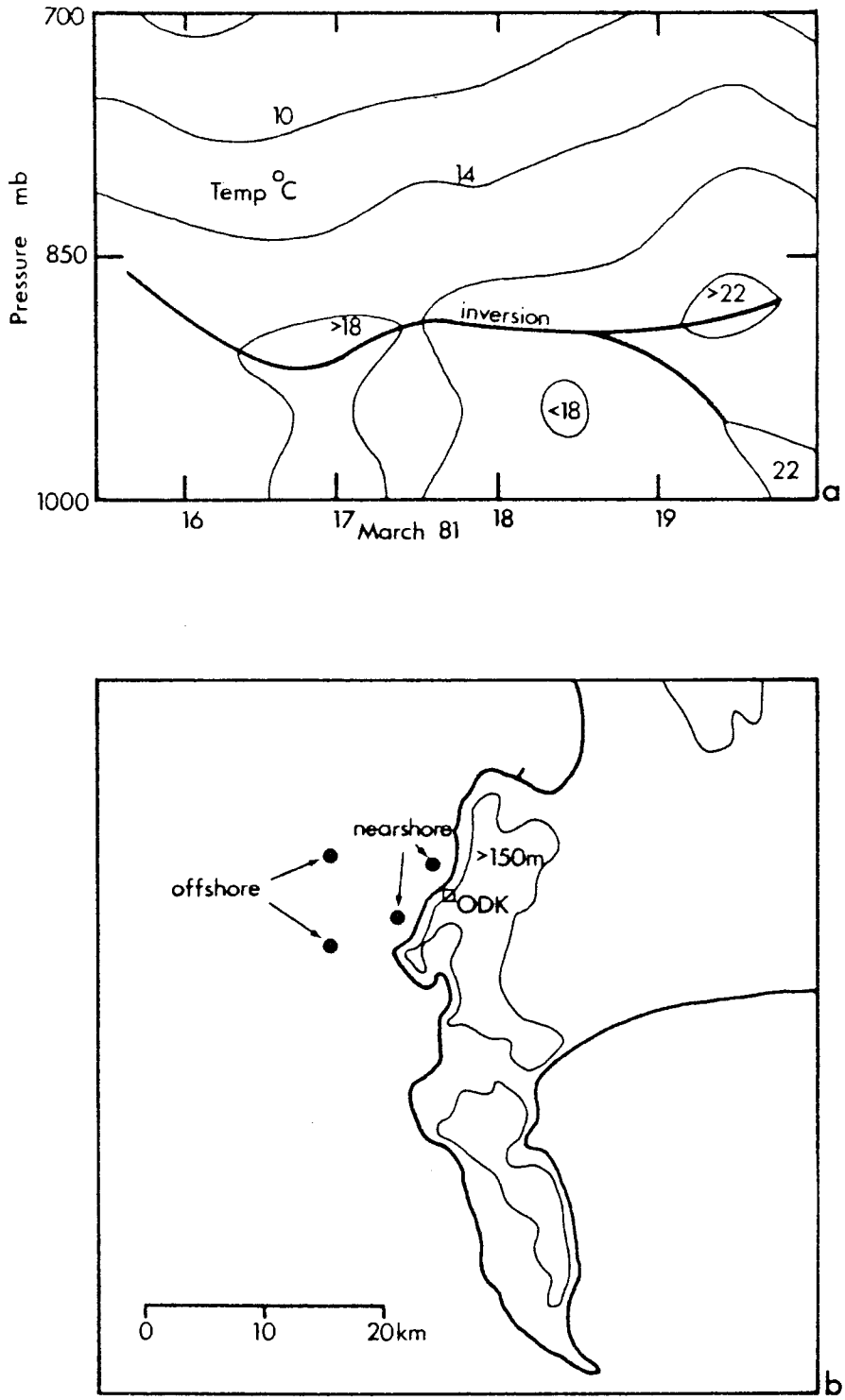

Fig. 40a: The radiosonde temperature time series for the period 16 to 22 March 1981. A temperature inversion layer is present near 900mb throughout the period.
40b: A reference map showing the positions of the buoy array and the Oudekraal (ODK) weather station.

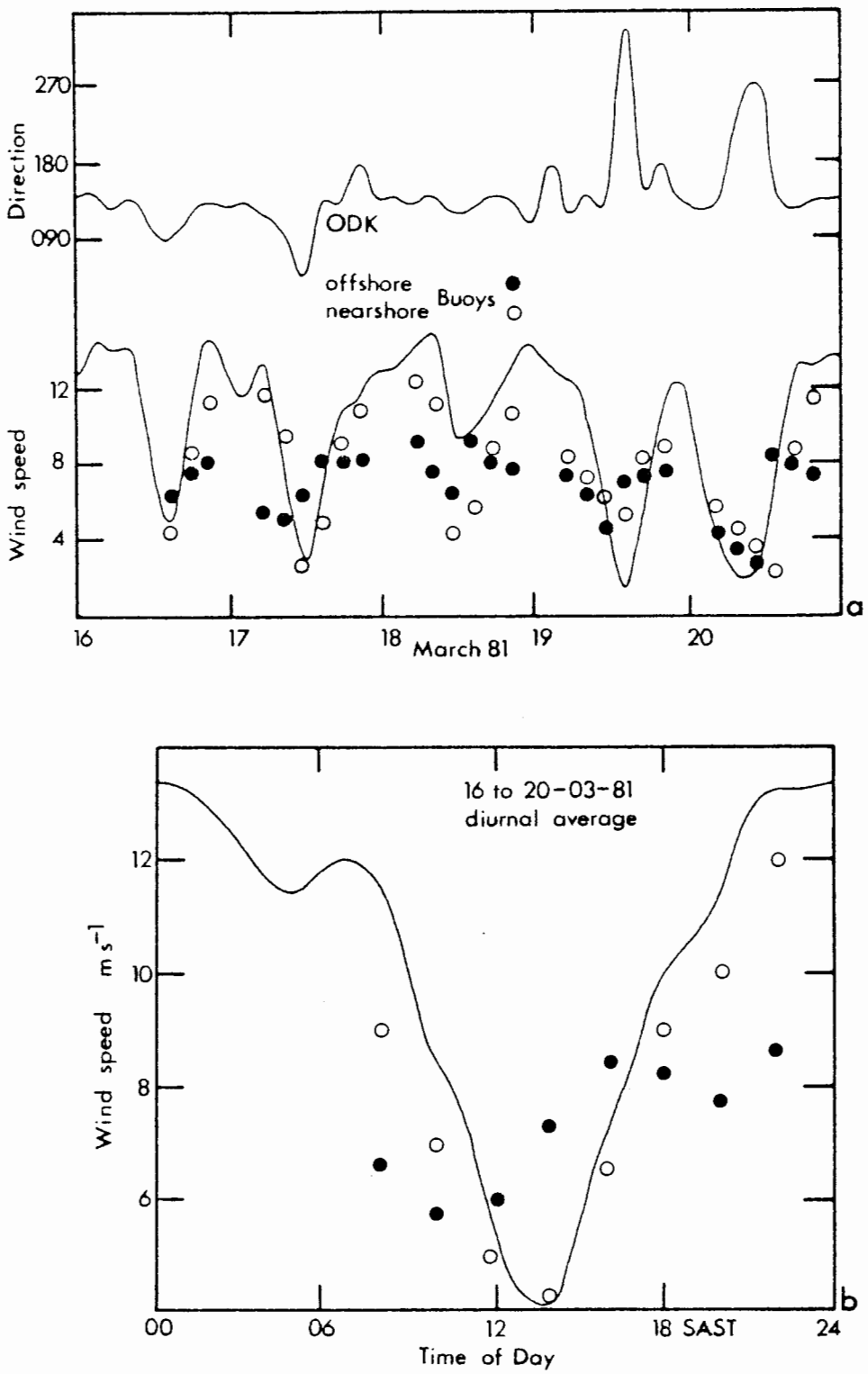

Fig. 41a: A time series comparison of moored buoy and coastal wind data for the period 16 to 20 March 1981. Diurnal cycles are evident in the downslope wind jet to the lee of Table Mountain. These cycles are highlighted by averaging over each hour in (b).

41b: The average diurnal wind speed observed at the coastal, nearshore and offshore positions. Lowest speeds occur at mid-day. The downslope jet becomes activated in the evening. The data void in the early morning hours was due to the manual method of data gathering.

CHAPTER 4: SUMMARY AND CONCLUSIONS

Wind shear driven coastal upwelling features have been described along the SW tip of Africa using mesoscale aerial survey observations. These results are embedded in a geographically unique setting consisting of mountainous peninsulas jutting seawards between the subtropical and temperate latitudes. Unlike other coastal upwelling areas, the west coast of Africa terminates abruptly at 35°S with no poleward land mass. The warm, Agulhas current flows near the cool, upwelling Benguela current off the SW tip, creating sharp contrasts in nearshore sea surface temperatures. The South Atlantic Anticyclone (SAA) and an interior low pressure cell create a favourable summer-time pressure gradient for equatorward winds. Temporal fluctuations in coastal upwelling activity result from the cyclical modulation of gradient winds by the interaction of the SAA and transient wave cyclones of the circumpolar jet stream.

On smaller scales topography and vertical wind shear play dominant roles in perturbing the alongshore wind. The topographic irregularities inherent along the SW tip of Africa ensure a variable surface friction and wind stress over the adjacent sea. The key to the formation of cyclonic wind stress curl areas off the coastal headlands is the depth of flow. In developing the observational techniques to illustrate these phenomena, a background in mesoscale wind

driven upwelling research was sketched.

The background of information linking wind stress curl to alongshore variations in coastal upwelling was explored in Chapter 1. From the literature review a synthesis of two observation and analysis methods was formulated. These techniques utilize the gathering of mesoscale wind data by aerial survey and the processing of data by digital matrix analysis. The resolution of wind data into a uniform matrix array and the use of centered differencing techniques to identify mesoscale wind stress curl areas is a significant development in upwelling research. Through reduced time and space observational scales, the realignment of atmospheric and oceanic thermal fronts along the SW tip of Africa led to the subjective recognition of case study patterns.

The aerial survey data gathering procedure was outlined in detail in Chapter 2. The flight levels and sampling media were standarized for comparison with other mesoscale studies conducted in eastern boundary currents. The mesoscale aerial survey data gathering technique was customized to suit local time and space scales and a flexibility in scheduling and grid resolutions provided an insight into the mesoscale motions interacting along the coast. Of particular note was the aerial survey technique of sequential composite mapping with data analysis accomplished in near real-time. An operationally oriented interpretation of mesoscale wind and

upwelling patterns is required in the southern Benguela due to the high frequency of temporal cycles. In this manner physical environmental anomalies may be translated into timely and effective fisheries management policies.

In Chapter 3 selected case study results were presented using progressively diminishing time and space scales. Sequential case studies covered the cyclic events with periods from days to weeks and showed changes in wind and upwelling distributions with time. Individual case study days followed the sequential format. Various mesoscale dimensions were used in conjunction with synoptic time scales. Selected stages of two wind event cycles were compared and related to the central wind shear- differential upwelling theme. In the final case studies even smaller time and space scale were utilized to investigate diurnal seabreezes and thermally constrained downslope wind jets. Significant contrasts within these mesoscale phenomena were described using boundary layer data. Again, vertical wind shear was observed to play a prominent role in enhancing topographic friction on the microscale.

Case studies A and B chronologically illustrated wind shear and differential upwelling patterns over two 11 day cycles. The transient low level wind jets, coastal geometry and upwelling plumes were found to be spatially correlated to the W of the Cape Peninsula and within False Bay. A three

dimensional view of coastal winds using transect data indicated that vertical stratification determines the level of topographic deflections and differential upwelling. The origin of the Cape Hangklip upwelling plume and a nearby warm countercurrent were traced to the topographic channeling of a wind axis in semi-enclosed False Bay. The sequential case studies conclude that wind shear persists along the coastal mountains throughout the cyclic modulation of winds.

Case study results for individual days (C and D) were used to contrast the mesoscale variation of wind stress and vorticity. Different stages of the inversion cycle were chosen to interrelate the depth of flow with topographic controls (schematically shown in Fig.42a and b). Comparisons indicated that an alongshore thermal front becomes perturbed in the shallow flow depth cases. The temperature "wave" causes topographic controls to extend further seawards, particularly off Cape Columbine, Cape Hangklip and the Cape Peninsula. During the presence of a low inversion layer the alongshore wind jet was found to be deflected seawards by the coastal mountains. Downwind wakes or wind shadows inhibited upwelling and a differential pattern emerged. In a composite case study off Namaqualand, the formation of a warm, nearshore countercurrent was observed. A persistent cut-off low enhanced the inversion and led to a collapse of seasonal upwelling in the northern, topographically uniform portion of the study region.

Observations of thermal/diurnal effects, which operate on diminished time and space scales, form the third set of case study results in Chapter 3. As the SAA recedes eastward and the winds slacken, standing vorticies emerge downstream from the coastal mountains. At the wake boundaries, downslope wind jets form and abate in sympathy with the 24 hour thermal cycle. One example of this phenomenon (case study F) is the nocturnal maximum in wind/upwelling activity at Oudekraal, attributed to accelerations along an inversion interface as depicted in Fig.43a. The downslope jet pours onto the sea surface imparting additional stress curl and enhanced frictional drag (Fig.43b) before converging downstream.

With the collapse of pressure gradients, temperature contrasts between land and sea cause seabreeze circulations during mid-day. Two distinct seabreezes, the cool Table Bay westerly and the warm False Bay southerly were identified in case study E. These circulations were characterised by a cyclonic curvature around the Cape Peninsula and a convergence line across the Cape Flats. Light, summer winds result in onshore flow and upwelling relaxation to the NW of the Peninsula. Wind shadow zones were found to be particularly susceptible to seabreeze entrainment.

One of the aims of this thesis is to show that the physical processes which drive the southern Benguela upwelling gyres are interrelated in a descriptive framework. Another

important goal is the mesoscale quantification of these forcing functions. The differential upwelling circulations along the SW tip of Africa were accounted for by horizontal wind shear acting on scales of 10-40km. Vertical wind shears of $-2(10^{-2})s^{-1}$ were translated by surface friction into horizontal wind vorticities of $-6(10^{-4})s^{-1}$ and wind stress curl values of $-2(10^{-6})$ dynes cm^{-3}. The descriptive framework built up by the case studies includes a number of common points:

(1) a spatial relationship exists for topographically channelled winds, upwelling plumes and countercurrents,
(2) vertical stratification plays a dominant role in the production of wind stress curl and differential upwelling by capping and enhancing surface friction.
(3) atmospheric and oceanic thermal fronts react to orographic divergence and horizontal wind shear by perturbing out of coastal alignment, and
(4) low level winds accelerate over portions of the southern Benguela current through deflections forced by three pronounced capes.

The individual case studies each add a further dimension to this descriptive framework. Sequential and composite studies of wind/upwelling events have identified that:

(1) the upwelling circulations next to the headlands respond

quickly to wind forcing with cold plumes growing and decaying over a short lifecycle,

(2) seabreeze circulations develop during summer afternoons following a slackening of pressure gradients and are characterised by a cyclonic confluence of wind and an upwelling relaxation,

(3) a late evening peak in wind/upwelling activity occurs off Oudekraal due to the interaction of a topographic downslope jet and a sharp inversion interface aloft,

(4) the persistence of cut-off low pressure systems is linked to a collapse in seasonal upwelling off the SW tip of Africa,

(5) wind shear driven cyclonic circulations in False Bay cause a cold plume off Cape Hangklip and a warm countercurrent in Koëlbaai, and

(6) equatorwards winds of $20ms^{-1}$ may reverse under a capping inversion during their traverse of the mountainous peninsulas.

In the sequence of wind/upwelling events a coincident growth and decay in the temperature inversion or wind shear layer is observed. This secondary effect, from the adjustment of macroscale pressure cells, controls the topographic susceptibility of surface winds. In case studies A, C, and D the comparison of deep and shallow flow fields indicates the importance of the inversion layer. When vertical wind shears dip below 500m, horizontal vorticities result from

topographic friction. Wind stress curl values then build up next to the coastal mountains at Cape Hangklip, the Cape Peninsula and Cape Columbine. The marked alongshore variability in upwelling rates is ascribed to the interaction of flow depth and topography in the case studies in Chapter 3.

The above results reflect site-specific mesoscale phenomena which are paralleled in other international studies. Similar techniques of data gathering were employed to investigate the dynamics of downslope winds and leeward waves over the Rocky Mountains of the U.S. (24,52,76) and off Hawaii (64). Along the Washington coast, topographic flow patterns and mesoscale convergence were described from a combination of surface and aerial survey data (56,57). Wind shear patterns in the Somali jet were studied utilizing PIBALS (4) and aerial survey techniques (17). Using the observational studies as a foundation, other investigators have pursued three dimensional modelling of topographic flow patterns under varying conditions of stratification (18,75). Of particular relevance is the air-sea interaction modelling study of a seabreeze upwelling regime by Clancy et al (23). Oceanic response to longshore wind and seabreeze forcing and air-sea feedback during upwelling was investigated in the model through idealized numerical experiments. In developing the data base to construct and verify these models, aerial survey has been shown to be an efficient means of gathering synoptic

time scale information on transient mesoscale phenomena over remote coastal regions, particularly through this thesis along the SW tip of Africa.

Many gaps in knowledge, concerning the alongshore variation of upwelling in the southern Benguela, have been answered by the results presented in this thesis. The duration and intensity of standing vorticies embedded in the surface summer wind field has been attributed to the orographic wakes which form downstream of the coastal peaks. Along the wake boundaries positive feedback mechanisms enhance and maintain the extreme horizontal wind shear. As the coastal wind jet becomes compressed over the orography, offshore oriented accelerations occur. The jet is forced downward along an inversion interface, pouring onto the sea surface in a hydraulic jump with substantial turbulence and additional wind stress imparted via the enhancement of the frictional drag coefficient. The standing vorticies formed by the convergence of deflected flow and the alongshore jet (Fig.44), are spatially related to cold plumes of upwelled water. The sheltered wake areas in the "shadow" of the coastal peaks are characterised by positive sea temperature anomalies which act as a source for nearshore countercurrents. With these field data utilized as input and verification, numerical modelling of southern Benguela upwelling should move ahead with stimulating results.

Many new questions arise from the observations and hypotheses presented in this thesis. Additional research is necessary in the determination of vertical and horizontal wind shear, drag coefficients and turbulence leewards of Kogëlberg, Chapman's Peak, Oudekraal, and Stompneus. Time series measurements using marine based wind sensors would enable a better understanding of marine boundary layer conditions and downslope wind stress enhancement in these regions. A real time monitoring of anomalous synoptic-scale weather patterns, as shown by selected indicators, could lead to a more effective management of fisheries resources. In this regard, time-dependent coastal circulation models need development to enable the forecasting of Agulhas water penetration, Benguela current gyre spin off, oceanic thermal front realignment, upwelling relaxation, and nearshore countercurrent formation. Satellite remote sensing (ie. SEASAT) is beginning to provide direct data inputs to such modelling problems.

It is the unique coastal geometry of the SW tip of Africa which produces cold plumes and warm water pockets via wind shear. These mix during transitional phases of the meteorological cycle to provide a suitable environment for marine bioproductivity. This thesis has demonstrated a spatial relationship between mesoscale meteorological and physical oceanographic patterns. Understanding the interactions between wind shear and differential coastal upwelling processes is a step towards sustaining the renewability of one of the earth's many finite resources.

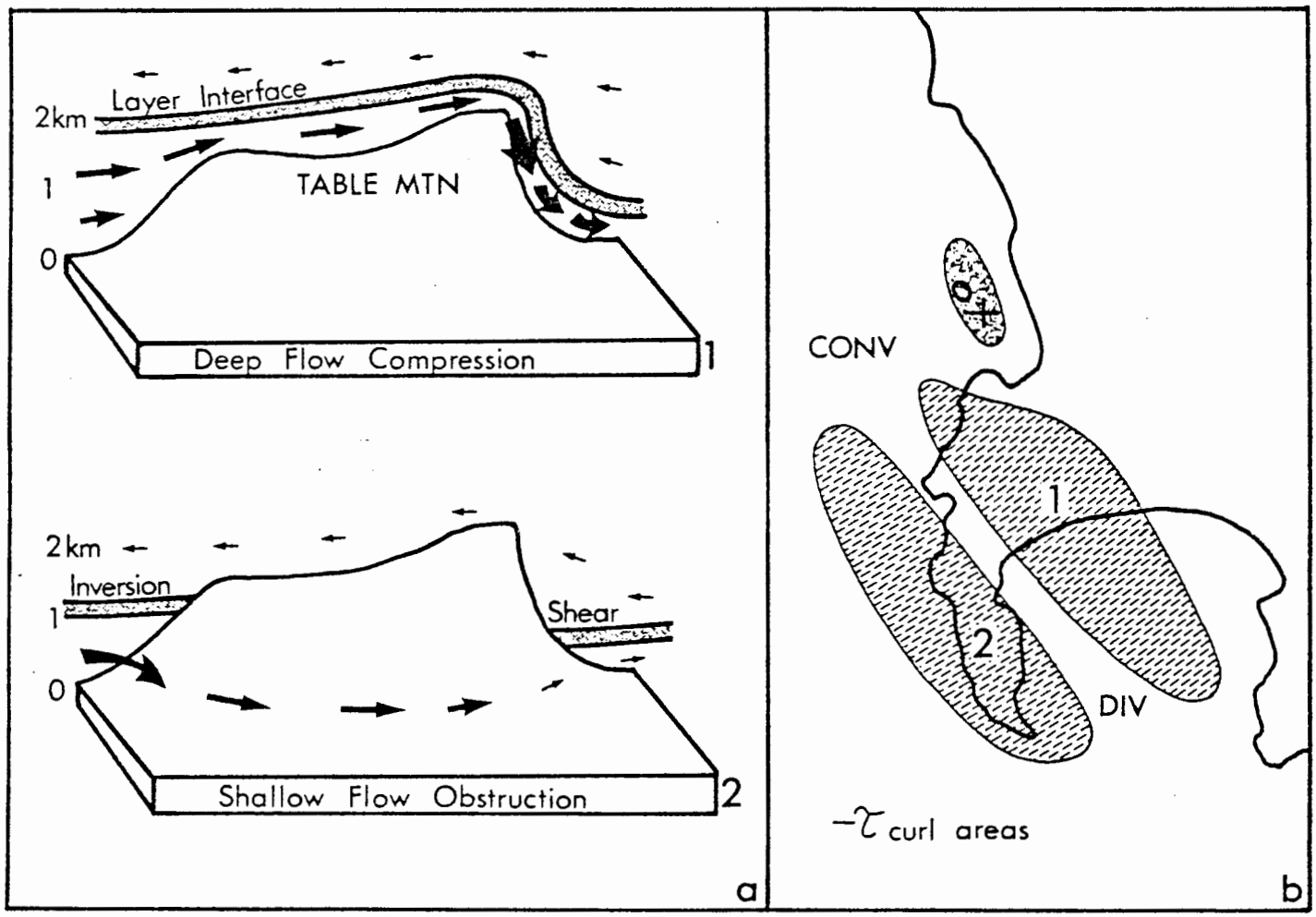

Fig. 42a: A schematic comparison of different flow depths in the vicinity of Table Mountain. Deep flow accelerates over the mountain while shallow alongshore winds are deflected around.

42b: A schematic representation of cyclonic wind stress curl areas in deep (1) and shallow (2) flow. The cyclonic maximum moves southwards and offshore as an inversion descends.

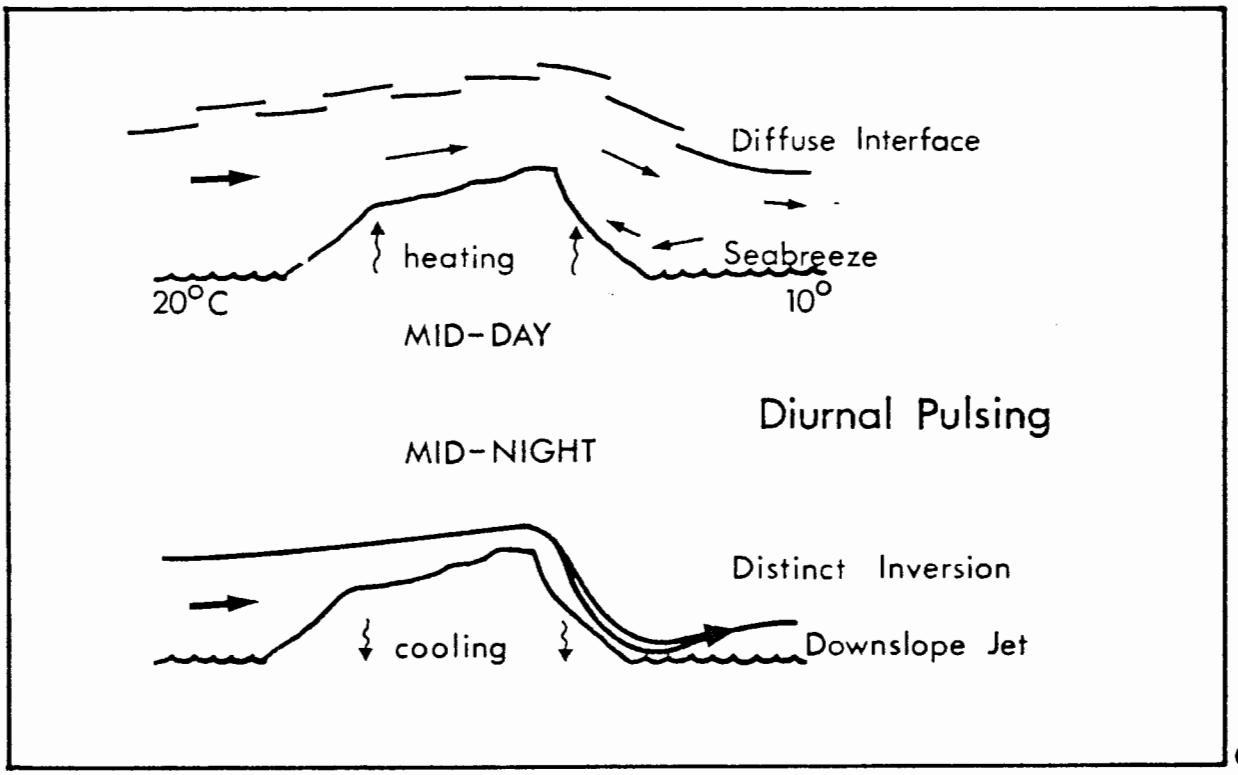

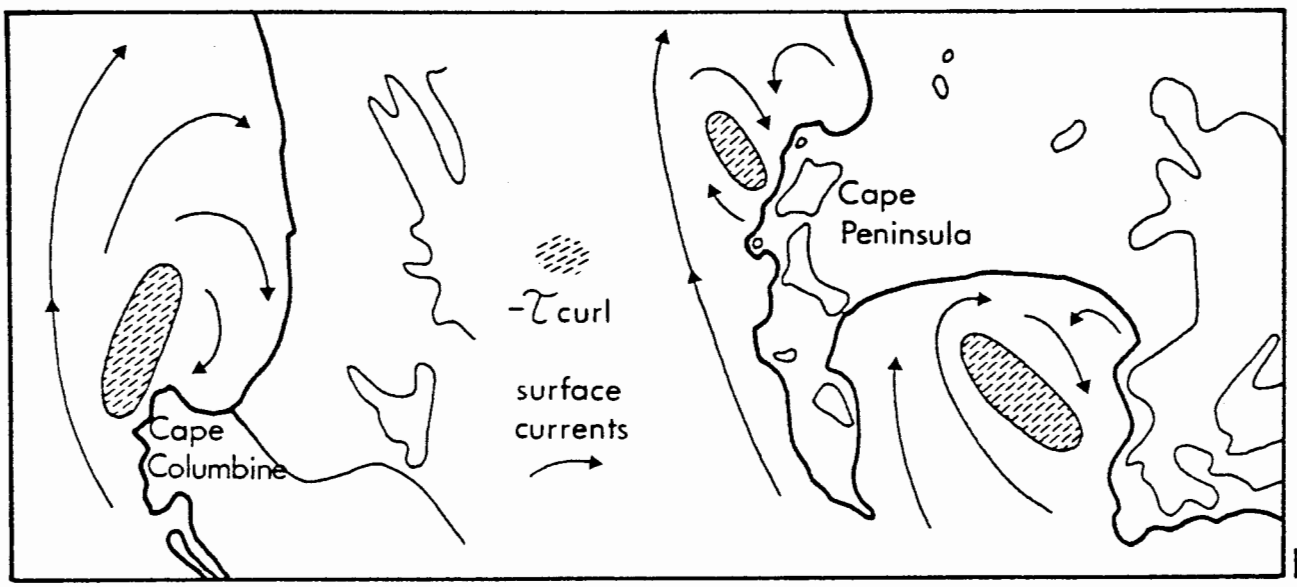

Fig. 43a: A schematic diagram of diurnal pulsing mechanisms which operate to produce a nocturnal downslope jet at Oudekraal.

43b: A schematic map showing the interactions possible between cyclonic wind stress curl and surface ocean currents in the lee of the Cape Columbine, Cape Hangklip and the Cape Peninsula headlands.

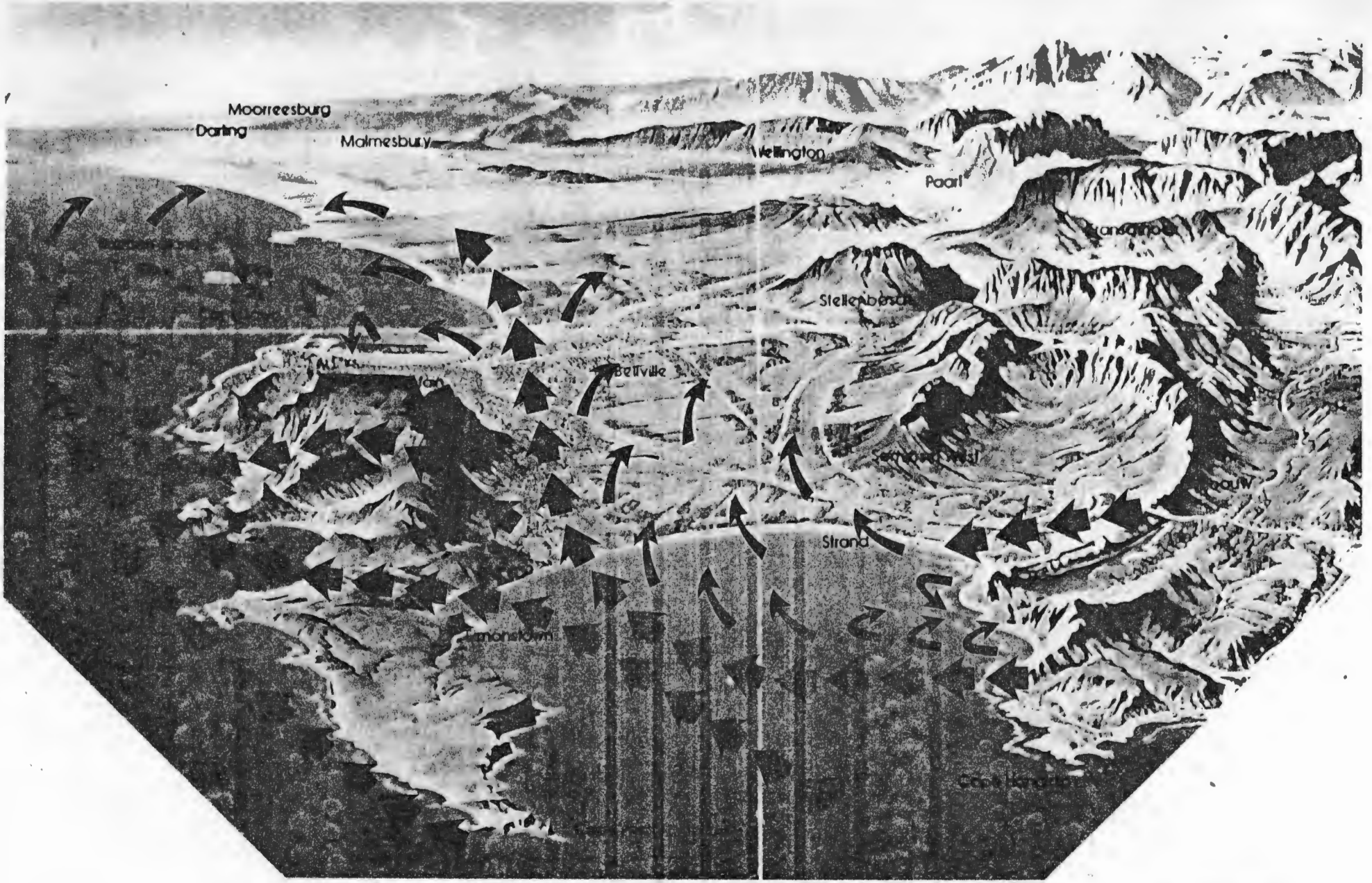

Fig. 44: A 3 dimensional view showing topographic deflections which are imposed on the shallow alongshore wind jet. Wake capture areas are seen in the lee of Kogëlberg and Table Mountain.

APPENDIX

Included in the appendix is the computer program used to calculate wind field variability parameters Fig.45, and the input data to the program. The matrix borders are shown in Figs. 46 to 48 immediately preceding the corresponding data tables.

```
C  MATRIX ADJUSTMENT.  DATA CARD 'MM,MM   'WIDTH X HEIGHT' FIRST CARD A
FTER
C  REDF. ADJUST 101 FORMAT  M(WIDTH) M(HEIGHT).
C  101   FORMAT(1H ,M(///...///,M(5X,F7.3)))
C  NUMBER OF ///'S AND VALUE OF 'S' BY INTUITION. P.S. MAX WIDTH = 120

      REAL NORMAL

      DIMENSION VAL(26,26),VANG(26,26),VSPD(26,26),DIV(26,26),
     /VORT(26,26),WSPD(26,26),STRESS(26,26),DUDY(26,26),DVDY(26,26),DUDX
     /(26,26),DVDX(26,26),POWER(26,26),TANGNT(26,26),NORMAL(26,26)
      DATA VAL/676*0./,VORT/676*0./,STRESS/676*0./
C  A MAXIMUM OF 90X90 MATRIX SIZE
      READ 100,M,M
      READ 100,ID,IM,IT
      PRINT 103,ID,IM,IT
103   FORMAT(1H1,'    DATE OF INTERPOLATED WIND FIELD  ',I2,'/',I2,'/',I
     12)
      READ 100,((VAL(I,J),J=1,M ,1),I=1,M ,1)
      RHO=.00122
      CD=.0013
      DX = 2.
      DY = 2.
      PCONST = 0.0000000061Z5
      DO 4 I=1,M
   15 DO 5 J=1,M
      VANG(I,J)= FLOAT(IFIX(VAL(I,J)))
      VSPD(I,J)= 50.*(VAL(I,J)-VANG(I,J))
      VANG(I,J)=FLOAT(IFIX(VAL(I,J)))*3.141   /180.
      WSPD(I,J)= VSPD(I,J)*100.
    5 CONTINUE
4     CONTINUE
      DO 6 I=2,M-1
      DO 7 J=2,M-1
      IF(VAL(I-1,J).EQ.0. .OR. VAL(I+1,J).EQ.0. .OR. VAL(I,J-1).EQ.0.
     &.OR. VAL(I,J+1).EQ.0.) GOTO 7
      DUDX(I,J)=(-VSPD(I,J+1)*COS(VANG(I,J+1))+VSPD(I,J-1)*COS(VANG(I,J-
     11)))*(1/DX)
      DVDY(I,J)=(-VSPD(I-1,J)*SIN(VANG(I-1,J))+VSPD(I+1,J)*SIN(VANG(I+1,
     1J)))*(1/DY)
      DUDY(I,J)=(VSPD(I+1,J)*COS(VANG(I+1,J))-VSPD(I-1,J)*COS(VANG(I-1,J
     1)))*(1/DY)
      DVDX(I,J)=(VSPD(I,J-1)*SIN(VANG(I,J-1))-VSPD(I,J+1)*SIN(VANG(I,J+
     1J)))*(1/DX)
      VORT(I,J)=DVDX(I,J)-DUDY(I,J)
      DIV(I,J)=DUDX(I,J)+DVDY(I,J)
      STRESS(I,J)=WSPD(I,J)*WSPD(I,J)*RHO*CD*.7
      POWER(I,J)=WSPD(I,J)*WSPD(I,J)*WSPD(I,J)*PCONST
      TANGNT(I,J)=WSPD(I,J)*COS(VANG(I,J)-160.*3.141/180.)*.01
      NORMAL(I,J)=WSPD(I,J)*COS(VANG(I,J)-250.*3.141/180.)*.01
7     CONTINUE
    6 CONTINUE
      PRINT 110
110   FORMAT(1H1,60X,' **DATA INPUT MATRIX**')
      PRINT 101,((VAL(I,J),J=2,M-1 ),I=2,M-1 )

      PRINT 102
  102 FORMAT(1H1,60X,' **(DIVERGENCE *.0001)**')
      PRINT 101,((DIV(I,J),J=2,M-1 ),I=2,M-1 )
      PRINT 105
  105 FORMAT(1H1,60X,' **(VORTICITY *.0001)**')
      PRINT 101,((VORT(I,J),J=2,M-1 ),I=2,M-1 )
      PRINT 106
  106 FORMAT(1H1,60X,' **(SHEAR *.0001)**')
      PRINT 101,((DVDX(I,J),J=2,M-1 ),I=2,M-1 )
      PRINT 107
  107 FORMAT(1H1,60X,' **STRESS**')
      PRINT 101,((STRESS(I,J),J=2,M-1 ),I=2,M-1 )
      PRINT 108
108   FORMAT(1H1,60X,' **POWER** ')
      PRINT 101,((POWER(I,J),J=2,M-1),I=2,M-1)
      PRINT 109
109   FORMAT(1H1,60X,'**TANGENTIAL**')
      PRINT 101,((TANGNT(I,J),J=2,M-1),I=2,M-1)
      PRINT 111
111   FORMAT(1H1,60X,'**NORMAL**')
      PRINT 101,((NORMAL(I,J),J=2,M-1),I=2,M-1)
      PRINT 104
  104 FORMAT(1H1' ')

  100 FORMAT()
101   FORMAT(1H ,11(/////////,10(2X,F10.3)))
      DO 77 I=2,M-1
      DO 77 J=2,M-1
      IF(VAL(I-1,J).EQ.0. .OR. VAL(I+1,J).EQ.0. .OR. VAL(I,J-1).EQ.0.
     &.OR. VAL(I,J+1).EQ.0.) GOTO 77
      IX=I
      YY=J
      WRITE(15,200)XX,YY,VORT(I,J)
      WRITE(16,200)XX,YY,DIV(I,J)
      WRITE(17,200)XX,YY,STRESS(I,J)
      WRITE(18,200)XX,YY,DUDX(I,J)
      WRITE(19,200)XX,YY,POWER(I,J)
      WRITE(20,200)XX,YY,TANGNT(I,J)
      WRITE(21,200)XX,YY,NORMAL(I,J)
200   FORMAT( )
77    CONTINUE
      STOP
      END
```

Fig. 45: The computer program used to calculate wind field variability parameters such as shear, vorticity, divergence, and estimated surface stress from data input tables.

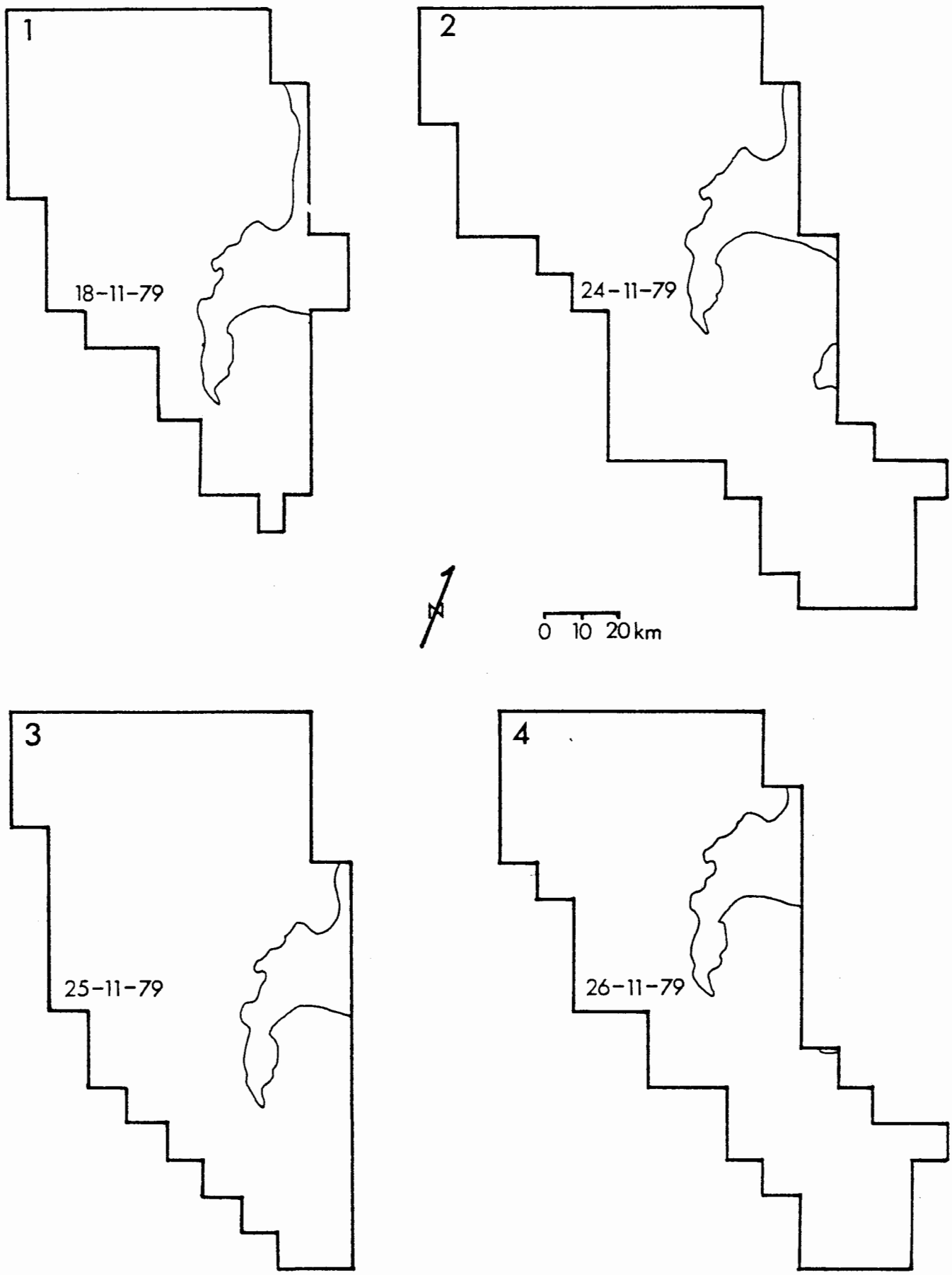

Fig. 46: (1,2,3,4) Wind data input matrix borders for 18, 24, 25 and 26 November 1979, corresponding to matrix tables 1, 2, 3 and 4.

MATRIX TABLE 1 18-11-79

	1	2	3	4	5	6	7	8	9	10
1	170/20	170/20	170/20	160/18	160/17	158/15	150/16	150/16		
2	164/21	162/22	166/22	160/20	160/19	159/16	155/14	160/15		
3	159/22	154/22	157/22	155/22	160/20	160/18	160/14	165/11	150/13	
4	153/22	150/22	153/22	152/21	150/20	161/17	164/14	165/12	145/14	
5	151/22	150/22	151/22	152/22	154/20	160/17	155/12	145/14	135/15	
6	150/22	150/22	149/22	150/22	151/21	149/18	142/12	140/17	150/15	
7		147/22	146/22	142/22	140/22	139/21	135/20	175/17	175/17	176/16
8		145/22	145/21	144/21	145/21	130/17	130/17	180/17	175/19	175/17
9		147/21	147/21	147/21	144/20	145/19	140/19	160/19	165/20	160/18
10			150/21	150/21	150/20	145/21	150/19	150/19	160/20	
11					150/20	150/21	152/19	153/20	155/21	
12					150/20	147/20	142/19	140/21	150/20	
13						145/21	143/21	142/21	140/21	
14						140/21	140/21	140/21	140/21	
15								140/20		

MATRIX TABLE 2 24-11-79

	1	2	3	4	5	6	7	8	9	10	11	12	13	14	15
1	137/25	138/24	141/22	149/20	155/15	155/12	165/10	170/07	175/10	179/16					
2	135/25	136/22	137/22	143/20	155/16	160/12	165/10	170/06	165/10	175/16					
3	133/26	133/24	130/22	140/20	160/16	170/14	174/10	173/07	160/10	161/17	175/16				
4	133/25	137/24	130/22	145/20	160/17	165/14	170/11	169/09	141/05	145/16	175/16				
5		129/23	130/22	150/20	163/17	163/15	165/12	166/11	120/12	165/16	170/15				
6		129/23	133/22	146/20	160/17	158/16	155/14	125/14	150/15	176/16	170/12				
7		130/23	131/22	132/21	139/20	139/17	140/17	145/17	120/17	180/16	140/12	130/11			
8				135/21	135/21	135/20	120/19	110/20	135/19	155/16	120/16	105/17			
9					133/22	129/22	124/21	140/21	121/21	125/19	100/15	095/13			
10						127/22	128/22	126/22	125/23	115/20	105/15	100/12			
11						128/24	127/23	126/23	125/23	122/21	119/17	120/15			
12						129/25	128/24	126/23	127/23	125/21	120/17	115/15	109/13		
13						130/25	130/24	130/23	130/23	129/21	129/17	120/16	116/14	110/14	106/13
14									130/22	130/21	128/18	127/16	126/15	118/14	108/13
15										125/18	120/17	119/16	120/14	121/12	
16										123/16	120/16	120/14	122/13	125/12	
17											120/14	122/14	123/13	123/12	

Matrix Tables 1 and 2: Wind data inputs for matrix points given in degrees from and ms^{-1}.

MATRIX TABLE 3

25-11-79

	1	2	3	4	5	6	7	8	9	10
1	170/01	190/01	220/02	240/02	250/02	270/02	270/02	280/02	280/01	
2	140/02	149/01	206/02	250/02	270/02	290/02	300/02	310/02	315/01	
3	135/03	139/02	190/01	270/01	290/01	315/02	315/01	315/01	315/01	
4	130/05	145/03	195/01	230/01	280/01	290/02	299/01	305/01	315/01	
5		150/04	195/02	212/02	278/02	283/01	290/01	300/01	309/01	300/01
6		150/04	190/03	190/02	210/01	220/01	230/01	250/01	280/01	280/01
7		130/05	135/03	145/02	152/02	160/01	175/02	190/02	230/01	280/01
8		119/06	120/04	140/03	150/03	165/01	195/02	230/04	250/01	310/05
9		110/07	120/06	141/04	150/03	175/01	220/03	195/02	220/01	330/05
10			130/07	142/05	150/03	150/01	150/01	160/02	190/02	340/01
11			142/08	142/07	143/05	144/02	145/02	140/03	130/02	200/01
12				110/10	095/07	110/05	120/05	130/05	120/03	100/01
13					100/10	100/07	110/03	120/03	110/04	099/01
14						095/07	100/04	095/05	085/06	080/06
15							080/07	075/07	065/08	075/06
16								060/10	061/10	062/10

MATRIX TABLE 4

26-11-79

	1	2	3	4	5	6	7	8	9	10	11	12	13
1	220/10	240/07	250/08	280/04	308/04	320/03	320/03	320/04					
2	220/10	230/07	240/07	271/04	340/02	320/02	310/02	300/03					
3	220/10	225/09	240/07	320/05	337/04	320/02	300/01	290/04	290/07				
4	222/11	225/08	250/07	340/05	335/07	330/04	320/01	270/10	290/09				
5	223/11	221/08	230/07	350/06	333/04	340/03	320/05	310/10	340/07				
6		225/10	290/07	340/06	330/05	320/05	325/07	330/11	353/07				
7			332/07	335/06	335/06	327/06	290/07	330/11	335/07				
8			320/10	325/07	330/06	330/07	325/07	320/11	360/08				
9			275/17	300/10	342/07	337/07	330/08	340/10	005/10				
10					332/10	333/08	335/08	320/10	315/10	320/08			
11					322/12	330/10	320/09	310/10	310/11	285/10	270/08		
12							305/11	300/11	310/12	315/13	320/12	295/11	270/12
13							312/12	309/12	310/12	310/14	316/14	290/12	275/12
14								305/12	307/13	305/14	302/15	289/12	
15									301/13	301/14	290/13	288/15	
16									300/13	298/14	296/15	295/15	

Matrix Tables 3 and 4: Wind data inputs for matrix points given in degrees from and ms^{-1}.

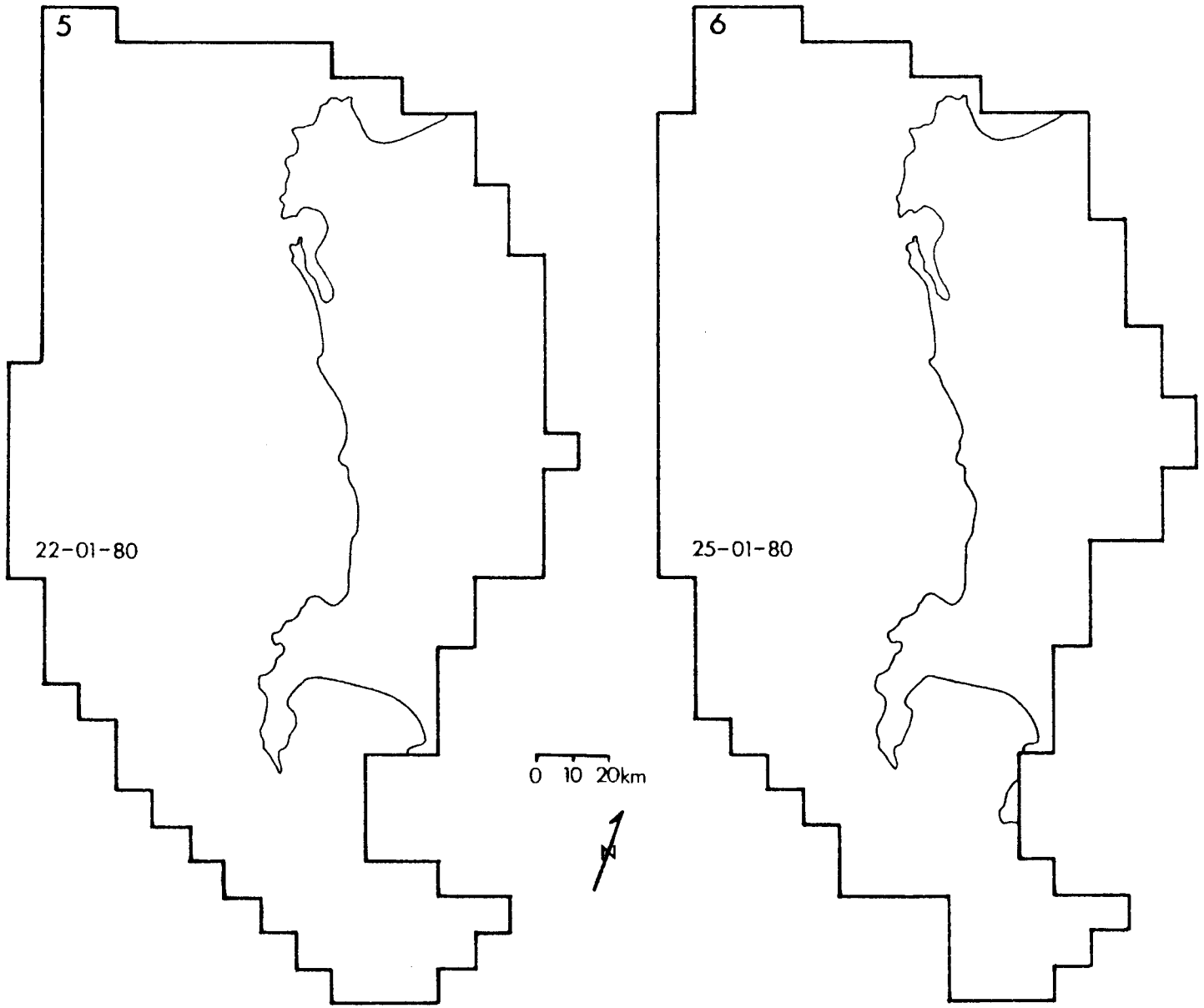

Fig. 47: (5,6) Wind data input matrix borders 22 and 25 January 1980, corresponding to matrix tables 5 and 6.

	1	2	3	4	5	6	7	8	9	10	11	12	13	14	15	16	17
1		164/19	167/19	165/19													
2		164/19	164/19	165/20	165/20	170/18	170/17	175/17	180/16	185/16							
3		165/19	167/19	170/20	170/20	170/18	175/17	175/16	185/16	185/15	205/15	205/14					
4		165/19	168/19	170/20	170/20	175/18	175/17	180/16	190/16	187/15	185/14	180/13	200/12	180/11			
5		164/19	167/19	168/20	172/20	177/18	180/17	185/16	183/16	182/15	182/14	177/12	175/11	170/09			
6		163/19	166/19	166/20	171/20	176/19	181/17	183/16	185/16	190/14	187/12	184/12	183/09	182/07	183/07		
7		161/19	165/19	163/20	170/20	175/19	183/17	187/16	190/15	188/14	184/12	180/10	175/08	170/07	182/07		
8		160/20	164/19	160/22	170/20	175/20	184/17	182/16	185/15	177/14	172/12	168/09	165/07	160/06	175/07		
9		168/20	166/19	162/22	175/21	180/20	185/17	190/16	185/15	180/14	175/12	160/10	160/07	159/07	155/08	130/07	
10		162/20	160/22	162/22	174/21	175/20	180/19	185/16	189/16	175/14	167/12	160/09	159/08	157/08	150/09	140/09	
11	145/20	147/20	150/20	160/22	168/21	170/20	172/18	178/16	180/15	179/14	170/12	160/08	157/09	152/09	147/09	130/10	
12	140/20	143/20	148/20	151/20	160/20	165/20	170/17	175/17	180/15	185/14	180/12	160/09	155/09	149/09	144/10	130/11	
13	145/20	147/20	150/20	155/20	160/20	166/20	171/18	175/16	183/14	182/14	178/13	159/10	157/09	147/09	130/10	129/12	140/13
14	140/20	145/20	150/19	155/19	160/19	169/19	166/18	170/16	175/13	178/12	178/13	163/10	159/10	146/10	133/12	127/14	140/15
15	138/19	143/19	149/19	155/18	155/18	160/18	163/18	165/16	170/12	175/12	179/13	165/12	160/10	145/09	130/12	125/16	
16	133/18	140/18	147/18	155/18	155/18	157/18	155/18	163/16	160/12	170/12	179/14	170/13	167/11	140/10	130/12	121/15	
17	130/17	132/17	145/17	155/17	155/17	155/17	145/17	143/17	141/11	140/12	170/15	173/15	175/12	160/10	130/11	120/15	
18		135/16	143/16	149/16	155/16	155/16	137/16	125/15	130/15	160/15	173/15	171/15	170/12	160/10			
19		136/15	142/15	148/15	155/16	155/16	140/15	130/15	160/16	175/16	175/16	168/15	130/12	120/13			
20		137/15	141/15	145/14	143/14	145/14	147/14	148/15	157/15	165/16	164/15	150/14	130/12				
21			130/15	134/14	137/14	140/14	143/14	140/15	153/15	160/16	161/15	140/14	130/14				
22				125/13	130/13	135/14	139/14	140/14	152/15	160/16	160/16	140/14	130/14				
23				120/13	127/13	130/13	137/14	143/15	140/15	150/15	135/15						
24					125/13	130/14	138/14	137/14	135/13	136/14	136/14						
25						130/14	130/14	130/14	135/15	140/14	143/14	150/14	150/13				
26							132/14	136/16	139/16	143/16	148/15	150/14	152/14	158/14	175/13		
27								130/15	131/15	130/15	133/14	134/13	135/13	136/13	150/12		
28									127/15	129/15	133/14	137/13	139/12	140/11			
29										125/16	130/14	135/13	138/12				

Matrix Table 5: Wind data input for matrix points given in degrees from and ms^{-1}.

	1	2	3	4	5	6	7	8	9	10	11	12	13	14	15	16
1		163/19	158/18	156/16	160/14											
2		162/18	159/18	158/16	163/14	167/12	170/10	175/09								
3		160/18	159/17	159/16	163/14	167/12	173/10	174/09	177/10	180/09						
4	156/19	158/18	160/17	161/15	164/13	168/12	172/10	174/09	180/10	180/10	177/10	177/10	175/10			
5	157/19	159/18	161/17	163/15	166/12	169/12	170/10	175/10	181/10	180/10	177/10	172/10	170/10			
6	158/19	159/18	161/17	164/15	167/13	170/12	173/11	175/10	182/10	183/10	176/10	171/09	170/09			
7	160/20	163/18	163/17	166/15	168/13	172/12	174/11	179/10	181/10	184/10	175/10	170/09	170/09	169/09		
8	162/20	160/19	168/17	167/15	169/12	171/12	175/11	179/11	183/11	185/10	173/09	169/09	166/09	164/09		
9	163/20	164/20	165/18	167/15	173/13	173/12	172/11	174/11	183/11	186/11	172/10	168/09	164/09	160/10		
10	162/21	163/20	164/18	165/16	165/14	164/12	170/11	171/11	182/11	186/10	173/10	167/10	160/10	155/10	150/10	
11	161/22	162/21	162/19	163/17	160/15	158/13	163/11	168/12	170/12	179/11	170/11	160/10	159/09	150/09	145/10	
12	160/23	161/22	161/20	159/17	155/15	154/13	160/12	162/11	165/11	168/11	165/10	158/09	150/08	147/09	143/09	140/09
13	159/24	159/23	160/22	155/19	153/16	151/14	160/11	160/10	165/11	170/12	165/12	155/08	143/08	139/09	137/09	135/09
14	158/25	158/24	157/22	156/20	155/17	152/15	160/12	155/09	165/11	173/12	170/10	155/07	140/07	137/08	135/08	135/08
15	159/25	158/24	158/23	155/21	155/18	154/16	160/13	150/08	160/09	176/14	180/10	153/07	137/07	135/08	132/08	
16	160/26	159/25	159/24	154/23	155/17	150/16	145/14	145/10	160/10	180/15	190/10	160/07	137/07	135/08	135/07	
17	160/26	159/25	158/24	153/22	145/19	140/17	137/15	130/15	150/11	200/15	190/10	158/06	136/05			
18		160/26	160/25	159/23	158/20	157/17	155/17	130/17	180/17	200/17	195/12	159/07	142/05			
19		161/26	162/25	163/24	163/21	155/19	135/18	160/18	190/18	200/17	190/15	159/10	130/05			
20		164/25	165/25	166/25	165/22	147/21	148/19	140/18	173/18	155/18	145/16	150/12				
21		167/24	167/25	167/25	155/24	142/22	145/21	147/19	160/20	150/19	125/17	125/15				
22			155/22	150/22	140/22	136/22	139/22	141/22	141/23	145/20	115/15	110/15				
23				145/20	135/20	133/21	135/21	138/21	140/21	145/20	115/17					
24					135/17	128/18	130/18	132/19	139/19	147/18	139/17					
25						130/16	132/17	137/17	141/18	145/18	140/17	138/15				
26						133/15	137/15	140/15	142/17	142/17	142/16	141/15	138/12	135/08		
27									142/15	147/16	148/16	148/15	153/12			
28									142/15	149/15	150/15	151/15	154/12			
29									142/14	150/13	153/13	155/14				

Matrix Table 6: Wind data input for matrix points given in degrees from and ms^{-1}.

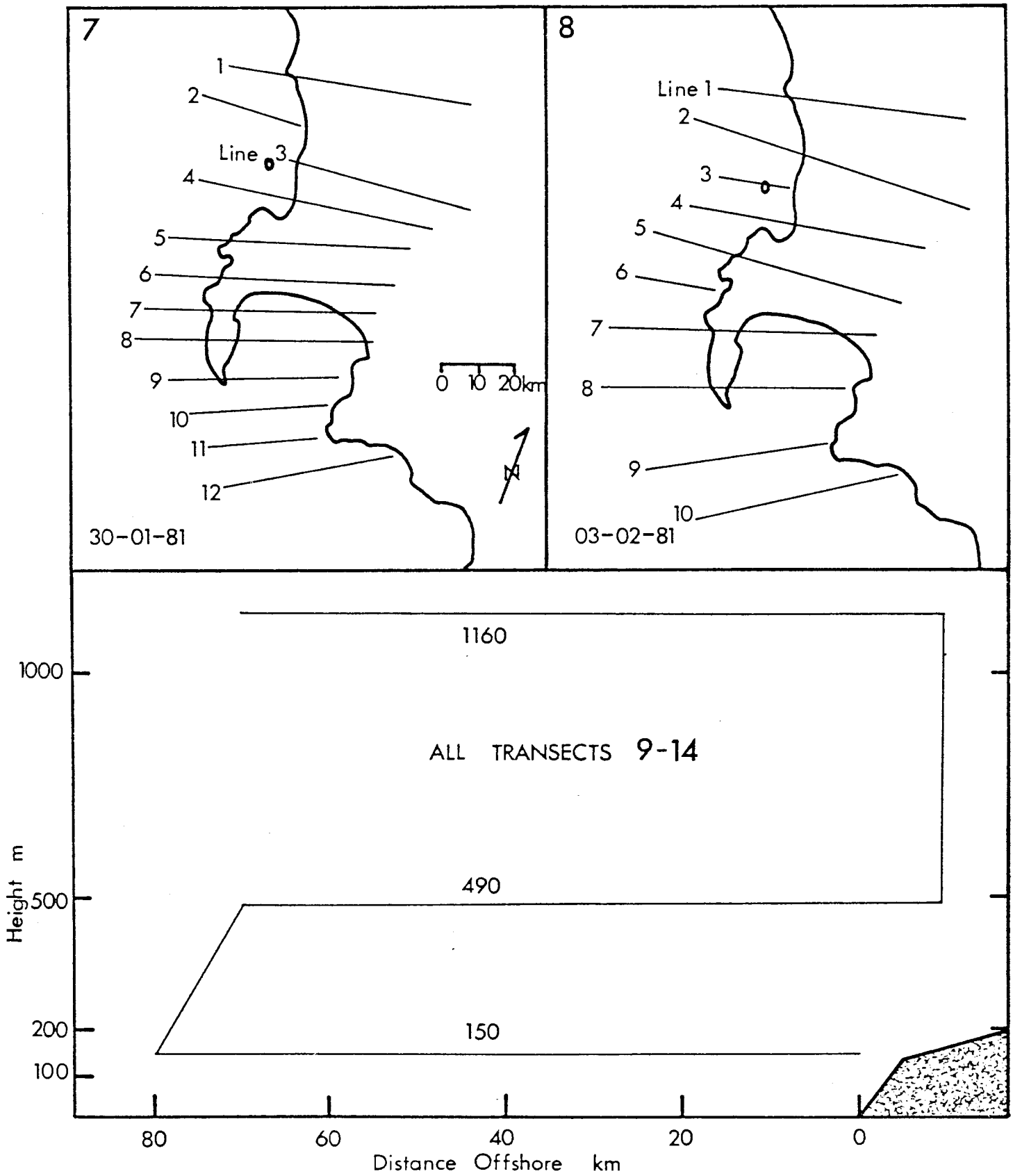

Fig. 48: (7,8) Wind data input lines for 30 January and 3 February 1981, corresponding to input tables 7 and 8. The standard cross section/transect grid is shown at the bottom, corresponding with transect tables 9 and 14.

INPUT TABLE 7 30-01-81

	1	2	3	4	5	6	7	8	9
LINE 1	190/13	180/12	176/11	178/16	178/14	175/10	175/09	190/08	
LINE 2	190/18	188/19	188/11	165/14					
LINE 3				165/16	175/14	180/14	180/13	175/11	145/05
LINE 4	170/15	170/15	130/04	175/17	200/14	220/10	190/09	220/04	
LINE 5	168/12	180/13	210/14	205/16	200/12	180/08	120/05		
LINE 6	160/13	178/10	190/15	195/14	195/15	210/12	190/06		
LINE 7	155/12	178/08	155/12	165/15	175/13	200/09			
LINE 8	150/12	150/12	175/09	150/12	155/14	160/15	130/06		
LINE 9		150/15	155/11	150/13	155/14	160/16	165/16		
LINE 10		145/13	142/12	145/11	150/11	140/11			
LINE 11			140/12	140/12	145/11	150/11			
LINE 12			140/12	140/12	138/12	130/10	130/09	125/09	

INPUT TABLE 8 03-02-81

	1	2	3	4	5	6	7	8	9
LINE 1	190/08	190/07	180/09	185/09	160/07	165/05	175/05	180/06	
LINE 2	190/10	190/07	185/07	160/12	160/09	158/08	140/08	135/07	170/05
LINE 3		180/04	140/07	155/13					
LINE 4		165/12	340/04	180/16	180/14	150/09	100/07	080/07	
LINE 5	155/14		130/16	190/12		210/12		170/05	
LINE 6	150/12		140/13						
LINE 7	150/12		145/12	160/10	170/14	175/10	135/05	120/06	
LINE 8	145/11	140/10	145/11	160/08	155/12	140/14	130/10		
LINE 9		140/11	135/08	130/08	135/08	140/11	150/12		
LINE 10			140/10	135/09	130/07	120/06	125/05	120/06	120/06

Input Data Tables 7 and 8: Wind data input for manual computation lines, given in degrees from and ms^{-1}.

TRANSECT TABLE 9 17-11-79

	1	2	3	4	5	6	7	8	9
LINE 1		145/11	148/11	155/12	160/17	160/18	150/18	145/14	135/10
LINE 2				155/17	160/20	170/20	175/19	170/19	185/19
LINE 3	155/15	150/18	155/16	155/16	150/14	150/14	150/12	130/12	130/17

TRANSECT TABLE 10 18-11-79

	1	2	3	4	5	6	7	8	9
LINE 1			165/07	160/09	145/09	130/11	135/15	136/16	136/16
LINE 2			132/16	135/15	135/12	125/15	130/12	144/12	140/20
LINE 3	145/23	145/22	140/20	140/23	150/21	145/17	140/15	145/15	170/17

TRANSECT TABLE 11 19-11-79

	1	2	3	4	5	6	7	8	9
LINE 1		315/09	310/07	308/06	310/06	310/05	300/05	290/03	295/02
LINE 2		300/05	310/06	312/07	315/07	290/05	235/05	235/06	225/06
LINE 3	130/10	145/09	150/06	155/05	170/05	170/01	170/01	170/02	225/06

Transect Data Tables 9, 10 and 11: Wind data input for vertical survey lines, given in degrees from and ms^{-1}. The lines correspond to the heights: Line 1 1160m, Line 2 490m, and Line 3 150m.

TRANSECT TABLE 12 22-11-79

	1	2	3	4	5	6	7	8	9
LINE 1	110/04	110/05	105/06	108/05	115/06	100/05	090/05	085/04	090/06
LINE 2	135/11	135/11	140/12	136/14	140/13	145/13	140/14	160/09	174/09
LINE 3	130/12	145/14	150/15	145/16	150/14	157/15	175/15	178/15	

TRANSECT TABLE 13 23-11-79

	1	2	3	4	5	6	7	8	9
LINE 1			083/12	082/12	080/13	070/11	070/10	076/09	078/07
LINE 2			145/22	145/22	145/20	145/18	130/12	120/10	110/06
LINE 3	125/22	130/21	125/22	120/25	123/24	128/22	140/22	120/20	165/20

TRANSECT TABLE 14 24-11-79

	1	2	3	4	5	6	7	8	9
LINE 1		075/05	055/06	065/07	080/07	085/04	060/04	055/04	
LINE 2				117/16	115/15	110/14	105/12	100/11	105/10
LINE 3	130/24	126/23	126/22	130/23	120/17	110/12	105/20	105/17	

Transect Data Tables 12, 13 and 14: Wind data input for vertical survey lines, given in degrees from and ms^{-1}. The lines correspond to the heights: Line 1 1160m, Line 2 490m, and Line 3 150m.

REFERENCES

1. ANDERSON, D.L.T., and GILL, A.E., 1975: Spin-up of a stratified ocean with application to upwelling, Deep Sea Res., 22,583-596.

2. ANDREWS, W and CRAM, D., 1969: Combined aerial and ship board upwelling survey in the Benguela Current, Nature, 224, 902-904.

3. ANDREWS, W.H.R., and HUTCHINGS, L., 1980: Upwelling in the Southern Benguela Current, Prog in Oceanogr., 9,1.

4. ARDANUY, P., 1979: On the observed diurnal oscillation of the Somali Jet, Mon. Wea. Rev. 107, 1694-1700.

5. ATKINS, G.R., 1970: Winds and current patterns in False Bay, Trans. R. Soc. S. Afr., 39, Part 2, 139-148.

6. ATKINSON, B.W., 1981: Mesoscale Atmospheric Circulations, Academic Press, London, pp. 495.

7. ARTHUR, R.S., 1965: On the calculation of vertical motion in eastern boundary currents from determinations of horizontal motion, J. Geophys. Res., 70, 2799-2803.

8. BAILEY, G.W., 1979: Physical and chemical aspects of the Benguela Current in the Lüderitz region, MSc. Thesis Dept. of Oceanogr., Univ. of Cape Town, pp. 225.

9. BAIN, C.A.R. and HARRIS, T.F.W., 1976: Coastal water movement study, Progress reports 1-6, NUCOR Research Unit, S.U.N.I., Faure.

10. BAKUN, A., 1973: Coastal upwelling indices, west coast of North America, 1946-1971, U.S. Dept. of Commer., NOAA TECH. REP. NMFS-SSRF - 671, pp.103.

11. BAKUN, A., 1978: Guinea Current upwelling, Nature 271,5641,147-150.

12. BAKUN, A., and PARRISH, R.H., 1980: Environmental inputs to fishery population models for eastern boundary current regions, IOC Workshops Rep. Series, Monterey, Calif.

13. BAKUN, A., and PARRISH, R.H., 1982: Turbulence, transport and pelagic fish in the California and Peru Current systems, Pacific Environ. Group Tech Dept., Southwest Fisheries Center, pp.34.

14. BANG, N.D., 1973: The Southern Benguela System: Finer oceanic structures and atmospheric determinants, PhD. Thesis, Dept. of Oceanogr., Univ. of Cape Town.

15. BANG, 1973: Characteristics of an intense ocean frontal system in the upwelling regime west of Cape Town, Tellus, 25, 256-265.

16. BANG, N.D. and ANDREWS, W.H.R., 1974: Direct current measurements of a shelf edge frontal jet in the southern Benguela system, J. Mar.Res., 32, 405-417.

17. BANNON, P.R., 1982: On the dynamics of the East African Jet: Arabian Sea branch, J. Atm. Sci., 39, 2267-2278.

18. BLUMEN, W., DIETZE, S.C., 1981: An analysis of three-dimensional mountain lee waves in a stratified shear flow, J. Atm. Sci., 38, 1949-1963.

19. BOYD, A.J., 1981: An intensive study of the currents and general hydrology of an anomalous upwelling area off South West Africa, MSc. Thesis, Dept. of Oceanogr., Univ. of Cape Town, pp.170.

20. BRUNDRIT, G.B., and VAN FOREEST, D., 1981: Benguela current modelling project reports, Dept. of Oceanogr., Univ. of Cape Town.

21. BUNKER, A.F., 1965: A low-level jet produced by air, sea and land interactions, Sea-Air Int. Lab., Rep. 1, J. Spar (ed.), Washington, pp.225-238.

22. BURT, W., ENFIELD, D.B., SMITH, R.L., and CREW, H., 1973: The surface wind over an upwelling region near Pisco, Peru, Bound-Layer Met., 3, 385-391.

23. CLANCY, R.M., THOMPSON, J.D., HULBURT, H.E. and LEE, J.D., 1979: A model of mesoscale air-sea interaction in a sea breeze-coastal upwelling regime, Mon. Wea. Rev., 107, 1476-1505.

24. CLARK, T.L. and GALL, R., 1982: Three-dimensional numerical model simulations of airflow over mountainous terrain: A comparison with observation, Mon. Wea. Rev., 110, 766-791.

25. CLOETE, C.E. (ed.) 1979: The transfer of pollutants in two southern hemispheric oceanic system, SANSP REP 39, CSIR, Pretoria.

26. CSANADY, G.T., 1982: Circulation in the Coastal Ocean, D. Reidel Pub. Co., Dordrecht, pp. 279.

27. DINGLE, R.V., MOIR, G.J., BREMMER, J.M., and ROGERS, J., 1977: Bathymetry of the continental shelf off South Africa, Dept. of Mines, Geological Survey, Marine Geoscience Series 1.

28. ELLIOT, D. and O'BRIEN, J., 1976: Observational studies of the marine boundary layer over an upwelling region, Monthly Wea. Rev., 105, Jan. 1977, 86-98.

29. EKMAN, V., 1905: On the influence of the earth's rotation on ocean currents, Arkiv Mat. Astron och Fysik, 2,11, Stockholm.

30. EVENSON, A.J., and VERONIS, G., 1975: Continuous represenation of wind stress and wind stress curl over the world ocean, J. Mar. Res., 33, 131-144.

31. FINDLATER, J., 1972: Aerial explorations of the low-level cross equatorial current over eastern Africa, Q.J.R. Met. Soc., 98, 274-289.

32. FOFONOFF, N.P., 1963: Dynamics of ocean currents, M.N. Hill ed., The Sea, Inter Science Pub., N.Y., 32-395.

33. GARCIA-MEITEN, R., 1975: Case study of a marine inversion on the Oregon coast, CUEA REP., 75-1, Dept. of Met., Florida State Univ., pp.108.

34. GILL, A.E., and CLARKE, A.J., 1974: Wind induced upwelling, coastal currents, and sea-level changes, Deep Sea Res., 21, 325-345.

35. GILL, A.E., 1977: Coastal trapped waves in the atmosphere, Q.J.R. Met. Soc., 103, 437, 431-440.

36. GOODWIN, J.A., 1979: A study of surface winds off the coast of Peru, CUEA TECH. REP. 58, Dept. of Met., Florida State Univ., pp.82.

37. HALPERN, D., 1976: Measurements of near-surface wind stress over an upwelling region near the Oregon coast, J. Phys. Oceanogr., 6, 108-112.

38. HANTEL, M., 1970: Monthly charts of surface wind stress curl over the Indian Ocean, Mon. Wea. Rev., 98, 765-773.

39. HAWKINS, J., 1977: A study of the mesoscale wind circulation in a land-sea breeze regime, CUEA TECH. REP. 32, Dept. of Met., Florida State Univ.

40. HAWKINS, J.D., 1979: Atmospheric structural variations that result in upwelling off Oregon, CUEA TECH REP. 52, Dept. of Met., Florida State Univ., pp.72.

41. HAWKINS, J.D., and STUART, D.W., 1980: Low level atmospheric changes over Oregon's coastal upwelling region, Monthly Wea. Rev., 108, 7.

42. HICKEY, B.M., 1979: The California Current system-hypothesis and facts, Prog. Oceanogr., 8, 191-279.

43. HOLLADAY, C.G., and O'BRIEN, J.J., 1975: Mesoscale variability of sea surface temperatures, J. Phys. Oceanogr., 5, 761-772.

44. HOLTON, J., 1975: An Introduction to Dynamical Meteorology, Geophys. Series 16, Academic Press, New York, pp.319.

45. HUSBY, D.M., and NELSON, C.S., 1982: Turbulence and vertical stability in the California Current, Cal COFI Report, Southwest Fisheries Center, pp.51.

46. HUYER, A., 1972: A comparison between wind and current observations over the continental shelf off Oregon, summer 1969, J. Geophys. Res., 77, 3215-3220.

47. HUYER, A., SMITH, R.L., and PILLSBURY, R.D., 1974: Observations in a coastal upwelling region during a period of variable winds, Tethys , 6, 391-404.

48. HUYER, A., SOBEY, E.J.C., and SMITH, R.L., 1979: The spring transition in currents over the Oregon continental shelf, J. Geophys. Res., 84, 6995-7011.

49. JOHNSON, A., and O'BRIEN, J.J., 1973: A study of an Oregon seabreeze event, J. Appl. Met., 12, 1267-1283.

50. JURY, M.R., 1980: Characteristics of summer wind fields and air-sea interactions over the Cape Peninsula upwelling region, MSc. Thesis, Dept. of Geogr., Univ. of Cape Town, pp.131.

51. KEEN, C.S., 1979: Meteorological aspects of pollution transport in the greater Cape Town area, Invest Rep., Dept. of Geogr., Univ. of Cape Town.

52. KLEMP, J.B., and LILLY, D.K., 1975: The dynamics of wave-induced downslope winds, J. Atm. Sci., 32, 320-339.

53. KRAUS, E.B., 1972: Atmosphere-Ocean Interaction, Oxford Univ. Press, London, pp.275.

54. LEETMA, A., 1970: The response of the Somalia Current to the SW Monsoon of 1970, Deep Sea Res., 19, 319-325.

55. LUTJEHARMS, J., 1979: Some dynamical characteristics of the South Atlantic upwelling system, Proc.Nat.Oceanogr. Symp., Univ. of Cape Town.

56. MASS, C., 1981: Topographically forced convergence in Western Washington State, Mon. Wea. Rev., 109, 1335-1347.

57. MASS, C., 1982: The topographically forced diurnal circulations of Western Washington State and their influence on precipitation, Mon. Wea. Rev., 110, 170-183.

58. Mc CREARY, J., 1976: Eastern tropical ocean response to changing wind systems, applications to El Nino, J.Phys. Oceanogr., 6, 632-645.

59. MOODY, G., 1979: Aircraft derived low level winds and upwelling off the Peruvian coast during March, April, and May, 1977, CUEA TECH. REP. 56, Dept. of Met., Florida State Univ.

60. MOOERS, C.N.K., COLLINS, C.A. and SMITH, R.L., 1976: The dynamical structure of the frontal zone in the coastal upwelling region off Oregon, J. Phys. Oceanogr. 6, 3-21.

61. NELSON, C.S., 1977: Wind stress and wind stress curl over the California current, NOAA TECH. REP. MNFS-SSRF-714, pp.87.

62. NELSON, G., (in prep.): Diagnostic models of upwelling in the Cape Peninsula region, PhD. Thesis, Dept. of Oceanogr., Univ. of Cape Town.

63. NEWTON, C.W., ed., 1972: Meteorology of the Southern Hemisphere, Met. Monogr. 13 Amer., Met. Soc.

64. NICKERSON, E.C. and DIAS, M.A., 1981: On the existence of atmospheric vortices downwind of Hawaii during the HAMEC Project, J. Appl. Met., 20, 868-873.

65. OVERLAND, J.E., and WALTER, B.A. Jr., 1981: Gap winds in the Strait of Juan de Fuca, Mon. Wea. Rev., 109(10), 2221-2233.

66. PARRISH, R.H., NELSON, C.S., and BAKUN, A., 1981: Transport mechanisms and reproductive success of fishes in the California Current, Biol. Oceanogr., 1(2), 175-203.

67. PEDLOSKY, J., 1974: Longshore currents, upwelling, and bottom topography, J. Phys. Oceanogr., 4, 214-226.

68. PHILANDER, S.G.H., 1976: Variability of the tropical oceans, Dyn. Atmos. Oceans, 3, 191-208.

69. PHILANDER, S.G.H., 1977: The effects of coastal geometry on equational waves, J. Mar. Res., 35, 509-523.

70. PHILANDER, S.G.H., 1978: Upwelling in the Gulf of Guinea, J. Mar. Res., 37, 23-33.

71. RAMAGE, C., 1975: The response of El Nino to trade wind anomalies, Bul. Am. Met. Soc, 56, 234-242.

72. ROLL, H.U., 1965: Physics of the Marine Atmosphere, Academic Press, London, pp.426.

73. SCHELL, I.L., 1968: On the relation between the winds off South West Africa, the Benguela Current and the Agulhas penetration of the south Atlantic, Deutsche Hydrographische Zeitshrift, 21, 109-117.

74. SHANNON, L.V., Nelson, G., and JURY, M.R., 1980: Hydrological and meteorological aspects of upwelling in the southern Benguela current, Coastal Upwelling, Amer. Geophys. Union, 146-159.

75. SIMARD, A., and PELTIER, W.R., 1982: Ship waves in the lee of isolated topography, J. Atm. Sci., 39, 587-609.

76. SMITH, R.B. 1982: Synoptic observations and theory of orographically disturbed wind and pressure, J. Atm. Sci., 39, 60-70.

77. SMITH, R.L., 1968: Upwelling, Oceanogr. Mar. Biol. Annu. Rev., 6, 11-46.

78. SMITH, R.L., 1974: A description of current, wind, and sea level variations during coastal upwelling off the Oregon Coast, J. Geophys. Res., 79, 435-443.

79. SOUTH AFRICAN NAVY, 1980: Charts SAN 1013, 1015, 1016, Gov. Printers, Pretoria.

80. SOUTH AFRICAN WEATHER BUREAU, 1980: Daily Weather Bulletin, Gov. Printers, Pretoria.

81. SOUTH AFRICAN WEATHER BUREAU, 1980: Monthly Newsletter, Gov. Printers, Pretoria.

82. STUART, D.W., 1979: The mesoscale meteorology of selected upwelling regions, Proc. Nat. Oceanogr. Symp. Univ. of Cape Town.

83. STUART, D.W., GOODWIN, R.J., and DUVAL, W.P., 1981: A comparison of surface winds and winds measured at 152m during JOINT I 1974 and JOINT II 1977, Coastal Upwelling, Amer. Geophys. Union, 39-43.

84. TRAGANZA, E.D., and CONRAD, J.C., 1981: Satellite observations of a cyclonic upwelling system and giant plume in the California Current, Coastal Upwelling, Amer. Geophys. Union, 228-241.

85. UHART, M., 1976: A case study of a land-sea breeze phenomena over the Western African coast, CUEA TECH. REP. 28, Dept. of Met., Florida State Univ., pp.125.

86. VAN FOREEST, D., 1980: A two-mode numerical model with applications to coastal upwelling, Ph.D Thesis, Dept. of Oceanogr., Univ. of Cape Town.

87. VAN IEPEREN, M.P., 1971: Hydrology of Table Bay, Dept. of Oceanogr., Univ. of Cape Town, pp.48.

88. WALTER, B.A., Jr., and OVERLAND, J.E., 1981: Response of stratified flow in the lee of the Olympic Mountains, Pacific Marine Environ. Lab. Tech. Rep., pp.48.

89. WATSON, A.I., 1978: A study of low level mesoscale winds observed off the Peruvian Coast during March and April 1976, CUEA TECH. REP. 41, Dept. of Met., Florida State Univ., pp.121.

90. WYRTKI, K., 1975: El Nino - The dynamic response of the equatorial Pacific Ocean to atmospheric forcing, J. Phys. Oceanogr., 5, 572-584.

91. YOSHIDA, K., and MAO, H.L., 1957: A theory of upwelling of large horizontal extent, J. Mar. Res., 16, 40-54.

92. YOSHIDA, K., 1967: Circulation in the eastern tropical oceans with special reference to upwelling and under currents, Japanese Jrn. of Geophys., 4, 1-75.